Creation of Magnetic Flux

Gordeeva, Anna

Publication date:
2011

Document Version
Early version, also known as pre-print

Creation of Magnetic Flux in Quenched Superconducting Rings and Josephson Junctions

Ph.D. dissertation at DTU Physics

July 31st 2011

Anna Gordeeva

Contents

Abstract

It is a well-known experimental fact that magnetic flux may be trapped in superconductors cooled through the phase transition from the normal to the superconducting state even in zero external magnetic field. The trapped magnetic flux is quantized and appears in the bulk as an Abrikosov vortex and in superconductors with annular geometry as a fluxoid, both containing one flux quantum.

For a long time the spontaneous trapping was considered as a mere disturbing factor accompanying the quenching of superconductors. The situation changed after the pioneering works by T. Kibble and W. Zurek who proposed the superconducting phase transition as a promising candidate for testing the "cosmological" scenario of the continuous phase transitions following right after the Big Bang. In the general picture, believed to be valid for any system undergoing such a phase transition, it is the interplay between the finite speed of the transition and the divergence of the relaxation time during the quench that leads to production of topological defects. In superconductors both types of topological defects (Abrikosov vortices and fluxoids) are expected to satisfy the proposed general scenario.

The main focus of this thesis is an experimental and theoretical study of the spontaneous production of fluxoids as well as Abrikosov vortices in small superconducting niobium rings. Experimentally we have measured the trapping probability as function of the quench rate, which is varied over several decades. For a given quench rate the trapping statistics is usually based on thousands of thermal cycles executed both without and with an applied symmetry breaking external magnetic field. Various configurations of Josephson junctions as well as SQUIDs have been used both as flux detectors and as rapid thermometers. The samples are specially designed superconducting circuits integrated on small chips fabricated in Russia. The experimental results are compared to theoretical predictions and numerical simulations. The work has been done as part of an international collaboration between researchers from Italy, England, Russia and Denmark.

Dansk resumé

Det er et velkendt eksperimentelt fænomen, at magnetisk flux kan indfanges i superledere, som køles gennem faseovergangen fra den normale til den superledende tilstand. Man taler om spontan flux-indfangning, hvis det sker uden påtrykt ydre magnetisk felt. I superledere fluxen er kvantiseret. Inde i selve superlederen findes fluxkvantet i en såkaldt Abrikosov hvirvel, mens kvantiseringen i en superleder med ringformet geometri sker i form af fluxoider, som hver indeholder et helt antal fluxkvanter.

I lang tid betragtedes spontan flux-indfangning som et uinteressant artefakt knyttet til nedkøling af superledere. Dette ændredes, da T. Kibble og W. Zurek foreslog den superledende faseovergang som en lovende kandidat til afprøvning af de kosmologiske teorier for de kontinuerte faseovergange, der skete umiddelbart efter Universets skabelse (Big Bang). Kontinuerte faseovergange er et generelt fænomen, og det antages, at det er konkurrencen mellem den begrænsede faseovergangshastighed og den divergerende relaksationstid under faseovergangen, som giver anledning til dannelse af såkaldte topologiske defekter. I superledere forventes begge typer af topologiske defekter (Abrikosov vortex og fluxoid) at følge det generelle scenario.

Denne afhandling lægger hovedvægten på en eksperimentel og teoretisk undersøgelse af den spontane indfangning af fluxoider og Abrikosov hvirvler i små superledende ringe af niobium. Eksperimentelt har vi målt indfangningshyppigheden som funktion af nedkølingshastigheden (quench rate), varieret over flere dekader. For en given nedkølingshastighed er den statistiske hyppighed baseret på tusindvis af termiske passager af overgangstemperaturen, udført både med og uden et symmetribrydende eksternt påtrykt magnetfelt. En række særligt udformede Josephson-elementer samt SQUIDs er blevet anvendt både som flux-detektorer og som hurtige in-situ termometre. Prøvestykkerne er special-designede superledende kredsløb integreret på små silicium chips, som er blevet fremstillet i Rusland. De eksperimentelle resultater er sammenlignet med teoretiske forudsigelser ved bl.a. numerisk simulering. Arbejdet er udført som en del af et internationalt samarbejde mellem forskere fra Italien, England, Rusland og Danmark.

Acknowledgements

Here I want to thank, in random order, those who made this research possible.

First, I thank my supervisor Prof. Jesper Mygind. With his enthusiasm, his inspiration, and his great efforts to explain things clearly he helped to make the research a unique experience for me. Throughout my thesis period he provided ideas, encouragement, guidance but let me free to pursue my own goals in my own way. It has been a great pleasure to have him as a supervisor.

It is difficult to overstate my gratitude to Prof. Roberto Monaco for making exploration of the experimental world of superconductivity the pleasure it has been. I consider it an honor to work with him.

I wish to express my gratitude to Prof. Mads Peter Sørensen, Prof. Ray Rivers, David Weir and Prof. Mogens Samuelsen for stimulating discussions which contributed significantly to my understanding of the subject.

Furthermore I gratefully acknowledge the discussions and correspondence with Prof. Andrey Pankratov, who have had a strong influence on my work. A special thanks goes to Prof. Claus Schelde Jacobsen for assistance at the late stage of the project. I thank Prof. Valery Koshelets, who have provided our group with all the samples covered in this thesis as well as many others. I thank Prof. Preben Buchhave for giving useful guidance in the use of the lasers. I thank my predecessor Morten Aaroe for introduction to the project and willingness to help during these three years.

I would like to thank the workshop, who helped build the equipment that allowed me to run the experiment.

I thank the staff of Physics Department (DTU Physics) in the Danish Technical University for creating excellent working conditions and friendly atmosphere, in particular, secretary Dorte Glass for helping in diverse ways and Ole Mogensen for technical support.

I would also like to thank my parents and sister for the support they provided me through my entire life. Without their love and encouragement I would not have finished this thesis.

Introduction

The problem considered in this dissertation is the spontaneous defect production in second order phase transitions in superconductors. What is the defect and why does it appear?

One of the fundamental properties of superconductivity is the Meissner effect, the expulsion of magnetic field from the interior of a superconductor. However under certain conditions the magnetic field penetrates the superconductor in the form of quantized vortices. From the point of view of gauge theories such a vortex represents a topological defect.

The superconducting state is a macroscopic coherent state in which a large number of Cooper pairs are synchronized in phase, i.e. described by a single wavefunction ψ.

In the "normal" state the phases of all particles are uniformly distributed along the trigonometric circle. That is why, despite every particle obeys quantum-mechanical laws, it does not result in quantum relations for macroscopic variables.

The transition from the uncorrelated to the correlated state is an intriguing question and a subject of the theory of non-equilibrium superconductivity. This field appears to be very challenging both for theoreticians and experimentalists. Therefore every new achievement in the field is regarded as a significant.

One of such achievements is the Kibble's theory of defect formations in the course of second order phase transitions. His analytical and rather intuitive approach allows to get some insights into the processes near the critical temperature, governed by fluctuations. The essence of the theory is that the probability for topological defects to be created depends on the cooling rate. Kibble obtained a relation from which one, informed about transition rate, can evaluate the density of topological defects.

As a cosmologist Kibble was interested primarily in the possible consequences of his theory for the Universe. We see today that the Universe is not completely homogenous over all scales, there are structures on various scales. It is believed that the structures we see today started out as small inhomogeneities in the distribution of matter in the early Universe.

Furthermore the applicability of the theory is not restricted to cosmology. Many features of the early Universe have analogues in condensed matter

physics: as the Universe expands and cools it might acquire a domain structure, such as, for example, in a ferromagnet cooled through its Curie point.

The adaptation of Kibbles' ideas to solid state systems, made by W. Zurek, attracted much attention and motivated a number of research groups to seek for experimental verification of the predictions. However for the experimentalists the task to prove/disprove the theory turned out to be difficult. A number of experiments have been conducted with different systems, such as helium 3, helium 4, liquid crystals and superconductors. However their outcomes deviated somewhat from the expectations and in the best cases were concluded as "non contradicting" the theory. New mechanisms of defect formation were proposed to link some of the experiments and the theory. Sometimes preliminary results were promising and the experiments were required to be continued but unfortunately they have been abandoned. The most successful experiments are reviewed in Ref.[1]. Since 2007 when this review was written several new publications on this subject have appeared. They will be described in the following chapter.

Thus 30 years have passed since the first Kibble's publication and there is still no unambiguous experimental demonstration of the KZ-law. But despite this fact the original theory became widely accepted and is believed to be correct so far.

As for superconductors before the appearance of the KZ-theory the speed of transition was not recognized as a factor influencing the trapping probability. The picture was as follows. While the cooling in zero field results in a homogenous state without vortices, the cooling in the presence of a field causes freeze-in of the vortices. What the KZ scenario says is that zero field and fast speed of transition together may also result in trapping of the vortices.

Probably the most informative experiment with superconducting systems that showed an undeniable scaling of defect density with the quench rate over four decades, was the experiment with annular Josephson junctions by R. Monaco et al. Indeed the trapping probability decreased as function of the quench time but the scaling exponent appeared to be two times larger than expected. Also the probability did not depend much on the circumferences of the rings. The interpretation of the results involved some difficulties due to complexity of the system. And for the further experiments the choice was made in favour of a single ring rather than the annular Josephson junctions.

This thesis is a continuation of the above project. Its main goal is to advance in the understanding of the mechanism of vortex formation in superconducting systems (Josephson junctions and single rings) in order to answer the question: is the KZ mechanism the only one mechanism responsible for the defect formation in superconductors. To achieve this goal the research was conducted in two directions.

The directions are determined by two competitive factors. On the one hand, in the ideal case the ring undergoing the phase transition has to be fully isolated from the environment. The situation when the transition occurs in magnetic field will be discussed in the thesis as well. On the other hand, the magnetic flux, when trapped, has to be detected somehow. For this purpose a magnetic sensor is required, consequently the ring is inevitably disturbed by the presence of it.

In the first approach the isolation of the ring is regarded as a condition of primary importance. Based on this principle an optical detection system had been designed by Morten Aarøe during his PhD project. However the realization of this idea required more resources than were available and due to this it was not completed. In the present thesis this direction has its development as the "SQUID" experiment.

In the second approach the isolation of the ring is sacrificed to a more simple detection system. In this case the ring is a part of the detection system - it forms one of the electrode of a Josephson junction, used as a magnetic sensor.

As a compromise between the two approaches the SQUID experiment was designed and performed. In this experiment the ring is isolated on the chip (no current leads, no Josephson junctions on top), but it is magnetically coupled to a SQUID. At first glance the consequences of the magnetic coupling between the ring and the SQUID for the trapping rate are not obvious. Experimental results and discussion will be given in the thesis.

The very important part of this project is a collaboration with the theoretical group at London Imperial college. Numerical simulations, performed by David Weir, considerably enriched our understanding of defect formation in superconducting rings. They revealed that the original KZ-theory did not work in the range of parameters where we could perform measurements. Therefore a direct comparison with the theory is not possible. The theory has been extended numerically to the experimentally achievable parameters.

The essential part of the research which makes it different from other projects is the ability to vary the quench time over several orders of magnitude. The technique of electrical heating was developed already in 2005 while during this project the laser heating is successfully implemented.

The dissertation starts with a literature survey, given in chapter 1, which lays out the theoretical grounds to be covered in the following chapters. In chapter 2 the used equipment and description of the setup are presented. The experimental part starts with chapter 3, where the SQUID experiment is discussed. In chapter 4 the trapping of Abrikosov vortices is studied in short Josephson junctions. The investigation of Abrikosov vortices is continued in chapter 5 for long Josephson junctions. Finally, the last chapter 6 deals with trapping of flux quanta in a ring, detected by an inline Josephson junction on top of the ring.

Chapter 1

Theory

This opening chapter is intended to give a literature survey and the background theory dedicated to the field of spontaneously generated topological defects in the course of a second-order phase transition. It is kernel is to form the foundations on which the following experimental chapters will rest.

1.1 Kibble-Zurek predictions

1.1.1 Second order phase transition

The dynamics of a system undergoing a second-order phase transition is described by a complex order parameter ψ, equal to zero in the symmetrical phase (before the transition) and non-zero in the asymmetrical phase (after the transition) [2].

The second order phase transition occurs when the state of a body changes gradually while its symmetry changes discontinuously at the transition temperature. The low-temperature phase is the one of reduced symmetry, i.e., it is more ordered.

Below the critical temperature while the whole body is in the state of reduced symmetry, an inclusion of the symmetrical phase is called "topological defect". Normal core of Abrikosov vortex is an example of such an inclusion in case of superconductors.

The simplest case of the continuous phase transition without external fields is described by the effective Ginzburg-Landau potential (Fig.1.1):

$$V(\psi) = \alpha(T - T_c)|\psi|^2 + \frac{1}{2}\beta|\psi|^4, \tag{1.1}$$

where α and β are phenomenological expansion coefficients, T is temperature and T_c is the critical temperature.

In equilibrium the value of the order parameter ψ is determined by the

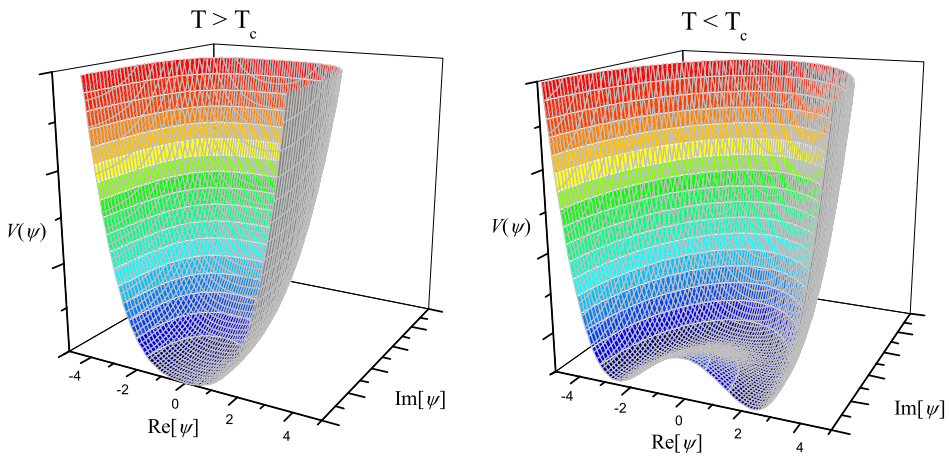

Figure 1.1: Ginzburg-Landau potential. Left: above the critical temperature. Right: below the critical temperature.

minimum of the appropriate potential V at a given temperature:

$$\frac{\partial V}{\partial \psi} = 0 \tag{1.2}$$

If this condition is not fulfilled the order-parameter experiences a relaxation process until the equilibrium value, determined by Eq. 1.2, is reached [3].

The relaxation process can be characterized by a relaxation time τ and a correlation length ξ. The correlation length ξ is as a characteristic length which measures the spatial response of the low-temperature phase to some perturbation (e.g. the distance over which the superconducting state develops at a normal metalsuperconductor boundary). Near the critical temperature T_c both quantities diverge according to the power laws [4]:

$$\xi \sim \mid 1 - \frac{T}{T_c} \mid^{-\nu}, \tag{1.3}$$

$$\tau \sim \mid 1 - \frac{T}{T_c} \mid^{-\gamma} . \tag{1.4}$$

The critical exponents ν and γ need to be specified for different systems, several examples can be found in [4], [5] or [6].

Suppose that the temperature T is varied with time t so that near T_c the expansion is valid: $T(t) = T_c(1 - t/\tau_Q)$, where τ_Q is a characteristic time of the transition, called the "quench time".

Above the transition temperature, the minimum energy is degenerate with respect to the order parameter phase φ. As the temperature falls below T_c the potential acquires the "Mexican-hat" shape. The order parameter

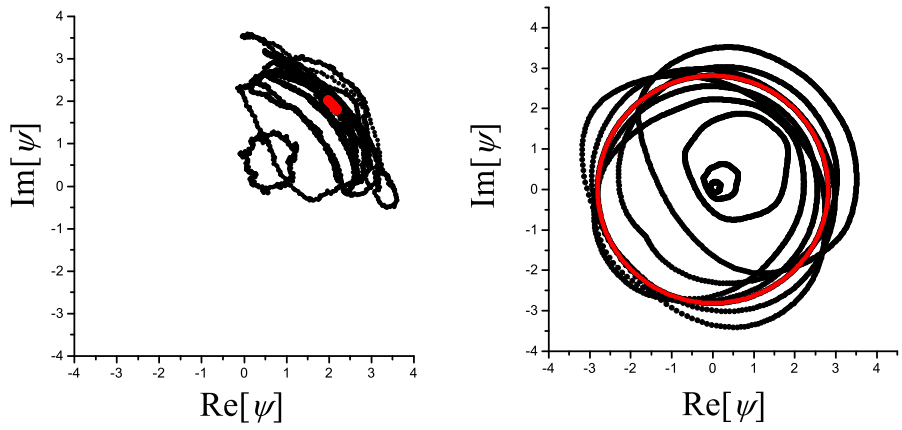

Figure 1.2: Snapshots of the order parameter of a 1D ring during the phase transition in the presence of fluctuations. The final states are shown by red. Left: At the end of the evolution the order parameter has a single valued phase. Right: At the end of the evolution the phase changes along the contour from 0 to 2π, giving one topological defect in the contour.

grows up and its phase becomes a well defined quantity. In the absence of an external field no value of the phase is preferred. The choice is governed by the thermal fluctuations only.

At this point the sample size and shape become important. For a single connected body with size of the order of the correlation length the same phase is established over the whole volume. If the size is larger than ξ the phase may be chosen independently in different domains, each of the size of ξ.

Two examples of the evolution of the order parameter of one dimensional ring are shown in Fig.1.2. The evolution starts in the minimum of the left potential in Fig.1.1 and continues driven by two factors: the changing potential shape and the thermal fluctuations. In the left plot of Fig.1.1 the order parameter slopes down and shrinks into one point. In the right plot it spreads into different directions, enveloping the grown maximum. Despite this state is less energetically favorable the order parameter remains in it as long as the intensity of the fluctuations is less than the height of the potential maximum. The second case illustrates the trapping of a topological defect.

According to the Kibble's and Zurek's approach [7] two regimes can be specified. The first regime, called "adiabatic", is sufficiently far from T_c, where the relaxation time is smaller than τ_Q. In this regime the system has time enough to reach the equilibrium and thus the instantaneous value of the order parameter coincides with the equilibrium value. The second regime ("impulse") occurs when the quench is faster than the relaxation time and

therefore the order parameter can not adjust to the new thermodynamic parameters.

The crossover between two regimes occurs at the freeze-out time $\widehat{t}$. At this moment the character of evolution changes. New defects cannot appear and those already created become frozen in or can annihilate during the further evolution.

The initial density of defects $\widehat{\xi}$ is determined by the correlation length ξ corresponding to $\widehat{t}$ and the instantaneous temperature. By expressing $\widehat{t}$ through the transition time, τ_Q, and substituting it into Eq.1.3 one gets [8]:

$$\widehat{\xi} = \xi(\widehat{t}) = \xi_0(\frac{\tau_Q}{\tau_0})^{\nu/(1+\gamma)}. \tag{1.5}$$

The parameters ξ_0 and τ_0 characterize the low-temperature (T=0) equilibrium correlation length and the relaxation time, respectively. Following [9] it is convenient to introduce the exponent $\sigma = \nu/(1+\gamma)$. The expression (1.5) represents the main result of the theory and is to be tested experimentally in this work.

1.1.2 The Universe

Historically, attention to the defect formation in superconductors was attracted when it was recognized that experiments with them could be helpful in understanding the Universe evolution. At the present level of knowledge it is believed that in its early evolution the Universe has been undergone through a sequence of phase transitions of different orders. If so the scenario described in Sec.1.1.1 might take place and led to some, probably observable, consequences.

With regard to the Universe there are three types of possible topological configurations: domain walls, strings and monopoles [10].

The observed isotropy of the 2.7K background microwave radiation [11] gives strong constraints on the inhomogeneities in the early Universe. Some inhomogeneities are, however, needed to explain the formation of galaxies, which presumably evolved by gravitational condensation from an earlier near-homogenous state [12].

Domain walls must be excluded, because their gravitational effect would lead to an unacceptable anisotropy in the back-ground radiation. Networks of strings scale with time, so now one cannot expect to find significant numbers of cosmic strings in the visible Universe, but their presence may have had an important effect on the early evolution of the Universe. The number of monopoles could have been very large in the early Universe. Many of them are expected to annihilate up to now. To estimate their present density a mechanism of annihilation is required.

Therefore all three types of defects might have appeared in the early history of the Universe but few are likely to have survived to the present.

1.1.3 Superconductors

Because of the disability to verify the prediction of Eq.1.5 for the Universe the number of solid state systems, experiencing phase transitions, were proposed by Zurek for experiments [7].

Among other systems, such as superfluid helium 4 [13], helium 3 [14] and liquid crystals [15], the superconductors were pointed out as promising candidates for testing the theory.

In comparison with the original theory the superconductors impose an additional complication - the coupling of the order parameter with the magnetic field. It makes the theoretical analysis significantly more complex. The question is discussed, for example, in Refs.[7], [16] or [17].

According to Ref.[16] fluctuations of magnetic field provides a completely new mechanism for the formation of topological defects, additional to the KZ-mechanism. In order to distinguish these two mechanisms in experiment, one has to be able to detect both positions and signs of individual vortices. The mechanism, based on the field fluctuations, should lead to domains of vortices of the same sign whereas KZ-mechanism predicts, that nearby vortices have opposite signs.

For superconductors the critical exponents in Eqs. (1.3) and (1.4) are $\nu = 1/2$ and $\gamma = 1$ [18]. Thus the Kibble-Zurek mechanism predicts for one-dimensional (1D) systems $\sigma = 0.25$ and for two-dimensional (2D) systems $\sigma = 0.5$.

Bulk superconductors are difficult objects from the experimental point of view for two reasons. It is not a trivial task to realize a uniform quench over the whole volume of the superconductor without thermal gradients. Also the observation of defects inside the bulk is very difficult, if possible at all. Therefore only 2D and 1D objects are available for the experiments.

The magnetic field trapped somewhere in the interior of the superconductor represents a topological defect. Depending on the geometry of the superconductor the field can be trapped in different configurations: as an Abrikosov vortex or as a fluxoid.

Abrikosov vortices

In type-I superconductor ($\kappa = \xi/\lambda_L < 1/\sqrt{2}$) magnetic field, below the critical value, is screened from the interior of a superconductor with a characteristic scale λ_L, called the London penetration depth:

$$\lambda_L{}^2 = m/\mu_0 n_s e^2, \tag{1.6}$$

where n_s is the density of superconducting electrons [19].

If type-II superconductor ($\kappa = \xi/\lambda_L > 1/\sqrt{2}$) experiences the normal-superconducting phase transition in the presence of external magnetic field (less than the upper critical field) along with superconducting phase the inclusions of normal phase will be found in from of quantized vortices, called

the Abrikosov vortices (AVs). Due to the requirement that the phase of the order parameter has to be a single-valued function [20], each vortex holds one flux quantum Φ_0:

$$\Phi_0 = h/2e = 2.07 \times 10^{-15}\text{Weber}. \tag{1.7}$$

The AVs consist of a normal metal core and superconducting currents circulating around the core. The magnetic field produced by a single vortex decays exponentially at scales $r >> \lambda_L$ [21]:

$$H_z \approx \frac{\Phi_0}{2\pi\lambda_L^2}\ln\frac{\lambda_L}{r}, \tag{1.8}$$

meaning that the AV is a well localized object in space.

In ideal superconductors when the external magnetic field is turned off the AVs become energetically unfavorable and tend to escape from the superconductor. It happens if superconductor is a singly connected and does not have pinning centers. The pinning centers can trap some of the AVs, which in this case stay inside the superconductor until the temperature will rise to make them free.

The pinning centers in superconductors can be various types of normal inclusions, dislocations, grain boundaries or interfaces between superconductors with different parameters [22].

Different types of pinning centers are known to have different temperature dependence of the pinning force f_p [23]. In general case f_p can be approximated by a power-law dependence

$$f_p \propto (1 - \frac{T}{T_c})^n, \tag{1.9}$$

with n ranging from 2.5 to 3.8.

If there is a cavity in a bulk superconductor it interacts with AVs. Away from the cavity the vortex energy includes both the energy of the normal core and the energy of the circulating supercurrents. Vortex trapped by the cavity does not have the normal core and consequently is more energetically favorable. It means that there is an attractive force between the vortex and the cavity [19].

Fluxoids

In 1964 F.London showed that a superconducting ring should conserve the quantity which he called "fluxoid". The fluxoid is defined for any closed path within a superconductor as

$$\Phi = \mu_0{\lambda_L}^2 \oint \overrightarrow{j} \cdot d\overrightarrow{s} + \oint \overrightarrow{A} \cdot d\overrightarrow{s} = n\Phi_0, \tag{1.10}$$

where $\overrightarrow{j}$ is the supercurrent density and $\overrightarrow{A}$ is the magnetic vector potential.

The validity of Eq.1.10 was demonstrated in Ref.[24] more than 30 years ago for tin cylinders. For a superconducting cylinder with wall thickness large compared to the penetration depth the first integral in Eq.1.10 can be negligibly small, and the total magnetic flux trapped by a persistent current in the cylinder becomes precisely quantized in units of Φ_0.

The annular geometry has attracted attention both theoreticians [7] and experimentalists ([25], [26] or [27]) for the following reasons. It is the ring geometry of the sample that allows one to detect the magnetic flux, because it is indefinitely trapped in the hole. Also the annular systems are the easiest to analyze, since they can be described within the 1D model.

1.2 Numerical simulations

In parallel with the experiments a lot of numerical simulations have been done attempting to provide a convinced evidence of the theory. Numerical simulations help to get more insights and to learn new features not appearing in the theoretical analysis. The results of simulations occur to be helpful in the interpretation of the experiments.

One dimensional systems

The simplest case of the 1D systems (i.e. a real order parameter with the periodic boundary conditions) is solved numerically in Ref.[28]. In such a system during the phase transition many pairs of kinks and antikinks may be created. Since the total magnetic flux from one pair is zero, they are not observable experimentally. Furthermore such a pair is unstable and tends to annihilate. Nevertheless in simulations every single kink and antikink can be counted at any moment of the evolution. The obtained scaling exponent σ for the average number of kinks versus the quench time is 0.28 ± 0.02 and compares favorably with the theoretical prediction 0.25.

In another work [29], in contrast with Ref.[28], the order parameter is a complex variable, which is a more adequate description, because it allows the creation of a single vortex and not only in a pair with antivortex. The authors extended the range of τ_Q to very slow quenches, when the average number of trapped vortices $< n >$ per cycle is less than one.

The important result is that for slow transitions the crossover from the Kibble-Zurek to a new behavior was observed (see Fig.1.3, where $< n >$ versus τ_Q is presented for several ring circumferences).

The interpretation of all experimental results presented in Chapters 3 - 6 is based on work [29]. It revealed the applicability region of the Kibble-Zurek theory for the systems of finite size. Before it was assumed that if the Kibble-Zurek behavior was valid, it should be valid in the whole range of τ_Q.

Two dimensional systems

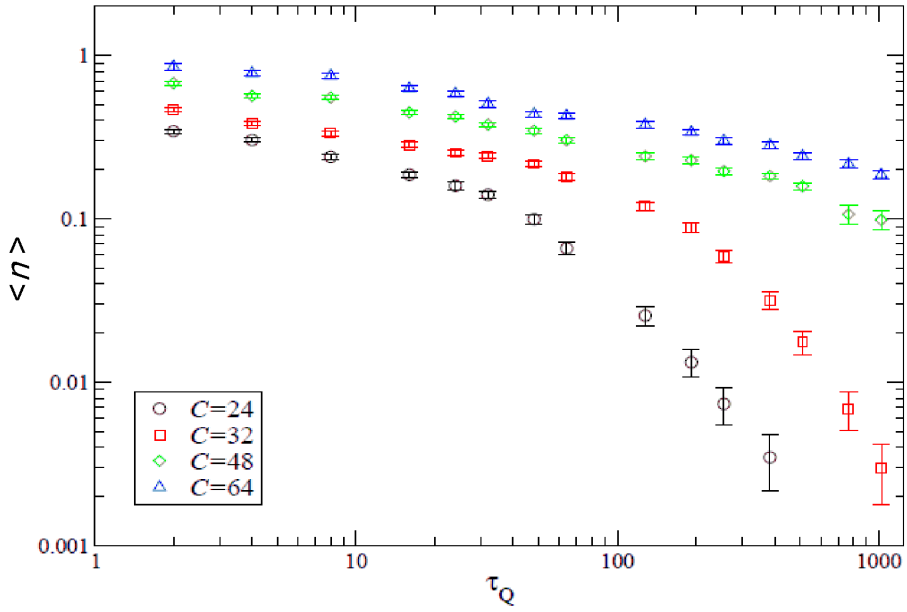

Figure 1.3: Average number of defects versus the quench time for several ring circumferences C. Results of simulations, showing change between KZ and exponential suppression regimes. When $< n >$ becomes smaller than 0.3 the trapping becomes suppressed for all curves. Above this value the KZ scaling $\sigma \approx 0.25$ is observed. The figure is reproduced from Ref.[29].

Defect formation in the course of the second order phase transition in two dimensions was studied numerically in Ref.[30] in the framework of the Abelian Higgs model (Ref.[31], p.318) coupled to a heat bath. It was shown that the density of topological defects scales with the quench time τ_Q with the exponent $\sigma = 0.44 \pm 0.1$, which is in a good agreement with predicted value 1/2.

The mechanism of fluxoid formation in a wide 2D ring in the course of the phase transition is described in Ref.[32] on basis of numerically solved time-dependent Ginzburg-Landau (TDGL) equations coupled to diffusion equation. In dimensionless units the inner and outer radii of the ring are 50 and 100, respectively. The diffusion equation is needed to model the cooling. Only one cooling rate has been investigated in this work.

Two stages of evolution of the order parameter of the ring are shown in

Fig.1.4. Right after the transition a huge number of vortices and antivortices are created in the ring body. During the next stage they annihilate randomly, some of them cross the outer or the inner border of the ring. Eventually all vortices leave the ring bulk. Those of them which entered the ring hole remain confined there infinitely. If the number of vortices entering the hole differs from the number of antivortices the magnetic flux trapped in the hole is not zero.

Also it is shown in [32] that the Josephson weak links in the ring can significantly increase the flux spontaneously trapped in the ring hole.

1.3 Experiments with superconductors

In this section the experiments with superconductors designed to test the KZ prediction are reviewed.

Array of rings

In order to observe KZ-behavior an array with 124 rings made from amorphous Mo_3Si was fabricated [25]. The sample was cooled through the normal-superconducting transition. The rings had inner and outer diameters 20 and 30μm, respectively. Indeed, for faster transitions more rings trapped magnetic flux. However the dependence on the quench time was much weaker than anticipated from the KZ-scenario.

Films

Another system used for testing KZ-behavior is superconducting films. They may contain a number of pinning centers, which can trap Abrikosov vortices during the transition. In such experiments one should be aware that the resulting density of vortices might be determined by the number of pinning centers rather than by the number of spontaneously generated vortices. If the number of the formers is known to be larger than the number of trapped vortices, such films can be used for testing KZ-scenario. Such experiment was reported in Ref.[33]. Measurements were made only for two cooling rates. For these two points density of produced vortices scaled with τ_Q exactly with $\sigma = 0.5$ in a full agreement with predictions for 2D systems.

Another way to create pinning centers in a superconducting film is to physically make holes through it. It was done, for example, in Ref.[34]. A high-T_c Josephson junction was used as a sensor for counting the number of flux quanta trapped in the normal conducting area inside the superconductor. But the authors were interested primarily in the sensitivity of their detector not in the rate of spontaneous trapping.

Josephson junctions

In Ref.[27] an array from 214 high-T_c Josephson junctions in series form-

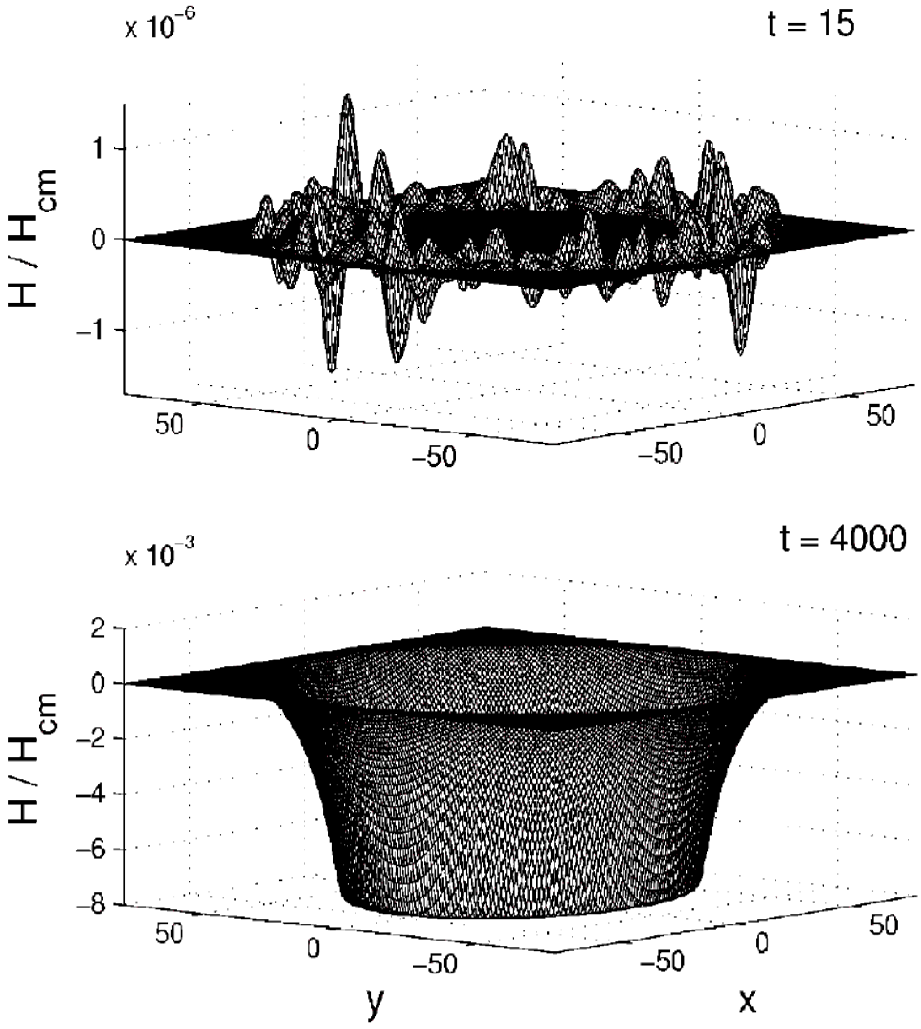

Figure 1.4: Recovery of superconductivity in the quenched ring. The figure is reproduced from Ref.[32]. Top: Initial stage of the evolution. Many vortices and antivortices randomly distributed over the body of the ring are created. Bottom: Last stage of the evolution. All vortices have left the ring body. Inside the hole a nonzero magnetic flux is trapped.

ing a loop was investigated. Values of the flux, trapped by the loop, measured at the end of each cooldown was found to satisfy a normal distribution. Dependence on the transition rate was not measured.

Another system tested for KZ-behavior was an annular Josephson junction: two superconducting rings on top of each other separated by a thin insolation layer [26]. The advantage of the system is that no additional magnetic sensor is required, the Josephson junction itself serves as the sensor. But the price is increased complexity.

In case of an annular Josephson junctions the "defect" is not an AV or fluxoid, it is a new object called "fluxon". A fluxon is created if one of the rings traps magnetic flux quantum and the other ring does not.

It was shown experimentally that the number of trapped vortices scaled with τ_Q accordingly to a power law with $\sigma = 0.5$ over four decades of τ_Q, which is twice larger than the expected exponent for a 1D system. A proximity effect [35] between two superconducting layers was involved for the explanation.

So far there are no more experimental works with superconductors about the KZ-behavior.

1.4 Josephson tunnel junctions

In this section necessary information about Josephson junctions (JJs) is given.

The Josephson tunnel junction consists of two superconducting electrodes separated by a thin insulating layer. Josephson phase ϕ is the difference in the phases of the wavefunctions in the two electrodes. The critical current I_c is a measure of how strongly the phases of the two superconducting electrodes are coupled through the weak link. The coupling free energy stored in the junction is the electrical work done by a current source in changing the phase:

$$F = E_j cos(\Delta\phi), \tag{1.11}$$

where $E_j \equiv (I_c/2e)$.

With regard to the JJs a new length scale has to be introduced - the Josephson penetration depth λ_J [36]. It determines the characteristic length, at which the external magnetic filed penetrates the Josephson region with suppressed superconductivity. The λ_J is given by [37]:

$$\lambda_J = \sqrt{\frac{\Phi_0}{2\pi j_c \mu_0 d'}}, \tag{1.12}$$

where j_c is the critical current density, μ_0 is magnetic permeability and d' is a thickness of insulator plus double λ_L of a superconductor. Sometimes it is required to get a more precise value. For example for the "window" type junctions the recipe is given in [38].

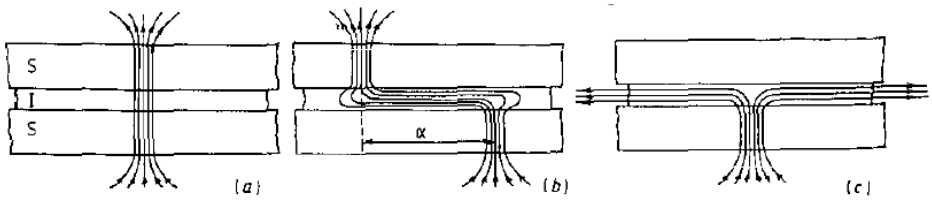

Figure 1.5: Types of Abrikosov vortices in Josephson tunnel junctions: (a) dipole, (b) misaligned vortex, (c) monopole. The figure is taken from [39]

All the Josephson junctions measured in chapters 4-6 are so-called "window"-type junctions. In the typical fabrication process the two electrodes are separated by an insulator that is thicker than the junction barrier to avoid short circuits. This part of the junction is called the passive or the idle region because no tunneling through it is possible.

Different types of AV are possible in the Josephson junctions composed by two superconducting electrodes and an insulating layer between them [39]. They are shown in Fig.1.5 from left to right: an aligned dipole vortex, a misaligned dipole vortex and a monopole vortex.

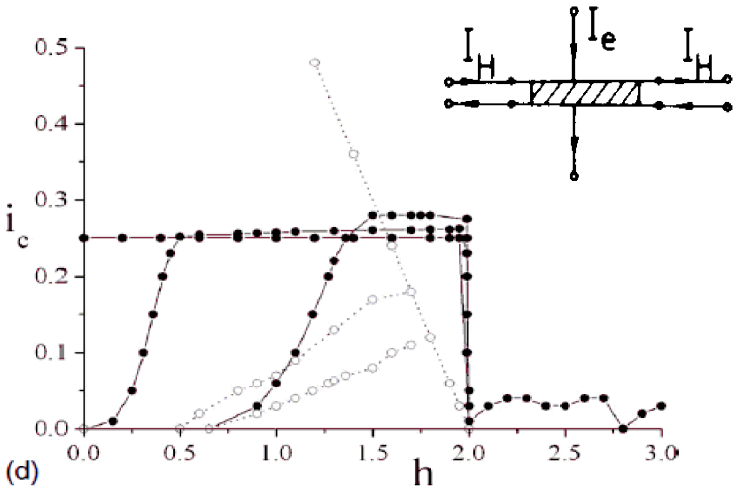

Figure 1.6: Numerically simulated magnetic pattern of a delta-biased Josephson junction. The figure is taken from Ref.[40]. Inset: A scheme of current injection for δ-biased Josephson junctions (from Ref.[36]).

Perpendicular field and parallel magnetic field lead to different magnetic patterns [41]. When a magnetic field is applied perpendicular to the plane of a junction, a complicated distribution of induced Meissner currents and magnetic fields is produced at the surface of the superconductor [42].These

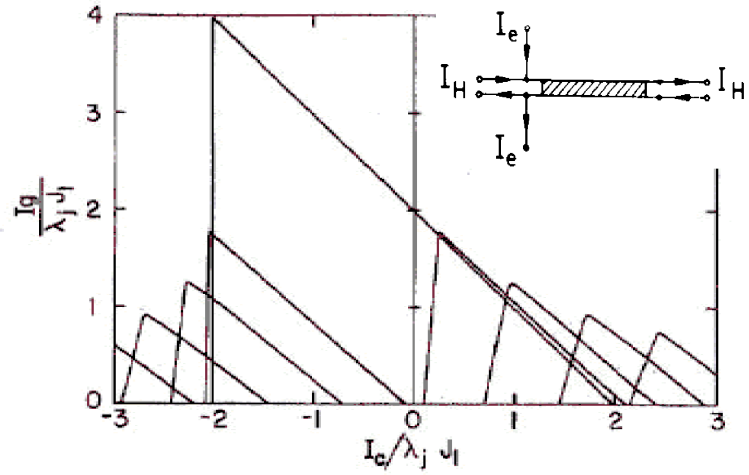

Figure 1.7: Theoretical magnetic diffraction pattern of a long inline JJ. Figure is reproduced from Red.[44]. Inset: A scheme of current injection for inline Josephson junctions (from Ref.[36]).

currents feed into the interior of the junction, where they generate local magnetic fields parallel to the plane of the junction. These fields, in turn, locally alter the Josephson phase [43].

The shape of the junctions and position of the current leads have a crucial effect on the critical current dependence on magnetic field, see, for example, [37]. Below two types of Josephson junctions are presented: the δ-biased junctions and the asymmetric inline junctions.

In Fig. 1.6 the magnetic diffraction pattern of a δ-biased JJ is shown. One can see that this kind of junction is nearly insensitive to magnetic field in a broad range of it [40].

The inline geometry was considered in Ref.[44]. In asymmetric inline geometry the bias current ia applied to the end of the junction electrode and is taken out from the same side of the second electrode (see inset in Fig.1.7). As the junction dimensions increase, the Josephson current density distribution becomes more non-uniform due to self fields. The slope of magnetic pattern, Fig. 1.7, is determined from condition $I_c = -I_B$, which is a consequence of the Meissner state.

As was shown analytically in [45] the Josephson energy does not vanish for $T \to T_c$. Their model consisted of two BCS superconductors coupled by a tunneling Hamiltonian. It means than the correlation between two superconductors appears simultaneously with superconductivity. This result can have an important consequence for experiments with superconducting rings with a Josephson junction on top (see Chap.6).

1.5 Thermal gradients

In our experiments we heat the samples and then wait until the heat dissipates to the environment due to diffusion processes. Inevitably there will be thermal gradients between different parts of the setup, for example between the sample and the sample holder, the sample holder and the exchange gas, etc. Also there will be thermal gradients within the sample volume. This is the most important problem, because it can influence the process of defect formation.

Analytically the general case of thermal gradients with no specified geometry is investigated in Ref.[46]. Two parameters, the cooling rate τ_Q and the velocity v_T of the transition front, determine the nucleation of topological defects. Depending on the relation between these parameters two regimes are found: in the regime of fast propagation, defects are created according to the Zurek scenario for the homogeneous case, while in the slow propagation regime, vortex formation is suppressed.

Consequences of the thermal gradients for a single ring. With regard to a single ring it is shown analytically and verified numerically that the thermal gradients drastically decrease the production of topological defects [47]. The region where the phase transition occurred first may impose its choice on the rest of the volume, thus suppressing or even halting production of topological defects.

In case of superconductors another serious consequence of thermal gradients is the appearance of currents due to thermoelectric effects. The existence of thermoelectric phenomena in superconductors was pointed out first by V. Ginzburg [48]. So far this field remains rather unexplored. A few experiments [49], [50] with incomprehensible outcomes did not clarify the issue. For review of the experiments see Ref.[51].

In order to observe nonzero current due to thermal gradients a sample has to posses some kind of anisotropy, for example to be composed of two different superconductors. Whereas in a conventional superconductor the thermal current has two components: normal and superconducting, which compensate each other, so the total effect is zero.

Consequences of the thermal gradients for a Josephson junction. For a Josephson junction inhomogeneity of temperature causes the following effect. The normal current flows in the direction of a gradient. This current is compensated by a supercurrent in the opposite direction. When the compensating supercurrent exceeds the critical current Josephson oscillations appear [51]. Experimental studies of the thermoelectric effects in SNS Josephson junctions [52] have provided ample verification of the above idea.

From the above considerations one can understand how much more complicated superconductors are in contrast with idealized system considered in KZ-picture.

Chapter 2

Materials and methods

This chapter will describe how the setup works. Throughout the project several kinds of samples were measured. Each sample required some modifications of the setup. Here common important components are identified and how they function together. Further details are provided in chapters dedicated to a certain type of samples.

2.1 Setup description

The diagram of the setup, including sample, sample holder, cryoprobe, electronics, instruments, computer hardware and software, is presented in Fig. 2.1. Arrows indicate the direction of data flow between different parts of the setup. Below the content of each block, its functions and interaction with other blocks are considered.

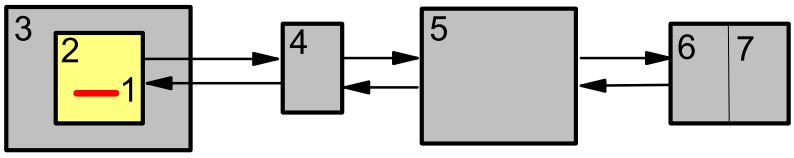

1 - sample, 2 - sample holder, 3 - cryoprobe, 4 - amplifier box,
5 - instruments, 6 - hardware, 7 - software

Figure 2.1: Diagram of the setup.

2.1.1 Samples

All samples were produced in the Institute of Radio Engineering and Electronics (IREE), Russian Academy of Science, in Moscow.

Layouts of all sample used in the course of the project are given in App. A.1. In total 5 different types of samples were used. Three of them were designed by Roberto Monaco, one by Morten Aarøe and one is a dc SQUID designed in IREE.

All samples are made by the vacuum deposition method on a silicon substrate. To fabricate Josephson junctions a trilayer structure $Nb-Al/Al_20_3-Nb$ was used. Details of the production process can be found, for example, in Refs. [53] and [54]. To contact the structure on the chip golden pads (0.6 by 0.6 mm^2) are deposited along the perimeter of the chip as the final stage of the fabrication.

The quality of the junctions is characterized by the leakage current. To quantify this current the parameter R_j/R_n is used, where R_j is the subgap resistance and R_n is the junction normal state resistance [36]. The larger the ratio the better the quality of the junction. At 4.2K for a given technological process junctions with $R_j/R_n > 30$ are considered to be good quality devices [55]. The ratio for the measured junctions in this project varied from 6 to 35.

Each chip contains one or two integrated 50 or 80 Ohm resistors, used as heaters. They were designed in form of a meander, see App.A.1. Hereafter we call these resistors the electrical heaters. The current is supplied so that magnetic fields from the two heaters cancel at the sample.

2.1.2 Sample holder

Two different samples holders are used: one of them is designed for cryoprobe 1 and another for cryoprobe 2 (see next section). Both sample holders have some common features: they consist of a metallic frame, a table supporting a sample, and coils. The table with the sample and the coils are fixed onto the frame by screws. All metallic parts are made from nonmagnetic materials: brass or copper.

The sample is pressed against the table by "fingers", i.e. wires formed as springs, soldered to a plastic board, which in turn is screwed onto the table. The contacting leads are printed on the board. The positions of the fingers are designed so that each finger touches the center of a certain contact pad on the chip. Thus the fingers have two functions: to mechanically fix the chip and to electrically contact the structures on the chip.

In the first sample holder the chip is directed vertically. Two coils can be mounted: one to generate the perpendicular magnetic field and one to generate the parallel magnetic field.

In the second sample holder the chip is placed horizontally and there is room only for one coil, which creates the magnetic field perpendicular to the sample plane.

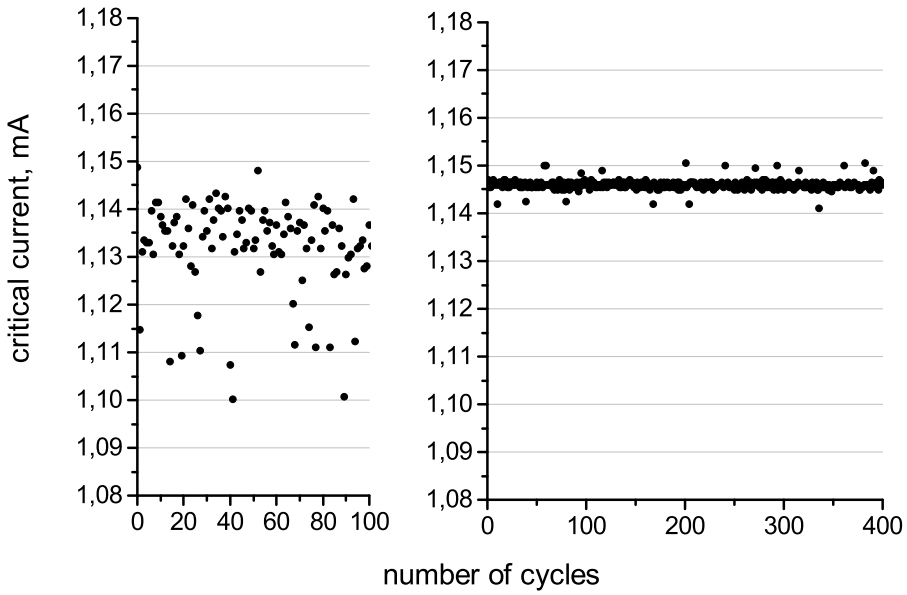

Figure 2.2: Comparison of the current noise for two different cryoprobes. Left: cryoprobe 1. Right: cryoprobe 2. In the cryoprobe 2 the noise is 2μA. Distinct points on the right plot are trapping of flux quantum. With noise presented on the left plot they can not be distinguished.

2.1.3 Cryoprobes

Two cryoprobes are used in the project. The measurements in chapters 4 and 5 (trapping of Abrikosov vortices) are made in the first cryoprobe. The measurements in chapters 3 and 6 (trapping of fluxoids) are made in the second cryoprobe.

The first cryoprobe is suitable for measurements which require different orientation of the magnetic field, because the sample holder fitted into this cryoprobe contains two coils.

In the second cryoprobe an optical fibre is installed for laser heating. Another distinction of this cryoprobe is a lower noise level. Therefore it was used to measure the production of fluxoids, which is a weaker effect in comparison with Abrikosov vortices and requires a lower noise level to be resolved.

The cryoprobes are characterized by different noise levels. A comparison is given in Fig. 2.2. Distributions of the critical current of a given Josephson junction, measured first in cryoprobe 1 and then in cryoprobe 2, are shown. The junction is heated above its critical temperature by the electrical heater in one case and by the laser beam in the other case. The pulse is long enough

to minimize the probability of spontaneous trapping of AVs or fluxiods. After cooling to 4.2K the critical current is measured. Such procedure is repeated many times. After a sufficient number of thermal cycles (for example, 100 cycles) one gets the distribution of critical currents.

Magnetic shielding

The resulting state of a superconductor after the phase transition is affected by external magnetic interference and noise of different sources. In order to eliminate all interference from the Earth's magnetic field the sample is put in a superconducting shield so that the experiments will result in accurate findings.

The magnetic shielding is provided by two layers. The first layer is a vacuum chamber of a cryoprobe made from superconducting Pb. The second layer is a high-Tc YBCO superconducting can inserted in the cryoprobe chamber.

Inside the YBCO can only nonmagnetic materials are allowed. All parts of the sample holder are made either from brass or copper.

2.1.4 Amplifier box

Block 4 in Fig.2.1 is the amplifier box and represents an electrical circuit regulating the exchange of data between the sample and the rest of the setup. The layout of the amplifier box can be found in App. A.3. Its functions are:

- to filter the external noise and prevent it from reaching the sample,
- to limit the maximum possible dc bias current through the Josephson junction
- to provide the primary amplification of the output signal (current and voltage across the sample) before it is transferred to the next parts of the setup, amplified again, recorded and analyzed.
- to disconnect the sample from the external instruments during the heating and cooling stages of the thermal cycle.

2.1.5 Instruments

Automatization

The experiment is automatized and run by a LabView program. The measurement technique is based on repetition of several manipulations, called a thermal cycle. One cycle can take from 2 to 15 seconds.

To realize automatization of the measurements Data Acquisition/Switch Unit, HP 34970A, was implemented [56]. It holds a number of relays which

can be operated by the computer. Commands to close/open the relays is given by LabView program.

The following four channels are connected to the relays. The channel called "trigger" is used to trigger the heating pulse from a pulse generator. The "Relay" channel is used to disconnect the sample from the environment during heating and cooling. The channel "heater" is needed to regulate the temperature of the sample during measurements. This channel is not used in this project. The channel "magnetic field" is used to apply the external field during the transition from normal to superconducting state.

Thermal cycle

The thermal cycle consists of the following steps, see Fig.2.3. At the moment t_0 the "relay" channel is open, isolating the sample from the environment and the "magnetic field" channel is closed, imposing the external field. These two manipulations prepare the sample for heating. At the moment t_1 the heating pulse is triggered. Time $t_2 - t_1$ is the duration of the trigger pulse. The duration of the heating pulse is shorter than duration of the trigger pulse. When the heating pulse ends the sample starts to cool down to 4.2K. To let the sample cool down the time interval $t_3 - t_2$ is set. At t_3 the "relay" channel closes, connecting the sample to the measurement system. From t_4 to t_5 the IV-curve is recorded on the computer. The cycle is finished.

All relays are connected to two control lines - L and H, Fig. 2.4. When a command is received the switch unit connects a specified channel to the control line. Only one channel can be operated by the switch unit at a time.

Two important points about the sequence of events during the thermal cycle have to be mentioned. First, due to the finite time needed to charge the coil the magnetic field has to be switched on before the arrival of the heating pulse. So that before the cooling the transient process in the coil has decayed and the magnetic filed becomes constant. Second, again due to the transient processes it is necessary to wait after connecting the "relay" channel and only then to start the measurements.

2.2 Quench time

The important part of the experiments is determination of the quench time. But before we describe how τ_Q is measured let us sketch a model of the heat flow in the setup.

The ring and the Josephson junctions used as thermometers are deposited on the silicon substrate. Typically the thickness of the substrate is 0.4mm. The chip is pressed against a copper or a brass table. The table is connected to the cryoprobe. Everything is surrounded by helium exchange

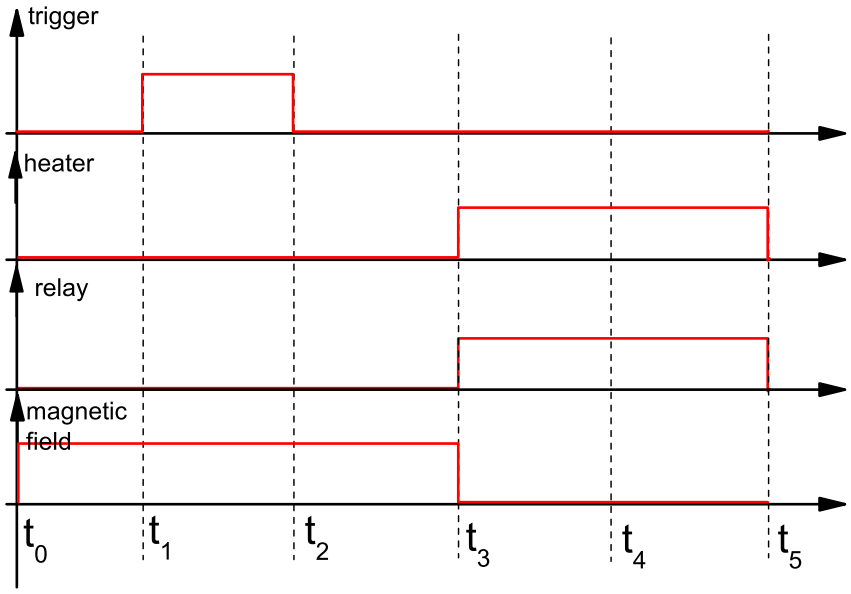

Figure 2.3: Scheme of the thermal cycle. Time interval during which the relays are closed are shown by the rectangular "pulses".

gas at low pressure, typically 10-15 millibars.

The quench time can be changed in two ways: by the duration/power of the heating pulse or by the pressure of the helium gas in the cryoprobe. Experimentally it was shown that the first method can vary τ_Q over four orders of magnitude: from 200μs to 1 s and more, if required.

The helium pressure is less effective, it gives a variation of only one order of magnitude. The smallest τ_Q can not be obtained by this method.

Heating. In the present setup the ring can be heated only together with the whole chip. The thermal conductivity of silicon at 4.2K is about 3W/cm K and it increases by one order at 10K [57]. The characteristic time for the heat propagation in silicon with length one millimeter is of the order of picoseconds [58]. In our experiments the minimal time scale is a few microseconds. It means that the approximation that the chip gets hot instantly is valid.

Cooling. The cooling of the chip occurs due to heat exchange with the metallic table and the helium gas. The most intensive heat flow is between chip and table. During the heating, if pulse is short, only the chip is heated, for longer pulses a part of the metallic table is also heated and must be included in the thermal model.

Model. In the simplest model the temperature of the chip T changes

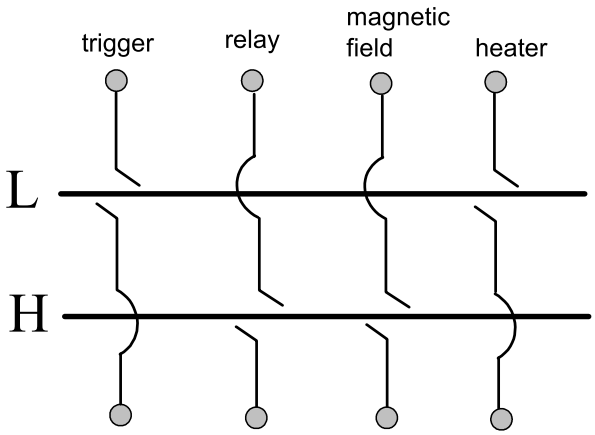

Figure 2.4: Scheme of relay connections.

exponentially with time:

$$T(t) = T_b + (T_0 - T_b)e^{-t/t_0}, \tag{2.1}$$

here T_b is the base temperature, T_0 is the initial temperature and t_0 is the time constant (can be viewed as RC with R - the thermal resistance between the chip and the table and C - the thermal capacitance of the chip). In this model we neglect the heat exchange with the gas as less intensive in comparison with the table.

By definition τ_Q is inversely proportional to a time derivative of the temperature at $T = T_c$:

$$\tau_Q = T_c(\frac{dT}{dt}|_{T=T_c})^{-1}. \tag{2.2}$$

In this model the quench time can be varied, for example, by means of t_0. Another parameter in Eq.(2.1), the quench rate depends on, is the base temperature. Different cooling rates can be obtained by keeping constant t_0 and regulating the base temperature. The base temperature for the chip is the temperature of the table only, since we excluded the gas from consideration. When we apply pulses of different duration we heat the table up to different temperatures. In such a way the base temperature depends on the pulse width, in turn the quench time depends on the base temperature and consequently also on the pulse width. It is easy to see from Eq.(2.1) that τ_Q can be varied over four decades by changing only T_b.

As the first approximation the whole table is supposed to be heated uniformly. In fact the part of the table, that is closer to the chip, is heated more. In a more complicated model the base temperature depends on time

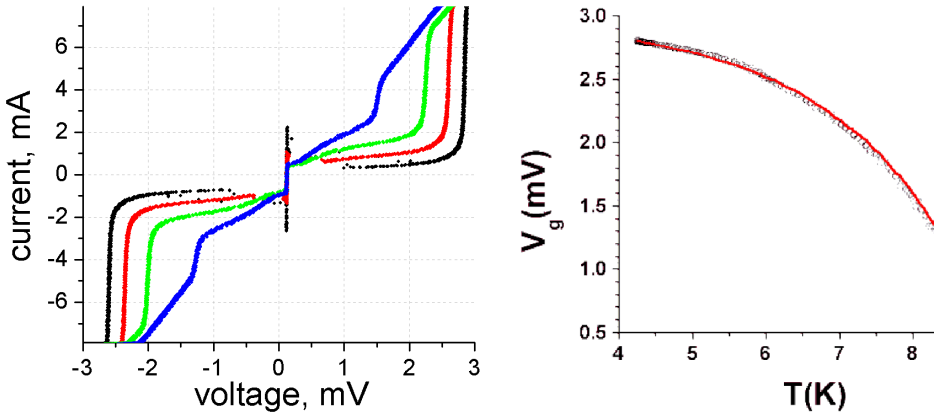

Figure 2.5: Left: IV-curves of a Nb JJ at several temperatures. Right: The temperature dependence of the gap voltage V_g. Circles - experiment, solid line - Eq.2.3. (reproduced from Ref.[60])

and it does depend in real setup. The above explanation is still valid in this case. Only instead of Eq.(2.1) one gets two exponents and consequently two time constants. One of them characterizes the heat dissipation from the chip and another - from the table.

Measurements. The Josephson junction is used as a thermometer. The dependence of the gap voltage of a niobium Josephson junction on temperature was first measured in Ref.[59]. For this particular technology ($Nb-Al/Al_20_3-Nb$) measurements were repeated in 2006 [60]. It was shown that $V_g(T)$ dependence is described very well by the following expression:

$$\frac{\Delta(T)}{\Delta(0)} = \tanh\frac{\Delta(T)}{\Delta(0)}\frac{T_c}{T} \approx [1 - \frac{T^4}{T_c}]^{2/3}, \tag{2.3}$$

where $\Delta(T)$ is the gap energy. Right side of Eq.(2.3) is an approximation, which makes calculations easier. The IV-curves of a JJ for several temperatures are shown in Fig.2.5, left.

Comparison of Eq.(2.3) with experiment is shown to the right. In order to measure temperature versus time the junction is biased at a certain current I_b above the critical current. The choice of I_b is an important issue. The best fit to the experimental data with Eq.(2.3) occurs at a bias current, which is 25% of the total current "jump" at the gap voltage [60]. A calibration plot of this procedure is given in Ref.[56].

A typical voltage response for a given I_b is given in Fig.2.6, left plot. The heating pulse lasts for 3 ms. At the moment the pulse starts the voltage jumps to a high value. When the pulse is off, the voltage is restored to the

initial value. The decay region of the gap voltage $V_g(t)$ is translated to $T(t)$ using Eq.(2.3). The result is shown in Fig.2.6, to the right.

Eq.(2.3) works only at temperatures below T_c, in reality even below 8.3K (for niobium the critical temperature is 9.2K). In order to determine the quench time at $T = T_c$ the measured dependence has to be extrapolated to higher temperatures. The extrapolation is shown in Fig.2.6 by the red solid line.

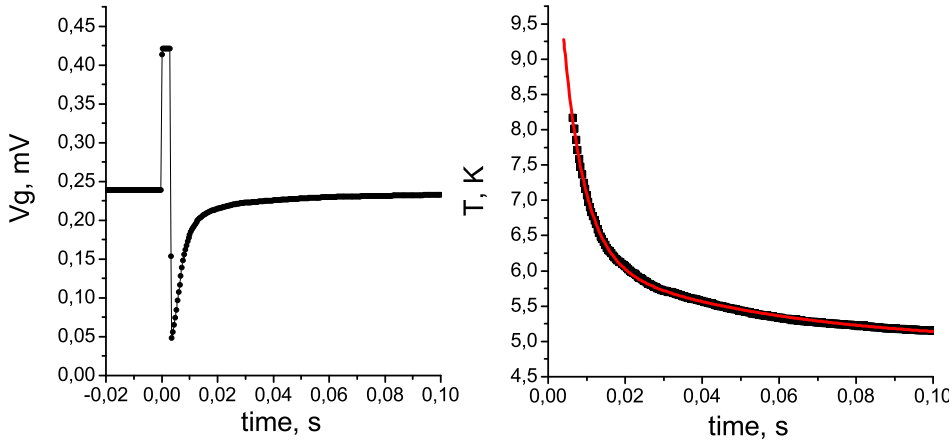

Figure 2.6: Left: The gap voltage versus time. Right: The corresponding temperature versus time. The black dots - experiment, the red line - extrapolation.

In Fig.2.7 τ_Q values obtained by the above recipe are presented. Three samples are measured in cryoprobe 1 and heated by the electrical heaters. One can see that the results do not differ from sample to sample. In log-log scale the dependence can be approximated by a linear law. In next chapters instead of τ_Q sometimes the pulse width is used for convenience.

In Fig.2.8 the τ_Q measurements are presented made in cryoprobe 2 both with electrical and laser heating. Again τ_Q is proportional to the pulse width. However the coefficients of proportionality are different.

There is can be a systematic error in all measurements. It originates from the offset of the amplifier, different critical temperature of the different batches or different bias currents. All these components give an uncertainty in the τ_Q values up to 20%.

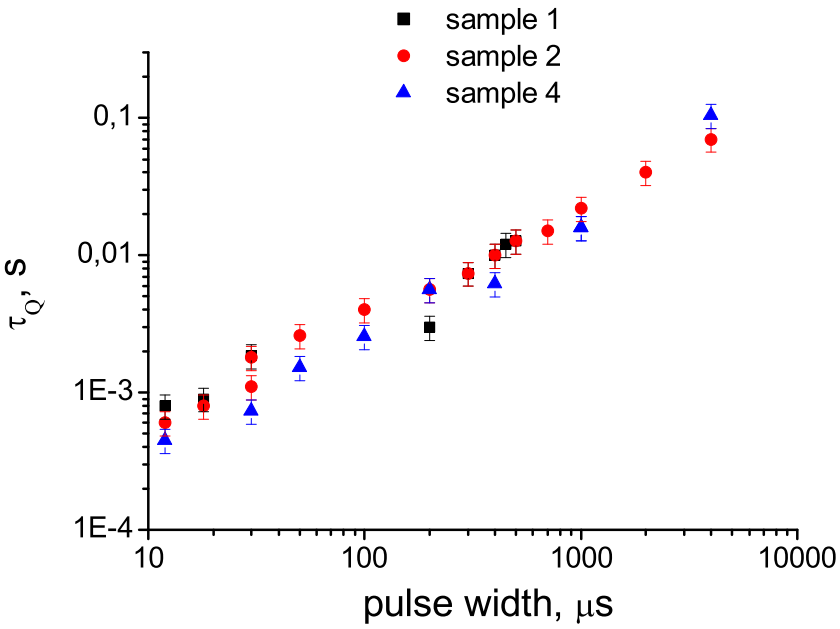

Figure 2.7: The quench time τ_Q versus width of heating pulse for electrical heaters in cryoprobe 1.

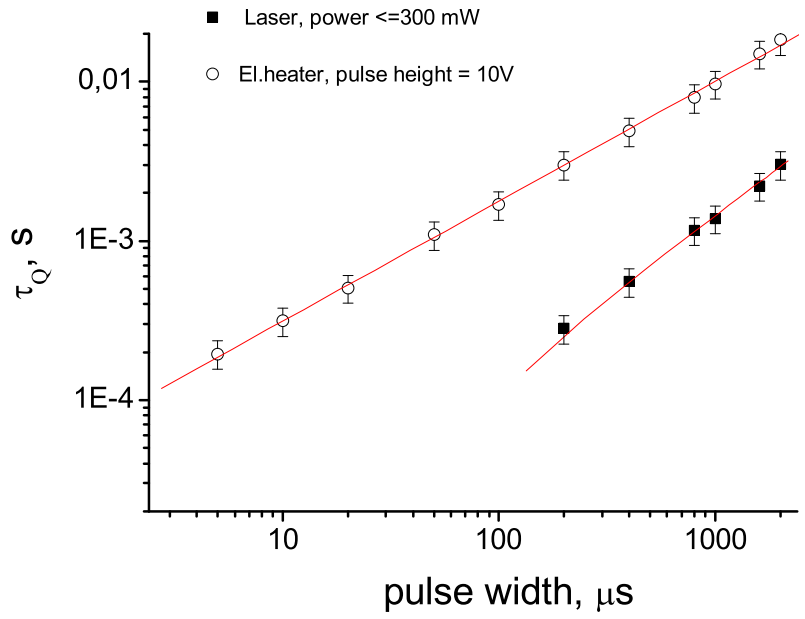

Figure 2.8: The quench time τ_Q versus width of heating pulse for electrical (circles) and laser (squares) heaters. Cryoprobe 2.

Chapter 3

SQUID experiments

In this chapter the spontaneous trapping of magnetic flux quanta in a niobium ring is investigated. The ring is loosely coupled to a low-Tc SQUID used as a magnetometer. Both the ring and the SQUID are shielded from the external magnetic field. The statistical distribution of the number of fluxoids trapped per cooling cycle is measured as a function of the quench time. Results are compared to the Kibble-Zurek predictions.

3.1 Description of experiment

The AFM-experiment was designed by Morten Aaroe during his PhD project as a realization of the idea about a ring fully isolated from the magnetic environment. The samples for this experiment were fabricated in IREE in Moscow. Only the last etching to free the cantilever was planned to take place at the DTU Danchip center. The etching procedure appeared to be more difficult than expected at the stage of design and has still not been completed. The results of this work are reported in Ref.[61].

While waiting for the etching procedure it was decided to measure samples with the cantilever stuck to the substrate. In this case the trapped flux quanta in the ring can be detected by an external magnetic sensor. A dc SQUID was proposed for this by Jesper Mygind.

The major challenge of the experiment is to place the SQUID close enough to the ring to obtain single-fluxoid resolution while still sufficiently far to avoid heating of the SQUID above its critical temperature during the thermal cycle. The SQUID has to be a passive detector, therefore its heating to the normal state is undesirable, since in this case the SQUID itself will experience all consequences of the KZ scenario. This problem could be solved by using a high-Tc SQUID close to a sample with a low-Tc ring on it. A significant difference in the critical temperatures of the high-Tc and the low-Tc superconductors enables that the SQUID stayed superconducting at all times. However, high-Tc SQUIDs generally are optimized for higher

temperatures and at 4.2K their sensitivity is reduced significantly due to the increase of the critical current density [62], [63]. Therefore a low-Tc SQUID was chosen. To keep the SQUID at low temperature a thermal insolation of several layers of mylar-foil was inserted between two chips.

High sensitivity of a SQUID is achieved by virtue of a large washer (multiply connected superconducting film, specially designed to focus the magnetic flux into the central hole of the SQUID). The presence of the superconducting washer significantly changes the magnetic environment of the ring compared to the ideal case considered in theory. The washer size is much larger than the size of the ring itself and the distance between the ring and the SQUID. Therefore, it is seen as an infinite superconducting plate for the ring. This has two consequences. First, being permanently in a superconducting state the washer screens the external magnetic field from the ring. On the one hand this is a positive effect. However, it deprives the possibility to investigate the influence of the external magnetic field on the trapping rate. Second, the washer may influence the process of magnetic flux formation in the ring for the same reason, because it screens any magnetic filed.

Samples with isolated superconducting rings are fabricated on a silicon substrate. The sample layout with the ring is shown in Fig. 3.1 (left). Two colors, red and blue, signify two different layers of superconductor. The superconducting ring is made from niobium and has the inner and outer diameters 156 μm and 162 μm, respectively. The thickness of the niobium film is 300 nm. Four Josephson junctions around the ring (small squares at the intersections of blue and red layers), connected in series, are used as thermometers. The size of the square Josephson junctions is 3μm by 3μm. Later this design happened to be very useful for the calibration of the SQUID.

Chip was designed and made in IREE RAS. Principles of operation of a dc-SQUID can be found elsewhere, for example in Refs.[64] and [65].

The SQUID has the following parameters. Its critical current is 22 μA. The outer size of the square washer is 2.5×2.5 mm^2, the size of the central hole is $70 \times 70 \mu$m^2. The declared flux noise of the SQUID is $3.6 \times 10^{-6} \Phi_0 / \sqrt{Hz}$ at 4.2K.

In Fig. 3.2 the current-voltage $I(V)$ and current-field $I_c(\Phi)$ characteristics of the SQUID are shown, indicating that the SQUID is a conventional dc SQUID. The only particularity of this SQUID is the asymmetry in the magnetic dependence of the positive and negative critical currents which originates from an asymmetric design of the base and the counter electrodes [66].

If a dc bias current is passed through a dc SQUID, the voltage V across it depends in a strongly nonlinear way on the magnetic flux threading the SQUID loop. This mode of operation is named "current bias" and used for all measurements presented here. The modulation depth (defined in

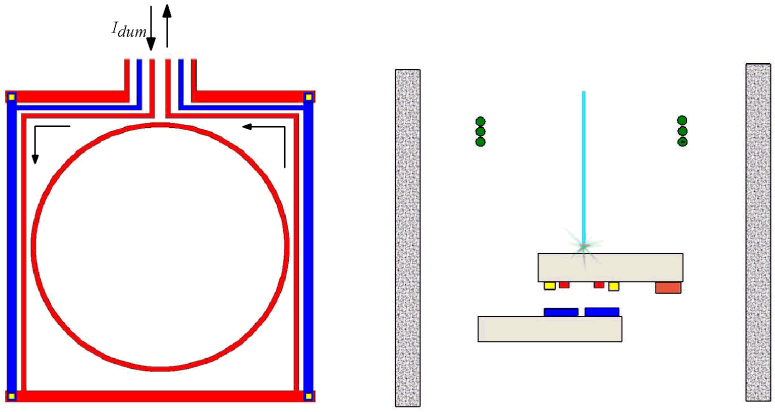

Figure 3.1: Left: Sample measured in the SQUID experiment. The superconducting ring traps magnetic flux quanta. Four small square Josephson junctions placed in the corners of the ring serve as thermometers to measure cooling rate and temperature gradients. I_{dum} is the current to calibrate the SQUID. Right: Scheme of SQUID-experiment. See details in the text

Fig.3.2(a)) is the range over which the voltage of the SQUID varies in response to the magnetic flux and depends on the bias current. In this experiment the optimal bias current, for which the voltage modulation is the largest, is founded to be 24.4μA.

The main elements of the setup are shown in Fig. 3.1 (right). Scale and relative dimensions do not correspond the real ones. The two chips are aligned so that the ring (marked by red) is coaxial with the inner hole of the SQUID (marked by blue). The Josephson junctions around the ring are shown by yellow color. The electrical heater is marked by orange color. The external coil (dark green) is placed approximately 1 cm away from the sample. The exact distance between the sample and the coil varies slightly from mounting to mounting. The cyan color with green light depicts an optical fibre used to supply the laser heating. All elements of the setup are inserted in a thick-wall can of high-Tc superconductor (vertical thick walls in the figure) screening the external magnetic fields.

Two chips are pressed face-to-face. Several layers of mylar-foil are inserted between them for thermal insolation. It keeps the SQUID below its transition temperature when the ring is thermally cycled.

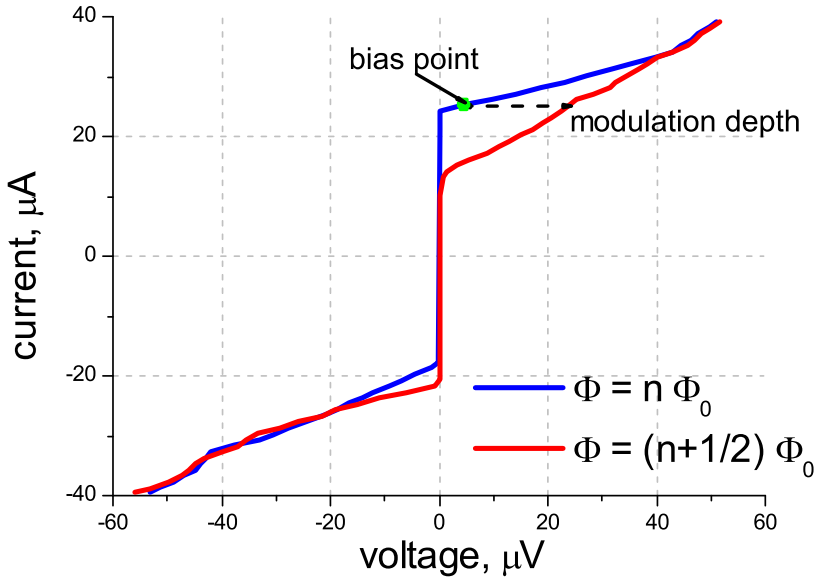

(a) SQUID IV-curves

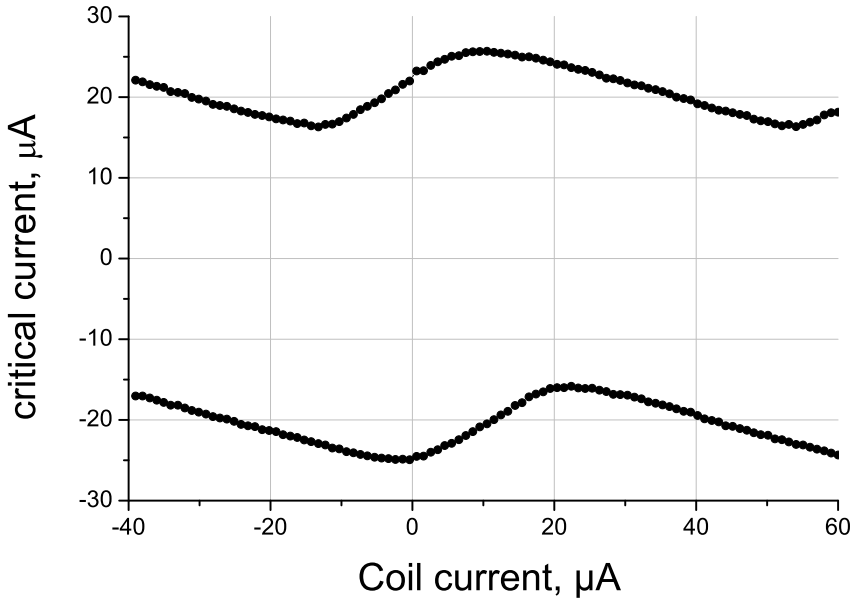

(b) Magnetic pattern

Figure 3.2: SQUID characteristics at 4.2K

In the beginning of the experiment the noise level of the setup was examined. The magnetic noise can be estimated by means of the SQUID. Every SQUID is characterized by a basic level of intrinsic noise usually stated by the producing company. All noise above this value is external and can be eliminated. The magnetic flux noise Φ_n is given by

$$\Phi_n = \frac{V_n}{\Delta V/\Delta\Phi}, \tag{3.1}$$

where V_n is a voltage noise and $\Delta V/\Delta\Phi$ is a flux-to-voltage transfer coefficient at the steepest part of $V(\Phi)$ dependence [67]. In order to measure Φ_n, a constant bias $I_b = 24.4\mu$A was applied to the SQUID and the voltage V of the SQUID was measured as a function of an applied current I_{coil} through the coil. The measured values are $\Delta V/\Delta\Phi = 90\mu V/\Phi_0$ and $V_n = 0.1\mu$V, which give the following value for the flux noise $\Phi_n = 0.001\Phi_0$. For a bandwidth $BW = 30$kHz the measured SQUID noise is $\Phi_n/\sqrt{BW} = 6 \cdot 10^{-6}\Phi_0/\sqrt{Hz}$, what is in a good agreement with declared value $3.6 \cdot 10^{-6}\Phi_0/\sqrt{Hz}$.

Every time after slow cooling (by lowering the cryoprobe in a dewar manually, in this case cooling from 10K to 4K takes about 20 minutes) SQUID was found in the same state, which therefore is believed to be a state without trapped vortices in the washer.

Next step is to detect whether the magnetic coupling between the SQUID and the ring is strong enough to resolve one trapped flux quantum in the ring. For our samples the calibration can be done in two ways. First way is to imitate the magnetic field distribution from a single trapped flux quantum. This possibility is given by four series connected Josephson junctions, which form a "dummy" square coil by their common contact lead. The area of the square loop is of the order of the ring area. If the current circulating in the ring with one trapped flux is known, by applying this current to the "dummy" coil, the resolution of the SQUID can be found. The path of the current I_{dum} is shown in Fig.3.1, left, by arrows.

Let us estimate how large the current I_{dum} has to be to create 1 flux quantum in the square loop. The inductance L of a ring with rectangular cross-section $a \times b$, a is the width, b is the thickness, if $a >> b$, can be estimated from the following expression [63]:

$$L = \mu_0 R(\ln\frac{8R}{a} - 0.5) = 3 \cdot 10^{-10}\text{H}, \tag{3.2}$$

where the radius of the ring is $R = 80\mu$m and its width is $a = 3\mu$m. Therefore the current circulating in the ring equivivalent to one trapped flux quantum is $I = \Phi_0/L \approx 4\mu$A.

Another way to calibrate the system is to cool the ring in the presence of magnetic field, then to switch off the external field and to measure the SQUID voltage. The value of trapped flux in the ring will be the closest

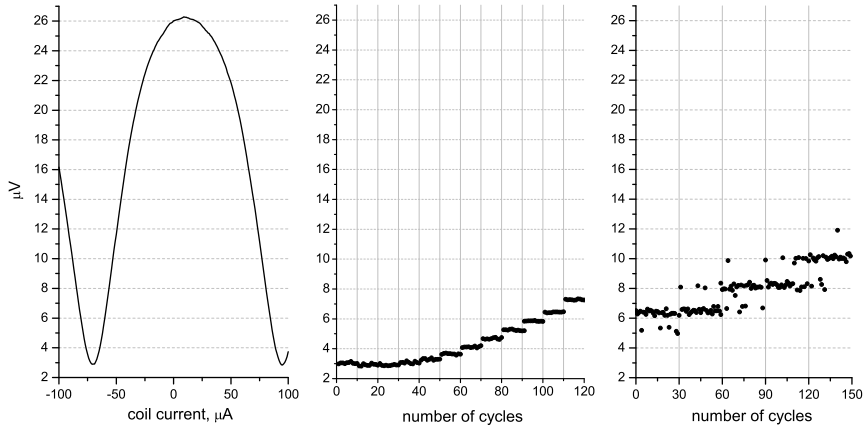

Figure 3.3: Calibration of the SQUID. Left: The voltage modulation by the field created by the external coil. Center: Calibration by means of the dummy coil. First 10 cycles are without coil. For every next 10 cycles the coil current is increased by 5μA. Right: Calibration by cooling in the external magnetic field. After every 30 cycles the current in the dummy coil is incremented to a new value: -40, -20, 0, +20, +40 μA. Electrical heater.

integer number of Φ_0 to the flux Φ imposed by the external field [24]. By repeating this procedure for different external fields one can observe a jump in the SQUID voltage every time the number of trapped flux quanta in the ring is increased by one.

The results of both calibrations are presented in Fig. 3.3. The figure consists of three plots. Left plot is the SQUID voltage as a function of the external magnetic field. In the current-biased mode of operation the voltage is a periodic function of magnetic field [64]. One period of modulation corresponds to one flux quantum entering the SQUID loop.

The central plot in Fig.3.3 is the calibration performed in the first way. First the SQUID voltage is measured 10 times with disconnected coil (first 10 points on the plot, the Y-axis is the voltage values and the X-axis is the number of measurement). After this coil is connected and the current $I_{dum} = 5\mu$A is fed in. With this current the next 10 points are measured, their numbers on the plot is from 10 to 20 on the X-axis. Then the magnetic field is increased again by the same amount and 10 more points are obtained, and so on. In general this plot repeats the left plot, the only difference being that every point is measured several times. Several points measured in a row give information about the voltage noise level.

The real coupling between the SQUID and the ring appeared to be stronger than between the SQUID and the "dummy" coil with the calculated

current (right plot in Fig.3.3). This is because the difference in the areas of the "dummy" coil and the ring was not taken into account.

Let us point out that the voltage separation between levels decreases when voltage approaches the minimum value of the modulation range. It means that magnetic field sensed by the SQUID changes by a fixed amount from one level to another.

From the broadening of the levels in Fig. 3.3, right, it is obvious that as soon as heater comes into play the noise increases. But even then the separation between neighboring levels is sufficient to distinguish different states of the ring.

Two heating sources were tested in this experiment: the electrical on-chip heater and a laser beam transmitted along an optical fiber placed from the back side of the ring chip, see Fig.3.1. In the next section data obtained with the electrical heater are compared to the data obtained with the laser.

The magnetic field can be obtained in two ways. It can be provided by the external coil (Fig. 3.1, right, dark green) or by the "dummy" coil on the ring chip (Fig. 3.1, left, shown by arrows). There are two moments about the coils to be mentioned:

- Field from the external coil is screened by the SQUID washer so that SQUID detects this field but ring does not feel it. Therefore to make the second calibration the "dummy" coil is used. Its position around the ring prevents screening of the field. The "dummy" coil gives the only possibility to cool the ring in the magnetic field.

- However the "dummy" coil can be used only for calibration. This coil is not suitable for measurements of trapping rate. It is not easy to maintain the same current in it because the whole chip is heated and as a result this coil changes its resistance rather fast during the thermal cycle. Nevertheless this experiment was attempted. Much higher trapping rate was found in comparison with the case without coil.

3.2 Results and discussion

Now when we know that the SQUID can resolve neighboring states of the ring: "$n\Phi_0$" and "$(n+1)\Phi_0$", we can measure the probability of trapping versus the quench time. In order to do this we need to determine the level which corresponds to zero magnetic flux in the ring. Every time when ring is found in a different state, it will be counted as a trapping. The probability of trapping is calculated as a ratio of "trap" events to the total number of thermal cycles.

The most populated level for cooling without external magnetic field is defined as a level of zero trapped flux.

Let us start this section from the discussion of difference between the electrical and the optical heaters. There are two main experimental observations:

- With the electrical heater it is possible to change the trapping rate by applying an external magnetic field. By regulating the current in the external coil one can switch between levels "nΦ_0" "(n+1)Φ_0" and so on, see Fig.3.4. With the optical heater the trapping rate does not depend on the external field, in other words the field is efficiently screened.

- For the same quench time τ_Q the ring traps significantly more often if it is heated by the electrical heater.

A possible explanation of the first point is the following. The electrical heater acts as a source of magnetic field when the voltage pulse is applied to it. When the pulse is on there is a certain distribution of supercurrents in the washer which screens the field generated by the heater. After pulse is finished the currents die out. But during a transition process the field near the washer is not zero, and this field influences the trapping in the ring.

The value of the magnetic field due to the electrical heater can be measured. A current of 1 mA in the heater creates one flux quantum in the SQUID. To heat the ring above T_c a current more than 28 mA is required, i.e. $28\Phi_0$.

The second point in the above list is obvious. The electrical heater adds noise to the system, thus increasing the trapping.

Therefore the measurements of trapping rate versus magnetic field are made using the electrical heater and the measurements of trapping rate versus quench time are made using the optical heater.

3.2.1 Trapping in a field

Fig.3.4 shows the results of trapping in the external field. In this section results are obtained with the electrical heater. The magnetic field is generated by the external coil.

In Fig.3.4 the ring states are denoted with a number n: $(n-1)\Phi_0$, $n\Phi_0$, $(n+1)\Phi_0$ and $(n+2)\Phi_0$. In our case it is reasonable to set n to zero. However, in general, n can be any integer number. The results presented below do not depend on the exact value of n.

In zero field the SQUID was observed in three different states, which correspond to three states of the ring: nothing trapped, one flux quantum trapped and minus one flux quantum trapped. In the figure the probability to find these states are red, blue and black respectively. One can see how the probability of the states changes periodically with the coil current. For the current 1200μA the most probable state is $+1\Phi_0$. The situation is fully

equivalent to zero magnetic field with the only difference that now the main state is $+1\Phi_0$ and two others are $0\Phi_0$ and $+2\Phi_0$.

3.2.2 Trapping versus the quench time

All results in this section are obtained with the optical heater. The ring chip was heated from the back side to avoid SQUID heating by the reflected light.

Fig.3.5 shows the reading of the SQUID for two different quench times. For most of the cycles the SQUID voltage is around 21μV (called the main level), but sometimes it is higher or lower than this value. The jump in both directions is about 1μV. The points above the main level signify that the ring has trapped "$+\Phi_0$", below - "$-\Phi_0$". The number of "$+\Phi_0$" is slightly larger than the number of "$-\Phi_0$". I.e. it is reasonable to suppose that there is a small residual field.

The bottom plot is taken for longer τ_Q. Again one can clearly see the most populated main level and two less populated levels. A difference from the top plot is that now the trapping of "$-\Phi_0$" dominates the trapping of "$+\Phi_0$". Hence the residual magnetic field has changed. From the bottom plot it is difficult to extract information about spontaneous trapping, because most of the traps of "$-\Phi_0$" happen due to the residual field rather than spontaneously.

The origin of the residual magnetic field and especially its dependence on the pulse remains unclear. However it is known that it is not due to insufficient shielding. Moreover the magnetic noise in the system is less then $0.001\Phi_0$, as shown by the SQUID measurements. This field should be generated during the thermal cycle, because it depends on τ_Q. A possible source for this field is the SQUID washer.

In Fig.3.6 one example of dynamics of the SQUID voltage during a thermal cycle is illustrated. The SQUID senses the moment when the heating pulse starts. Right after the arrival of the beam from the laser the voltage makes several fast oscillations (see the inset, where this region is enlarged) from 2 to 22 μV. This change is as large as the full modulation depth at the given bias current. The same effect should be observed if the magnetic field through the SQUID hole changes by several flux quanta. The further evolution of the voltage shows that the SQUID does not remain unaffected while the ring is quenched. It means that insolation consisting of 5 layers of mylar-foil is not sufficient to prevent the heat flow from the ring chip to the SQUID chip. However an increase of the number of insulating layers up to 15 yields a too dramatic reduction of the coupling.

Fig.3.7 summarizes the results of this chapter. The sum of probabilities to trap $+\Phi_0$ and $-\Phi_0$ is shown as a function of cooling rate. The degree of asymmetry between $+\Phi_0$ and $-\Phi_0$ discussed in relation to Fig.3.5 is included in the error bars ΔP. The more shift towards "preferred" sign the larger

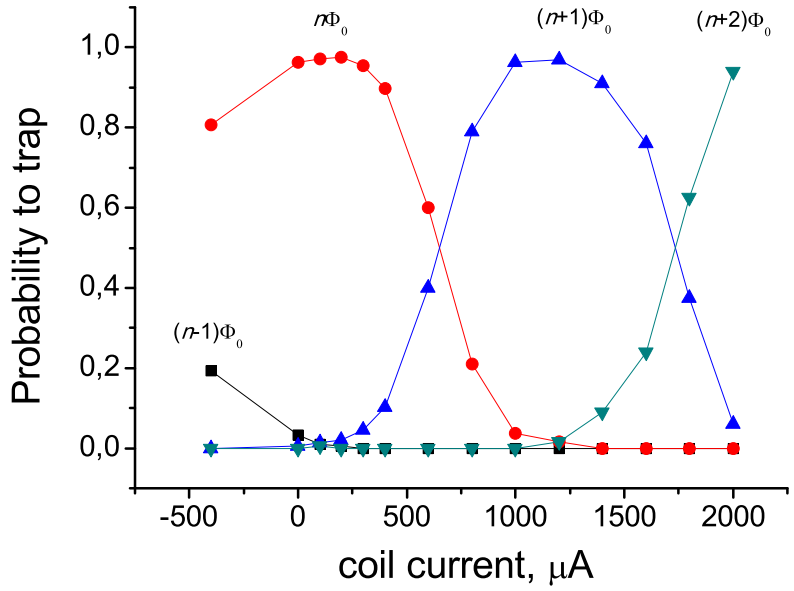

Figure 3.4: The probability to trap one flux quantum versus magnetic field/coil current in the external coil.

the uncertainty:

$$\Delta P = \frac{|N_{+1} - N_{-1}|}{N}, \tag{3.3}$$

where N_{-1} and N_{+1} are number of trapped $+\Phi_0$ and $-\Phi_0$ respectively, N is the total number of cycles. Longer τ_Q are not presented in this figure because of too large uncertainties.

Two sets of points are given in Fig.3.7: black and white, obtained with the optical and the electrical heaters, respectively. With the electrical heater the trapping probability is significantly higher.

One more moment to point out about the use of the SQUID for detection of magnetic fluxes is that we can hardly distinguish between flux trapped in the center of the ring and flux trapped in the body of the ring as Abrikosov vortex. Both cases are seen by SQUID as an increase in magnetic field by one flux quantum.

With all mentioned aspects the outcome of the presented experiment is to be taken with a good deal of scepticism. The main drawback of the SQUID experiment is the influence of the SQUID on the ring during the phase transition. Nevertheless let us remember this result as a reference point for its future comparison with results obtained in another systems.

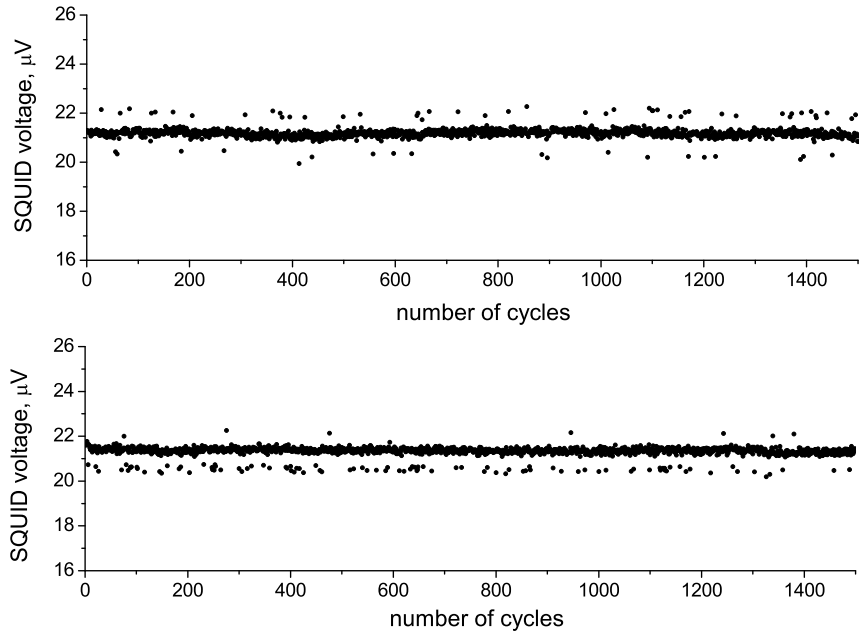

Figure 3.5: SQUID voltage for two different values of τ_Q. Top: power = 0.8W, pulse width = 300 μs . Bottom: power = 0.8W, pulse width = 20 ms.

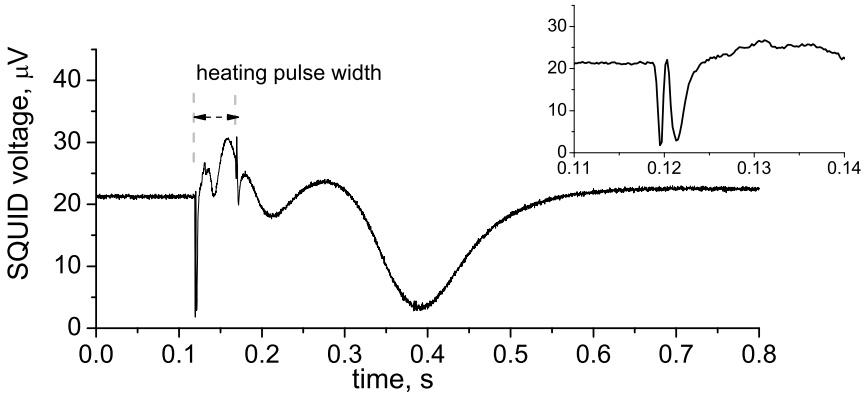

Figure 3.6: SQUID voltage versus time during one thermal cycle. Inset: moment of arrival of the pulse.

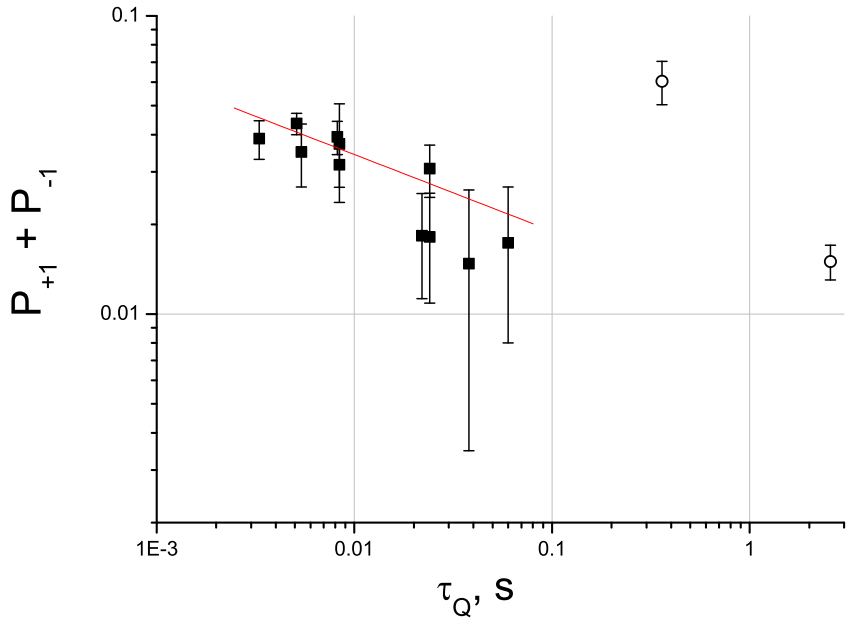

Figure 3.7: The probability to trap one flux quantum (both polarities) versus the quench time τ_Q. Black points are obtained with the optical heater, white points - with the electrical heater. Red line - power fit of the black points with exponent $\sigma = -0.26 \pm 0.11$.

Chapter 4

Abrikosov vortices in short Josephson junctions

> The hope is that, sooner rather then later, we can get as close as we can to some ideal reality or truth. It is misleading to assume that we can ever get to the absolute truth. Above all, we should always be open to the possibility of being wrong.
>
> /S. Oppenheimer "Out of Eden"/

The next three chapters are not written in historical order. The order is changed in such a way that complexity of the system increases from chapter to chapter.

In the beginning of the project the original idea was to use a superconducting ring whose circumference is much large than its width. For Kibble-Zurek mechanism such a ring was expected to show one-dimensional behavior. One-dimensionality means that the magnetic field can be trapped only as a fluxoid inside the whole ring but not as a single Abrikosov vortex in the body of the ring. A supporting argument for this belief is that the size of the defect scales during the phase transition. In other words, even if below T_c the ring is two-dimensional, near T_c it can be viewed as one-dimensional. Besides there was one more reason to think that our samples were not disturbed by AVs. It is known that AV in the absence of external magnetic field tends to escape from a superconducting film. It can stay there only if pinning centers prevent it from moving outside. Ideal superconducting film without defects does not have pining centers. Real Nb films are not perfect but still have so good quality that the ion gun may be used to create pinning centers. However, we believe that our samples do not contain pinning centers. So an Abrikosov vortex created during transition is expected to move out of the ring body.

However as we will see soon Abrikosov vortices play a significant role in our experiments. Therefore now the task is divided into two. The first is to understand Abrikosov vortex influence on our samples not to mix it with

fluxoid trapping. And the second is to study Kibble-Zurek effect for fluxoid trapping.

A single AV was studied in [68]. Magnetic diffraction pattern for different locations of the vortex. The location of the vortex within the junction is determined from the shape of the diffraction patterns.

4.1 Short overlap junctions

The simplest system for investigation of Abrikosov vortices is a superconducting film. However in case of a bare film an external sensor is required to detect the presence of the vortices. An alternative way is to modify the investigated system in such a way that it becomes a magnetic sensor itself. A realization of this idea is a Josephson junction. Abrikosov vortices in Josephson junctions have been studied quite intensively for several decades, see for example [69], [70]. However the variety of possible effects and their dependence on the specific system encourages more and more new investigations.

Most of researches are intended to understand the influence of AVs on the properties of Josephson junctions. For our needs the task is inverted, we are primarily interested in Abrikosov vortices. The Josephson junction is a mean to study them and it is interesting only if it can be used as a detector. Hence the JJ is an undesirable but necessary complication if we want to detect vortices.

AVs trapped in the electrodes are not the only possibility for the Josephson junction to interact with magnetic field. The magnetic field can penetrate into the junction region between the top/bottom electrodes also as a Josephson vortex. One Josephson vortex contains one flux quantum as well as the AV. But a characteristic size of the former, the Josephson length λ_J, is typically much larger than London penetration length λ_L. For example for our samples $\lambda_L = 90$nm, whereas λ_J varies from one batch of samples to another, depending on J_c, but is never less than few micrometers. The dimensions of the junction is a requirement for existence of the Josephson vortex. At least in one direction junction has to be longer than $4 - 5\lambda_J$ otherwise there is no room for a Josephson vortex. In this chapter we will consider only short junctions and every time the word "vortex" is used the Abrikosov vortex is meant. Longer junctions will be discussed in the next chapter.

The layout of the sample is presented in Fig. 4.1. Lets us describe it here in details because in the next chapters all samples will be presented in the same way. Junctions are formed by two overlapping layers of a superconductor, shown in two colors - blue and red. Between two superconductors there is a thin layer of AlOx (yellow). It does not coincide in area neither with the top electrode nor with the bottom one (so-called "window" type of

junction). The yellow layer in the picture is not seen in reality, because it is covered by the top electrode.

There are four junctions on the chip: two square and two circular. In turn every two differ by the geometry of the conducting electrodes: one circular and one square junction have the electrodes of a constant width which nearly coincides with the size of Josephson area just with a small correction for the idle regions, approximately 1μm. Another two junctions have narrow electrodes 2μm. The square junction have dimensions $10 \times 10\mu\text{m}^2$ and the circular ones have a diameter 12μm. The area of the square type is $100\mu\text{m}^2$ and the circular type is $113\mu\text{m}^2$. The critical current density is $\sim 3\text{kA/cm}^2$, which results in a Josephson length $\lambda_J \sim 7\mu$m. Hence these junctions are short they show near the ideal Fraunhofer diffraction pattern in magnetic field, see Fig. 4.2. Therefore these junctions can trap magnetic field only as an AV.

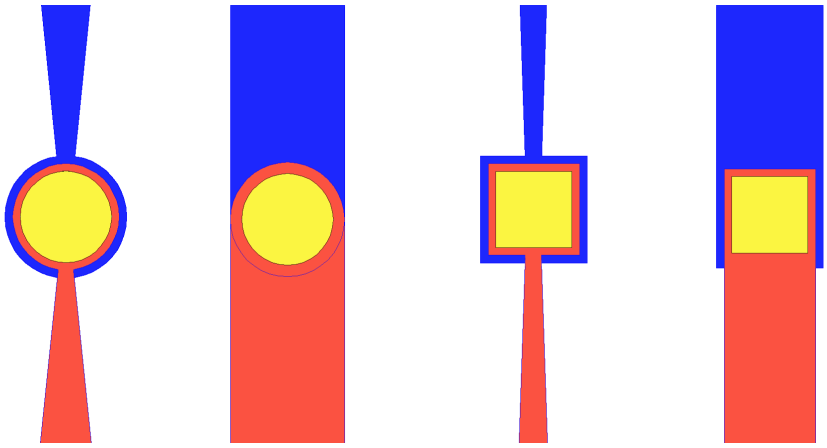

Figure 4.1: Layout of the sample with four short overlap Josephson junctions. Blue - bottom electrode, red - top electrode, yellow - Josephson region. From left to right: JJ_1, JJ_2, JJ_3, JJ_4. Junctions parameters are given in the text.

Two coils are used in this experiment. One creates a magnetic field in the direction perpendicular to the junction plane and is used during cooling. Another coil generates field parallel to the junction and is needed to obtain the I_c versus B dependence. The first coil can not be used for this purpose because it is known from [**?**] that JJs are less sensitive to the perpendicular field. And for the largest coil currents acceptable in the setup we can only trace the top of the main maximum of the $I_c(B)$ curve. Coil factors are 5μT/mA for the perpendicular coil and 28μT/mA for the parallel coil.

We measured all junctions on the chip except one JJ_1, which was not

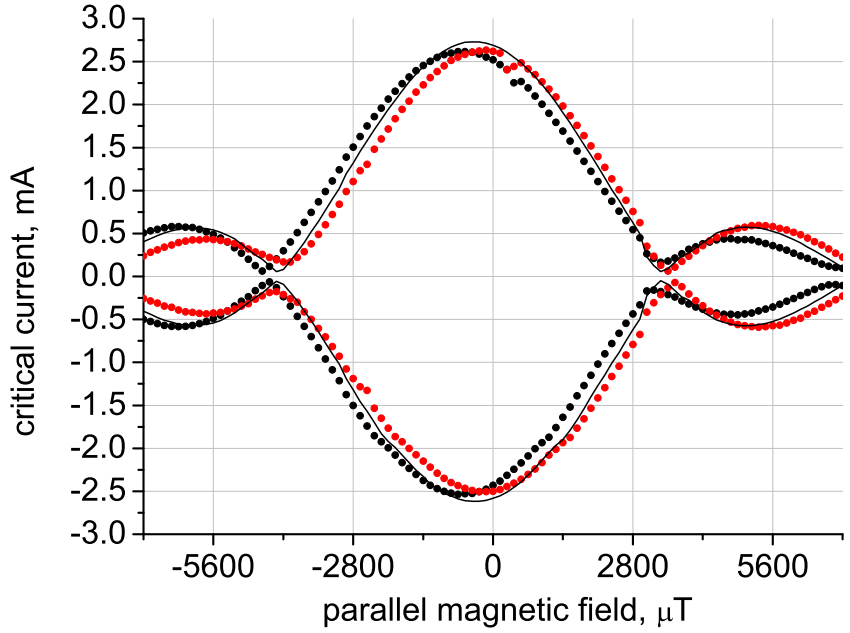

Figure 4.2: I_c dependence on parallel magnetic field for junction JJ_3. Solid line - without trapped vortices. Black markers - with a single trapped Abrikosov vortex. Red markers - with one trapped antivortex.

available for measurements because of the broken electrode.

In next two figures junction JJ_3 is considered in details. The I_c versus B dependence without trapped vortices is presented in Fig. 4.2 by the solid line. It is symmetric in regard to the direction of the magnetic field and is nearly perfect Fraunhofer-type, since this junction is short for $L/\lambda_J = 1.3$. The two other curves in this figure will be explained later.

In Fig. 4.3 the critical current of JJ_3 is shown after field cooling in both directions of magnetic field. Magnetic field was applied perpendicular to the junction plate during cooling and then removed before measurements. This procedure called calibration is made exactly as for Fig. 3.3. During the calibration junction is forced to trap more and more Abrikosov vortices. As a result the critical current changes in a stepwise manner, which in the plot looks like different levels. Every time a new AV enters the junction the critical current jumps to another value. Increase in magnetic field during cooling leads to the appearance of the new levels.

The junction starts to trap every cycle from the magnetic field 30μT or in terms of magnetic flux when density of magnetic field is enough to give one flux quantum through the junction area. This level continues until the

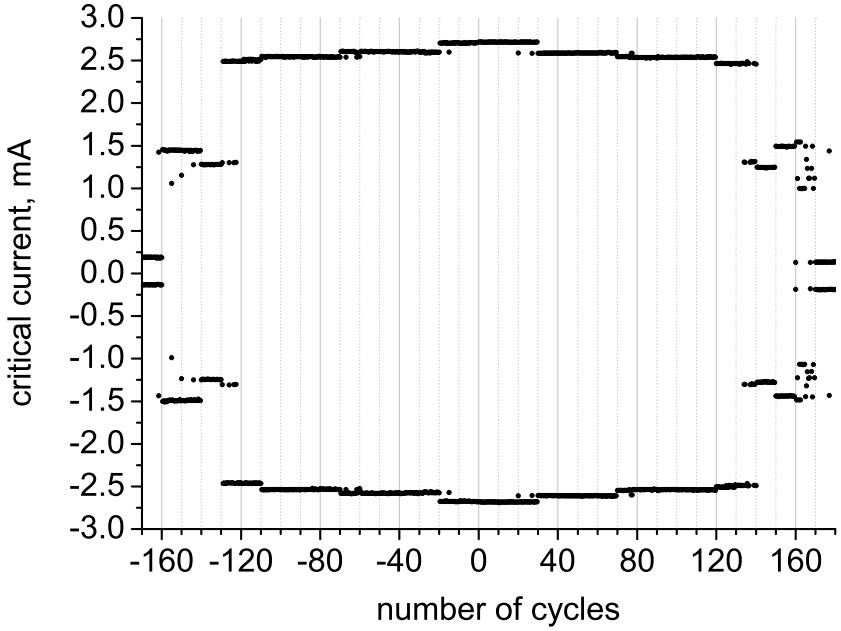

Figure 4.3: Calibration of the junction JJ_3. After every 10 cycles the magnetic field was changed by 10μT: cycles from 1 to 10 were measured without magnetic field, from 11 to 20 with magnetic field $+10\mu$T, and so on. The same in opposite direction: cycles from -1 to -10 were measured for -10μT.

magnetic field 70μT which corresponds to $3.5\Phi_0$.

In general the position of AV can be everywhere within the junction area or near the JJ. If it is far away from the JJ the junction properties are not affected by it. The fact that we see the levels and not randomly distributed values shows that AVs are trapped all the time in the same place. Similar observations were made, for example, in Refs. [69] and [68].

Now we will return to the discussion of Fig. 4.2. It shows the magnetic dependence of the critical current of JJ_3 in three different states of the junction: without vortices (solid line), with one trapped Abrikosov vortex (black markers) and with one trapped antivortex (red markers). To get the last two curves first the magnetic field required to trap one vortex was found with the help of Fig. 4.3. As discussed above we assume that for magnetic field from 30 to 60μT (cycles 30-70 in Fig. 4.3) the junction traps one vortex, and from -30 to -70μT (number of cycles between -21 and -70) one antivortex. Therefore to trap one vortex a middle value from the range $30 - 60\mu$T was taken. The junction was cooled in perpendicular

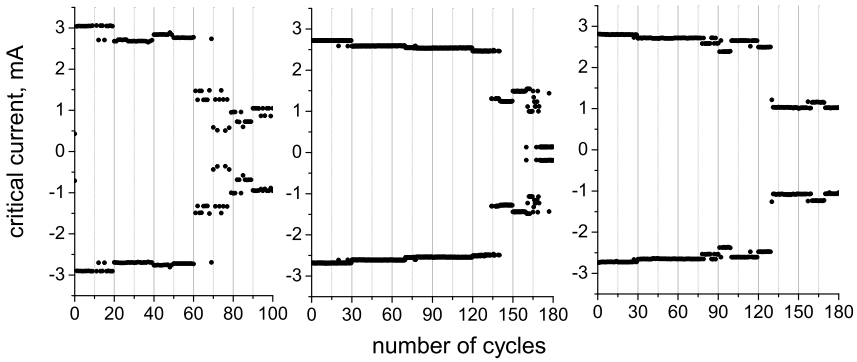

Figure 4.4: Calibration of the junctions. From left to right: JJ_2, JJ_3, JJ_4. After 10 cycles magnetic field was changed by 10 μT.

magnetic field $+50\mu$T and in this state the $I_c(B)$ dependence was taken (black markers). Then it was heated above T_c and cooled in the field -50μT to get the curve from red markers. Such magnetic fields create approximately two flux quanta through the junction area. We do not know exact number of trapped vortices at that field. However there is no reason to assume more than one AV. This could happen only if there were two equivalent pinning centers, what is unlikely.

The calibration patterns for three junctions, presented in Fig. 4.4, look in one fashion but every junction is characterized by its unique set of levels. An interesting question is what determines the position of the pinning centers. This could be either geometry of electrodes (for example, corners) or impurities in the films, which could appear during the fabrication process and should be distributed randomly over the junction area. For this kind of samples the question is not answered because only one sample was measured. However in the next chapter the long junctions prove the second proposal, namely that the pinning centers are different even for one junction type.

After calibration Kibble-Zurek measurements were performed for each of the three junctions available on this chip. No magnetic field was applied during the measurements. The result was the following: no junctions trapped Abrikosov vortices even at fastest cooling rate reachable for this setup. 2200 cycles were run with heating pulse 3μs and no traps were detected, the critical current was always the same.

For conclusion of this section let us underline several points, which may look trivial but are important, because later they will allow us to distinguish between Abrikosov vortex trapping and fluxoid trapping.

According to Fig. 4.2, when one vortex is trapped the maximal critical

current becomes smaller and shifts to the left or right depending on the sign of the vortex. Another thing to be mentioned is that two minor lobes around the main one change their shape and height when comparing to the state with no vortex trapped. Also the side lobes lose their symmetry in regard to the direction of magnetic field. Thus the trapped Abrikosov vortex results in the qualitative changes of magnetic pattern and therefore it is never equivalent to an added homogenous field.

The results presented in this section have been mostly known from previous theoretical and experimental work. They are needed here as a step toward more complicated systems. The most significant observation which we will need in the next chapters is that an Abrikosov vortex trapped in the junction leads to a qualitative change of the $I_c(B)$ diffraction pattern.

4.2 Delta-biased junctions

Now we start investigation of the next kind of junctions, namely delta-biased junctions. The samples were designed by Roberto Monaco and produced in IREE RAS in Moscow.

The main aim of the project is to develop such a design of the JJs, which would be sensitive to plus/minus one trapped flux quantum in a superconducting ring. Along with trapping in the ring, the trapping of Abrikosov vortices in the films is always present and can not be avoided completely, because the nature of two effects is the same. A design studied in this section is unsensitive to flux quanta inside the ring. For this type of samples we do need to separate two effects. Therefore we will use them to study the trapping of Abrikosov vortices.

The properties of δ-biased junctions are described in several works, see for example [71], [72] and [**?**]. In [**?**] the equivalence between δ-biased junctions in radial magnetic field and long uniformly-biased junctions in parallel magnetic field is shown.

We first consider a short junction with normalized length of the order of $5\lambda_J$. The critical current density for this junction is $\sim 100\text{A/cm}^2$. Then in next chapters we will proceed with longer junctions, $30\lambda_J$. As it is known the short junctions behave in one manner independently on the electrode geometry. They show Fraunhofer-type pattern in magnetic field. The junction, described in this section, has a length 200μm, Josephson penetration depth $\lambda_J = 35\mu$m and a normalized length $L = 5.3\lambda_J$, which is an intermediate length between "short" and "long" cases. In Fig. 4.7, plot 1 one can see the I_c versus B dependence for this junction.

Here the data is presented only for the inner junction from Fig. 4.5. Outer junction was measured by Roberto Monaco and demonstrated qualitatively similar results.

Calibration is made for this sample in magnetic fields from -6.5μT to

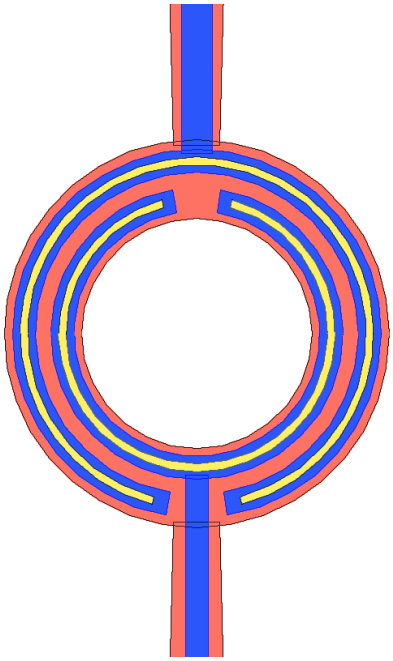

Figure 4.5: Layout of the sample with two delta-biased Josephson junction. One junction is placed closer to the outer border of the bottom ring-electrode and another - closer to the inside border.

$+6.5\mu$T, results are shown in Fig. 4.6.

Area of the junction is 400μm, four times larger in comparison with the previous junctions from Sec. 4.1. One can see that magnetic field at which one vortex is trapped is smaller now than for the overlap junction in Fig. 4.3. Increase of the junction area does not explain this difference. Therefore only geometry of electrodes can be responsible for much larger trapping in case of the δ-biased junction.

In Fig. 4.6 levels are enumerated from top to bottom, first for positive magnetic field and then for negative. They appear not exactly in this order, for example level 9 starts earlier than level 8. But we will steak to this numeration because it makes the reading of the plot easier.

Let us consider the level number 2. It appears when the junction is cooled in the magnetic field 0.5μT. At this level the critical current decreases from 0.32 mA to 0.29 mA. In the cold state if the external magnetic field increases by 0.5μT the critical current changes only by ≈ 1 percent. But inhomogeneities in the distribution of the Josephson phase introduced by trapped Abrikosov vortex lead to much more significant change of the critical current [73], [39].

New levels in the calibration plots do not appear suddenly, there is a smooth transition between them. This effect is also seen in Fig. 4.3 of the

last section but it is more pronounced in Fig. 4.6. For a given magnetic field we can see two or even more levels. Sometimes it means that different number of vortices are trapped. But sometimes number of vortices can be the same but they are trapped in different places.

As one can see the trapping event is a random process at the end of which junction can be found in one of possible states. Different states are realized with different probability, some of them are more frequent than others.

Thus the number of trapped vortices is not determined with one hundred percent of probability by external magnetic field but changes from one attempt to another. It proves that the effect we deal with has a statistical nature.

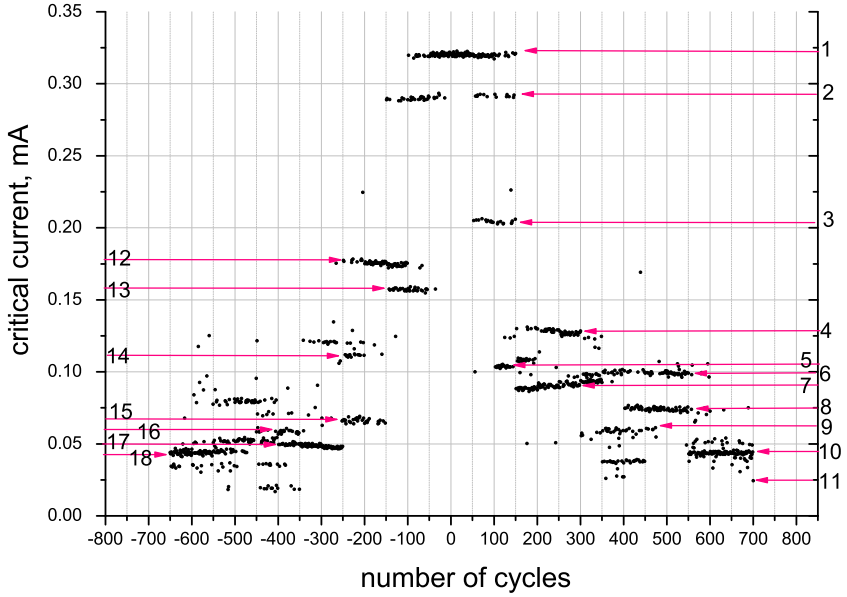

Figure 4.6: Positive I_c of the delta-biased short Josephson junction during the calibration. After every 50 cycles magnetic field was changed by 0.5μT in positive direction and by -0.5μT in negative direction. The levels are enumerated from top to bottom starting from the left side.

In next Fig. 4.7, which covers two pages, the dependence of the critical current on the perpendicular magnetic field is shown for several levels from Fig. 4.6.

Once vortex is trapped it stays there until the sample will be heated above the critical temperature. The stability of every state presented in Fig. 4.7 and earlier in Fig. 4.2 is proved by that that each curve was taken two times and results overlapped completely.

Not all levels from Fig. 4.6 are presented by magnetic patterns in Fig. 4.7. But those which are presented already can be classified and analyzed. Below some common trends are listed.

- With increase of magnetic field, applied during cooling, main maximum splits into two.
- Maximal critical current becomes smaller.
- The number of minor lobes between two maxima increases with number of trapped vortices.

From magnetic patterns both in parallel and perpendicular filed is it possible to figure out the positions and types (monopole, dipole or misaligned vortex) of trapped vortices [69]. It is not done here because it is not the aim of this thesis.

Kibble-Zurek measurements (probability of trapping versus the quench time) were also performed for this junction, see results in Fig.4.8 and Fig.4.9. The way the Kibble-Zurek measurements are carried out is described in the next chapter in details. Therefore here only results are shown.

Despite that the junction is also short in dimensionless units as the previous ones, it is larger in area. Also probability to trap Abrikosov vortex is higher because of shape of the electrodes.

In Fig.4.8 the critical current of the junction for a fixed τ_Q is shown. The thermal cycle was repeated more that 400 times. Trapping was minimized by adjusting a residual magnetic field with the perpendicular coil. Once in a while both positive and negative critical currents change, i.e. the junction traps AVs. One can see that for Kibble-Zurek measurements vortices are trapped in the same places as during the field cooling calibration. Each distinct point can be associated with a certain level on the right plot (shown by arrows).

However this junction turns out not to be a good detector for two reasons. First, it can not distinguish between vortex and artivortex. And second, the probability of trappings for this junction does not decrease with τ_Q. The probability of trapping for this junction versus the pulse width (which is proportional to the quench rate τ_Q, see Sec.2.2) is presented in Fig.4.9. The dependence on τ_Q is not clear.

Hence we investigated trapping of Abrikosov vortices in the short junctions for different bais and geometry of electrodes. Qualitatively results are similar for different geometries. Critical current decreases in a stepwise manner by increase of number of trapped AVs. By the example of the δ-biased Josephson junction it was shown that Abrikosov vortices trapped by the junction in perpendicular magnetic field manifest their presence by distirtion of magnetic pattern in various different ways.

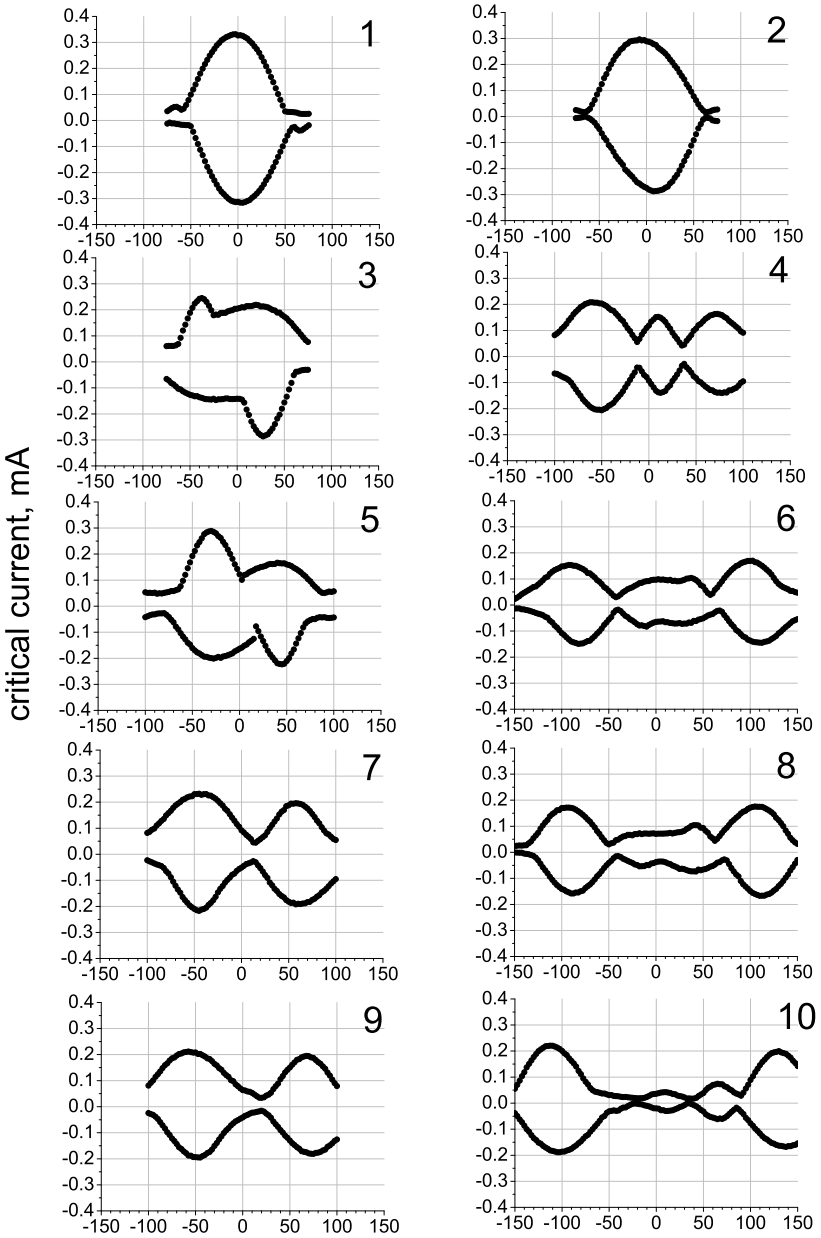
1
2
3
4
5
6
7
8
9
10
critical current, mA
magnetic field, μT

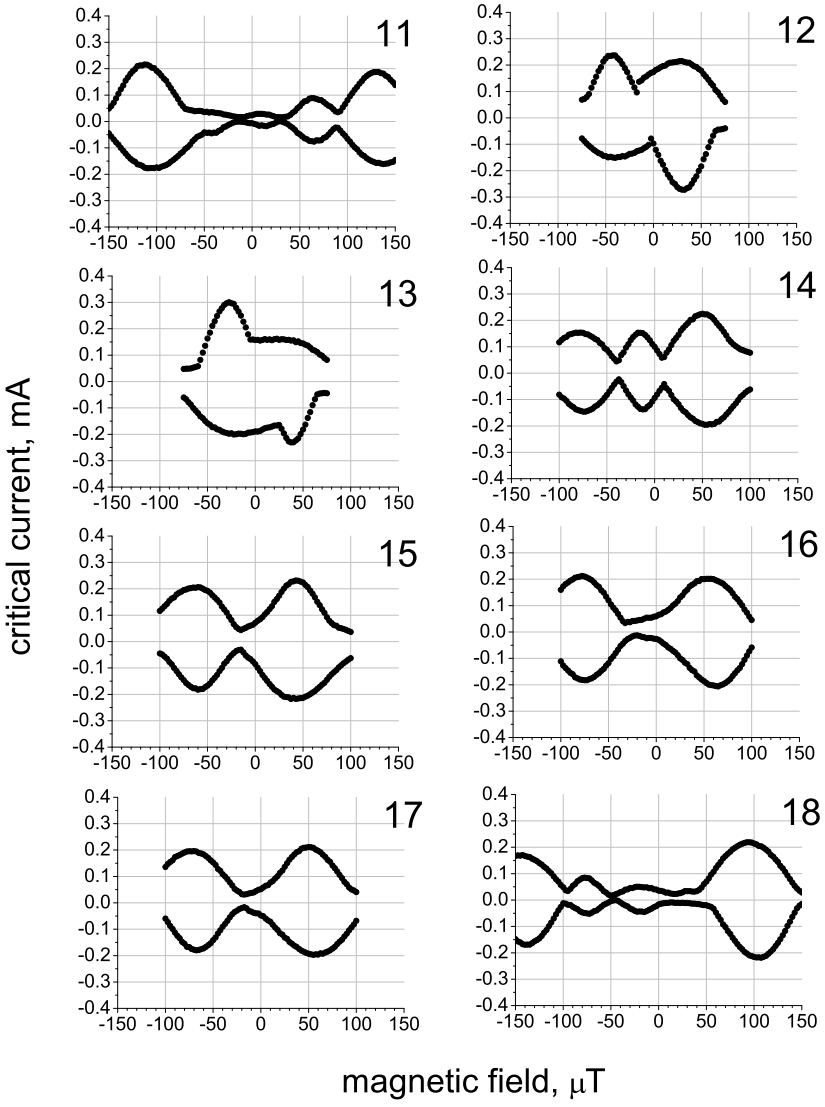

Figure 4.7: I_c in perpendicular magnetic field of the delta-biased Josephson junction. First page - first 10 levels. Second page - levels from 11 to 18.

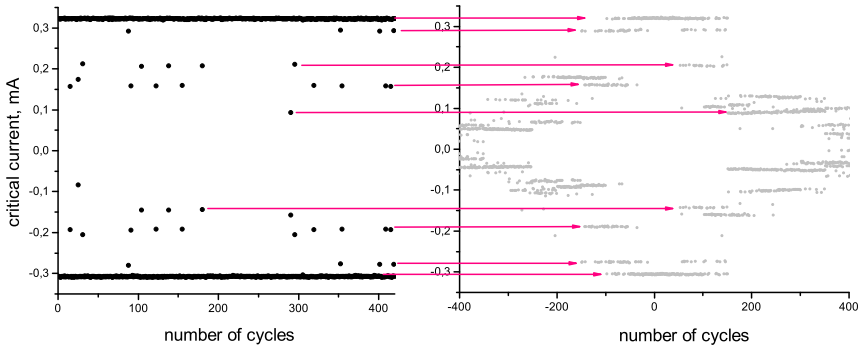

Figure 4.8: Left: Critical current of the junction. Pulse width $1ms$, pulse amplitude 10 V. Right: Calibration plot (the same as Fig. 4.6). Arrows identify values of the critical current with levels observed during the field cooling.

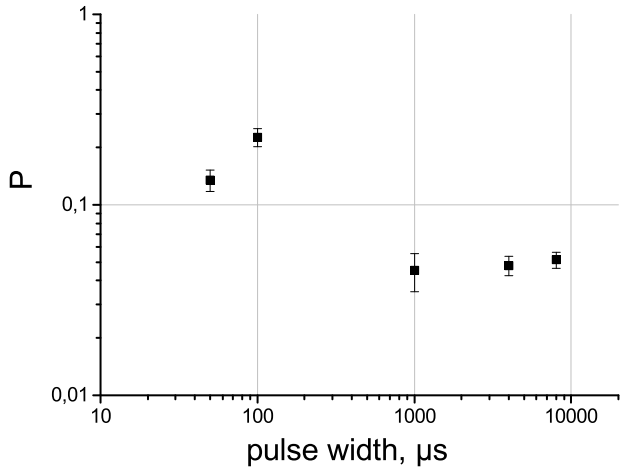

Figure 4.9: Probability of trapping of AVs versus pulse width for delta-biased short JJ.

Chapter 5

Long delta-biased Josephson junctions

We continue the investigation of the delta-biased Josephson junctions started in the previous chapter. But in this chapter we consider long junctions. The layout and geometry for several junctions are identical to the junctions described in Section 4.2. The long normalized length L of the junctions is due to the larger critical current density, $\sim 3\text{kA/cm}^2$.

Since the junctions are long, all three types of interaction with magnetic field are possible (described in chapter "Theory"):

- Abrikosov vortices. Can be trapped everywhere and may affect the critical current and the magnetic difraction patterns of the junctions.

- Flux quanta trapping in the ring. It is expected that the ring, which forms the base electrode traps magnetic flux quanta. The shielding current circulating near the inner edge of the ring will affect the inner junction. Below we will show that this design is nearly insensitive to the shielding currents.

- Josephson fluxon. Also can be trapped during the cooling. But due to the open ended top-electrode leaves the junction when a bias current is applied.

Consequently only AVs can be observed with this kind of junction detectors. Hence the aim of this chapter is to study the AV trapping as a function of the quench time τ_Q.

Our expectations are the following. The junctions are two-dimensional objects from the point of view of the AV. Therefore the scaling exponent of the linear part is expected to be 0.5 rather than 0.25. After the linear region we expect to see the exponential decay [29].

5.1 Experiment. Results

In this chapter five samples are analyzed. Their characteristics are listed in Table 5.1, such as ring size, junctions length and quality of the junctions. The criterion of quality is given in 2.1.1. Last column "Notes" summarizes the results of this chapter, discussed in details at the end of the chapter.

Table 5.1: List of measured samples

sample number	inner/ outer radii of sc ring, μm	normalized length of inner JJ, λ_J	quality	notes
1	30, 50	28	good	The lowest trapping rate
2	20, 60	19	average	Repeats sample 1 but with a tail
3	30, 50	28	bad	Traps much more than 1, but with exponential decay for larger τ_Q
4	30, 50	28	bad	Strong dependence on magnetic field
5	10, 30	12	good	The smallest sample with only one pinning center

The layout of the samples is presented in the previous chapter in Fig. 4.5. Two Josephson junctions are placed on the top of the superconducting ring. Depending on the position on the ring they are called the inner junction and the outer junction, respectively.

The experiment was made using the first cryoprobe (see Chap.2). One external coil was used to generate a magnetic field perpendicular to the junction plane. The coil factor is 5μT/mA. The two electrical heaters on the chip were connected so that the current through them created a magnetic field in opposite directions to minimize its influence on the ring.

In this chapter it is more convenient to use the pulse width instead of τ_Q values. The relation between them is given in the Chapter 2 in Fig.2.7. The amplitude of the heat pulse was kept to 10 V all the time, so the cooling rate was regulated only by changing the pulse width.

The typical magnetic patterns of the delta-biased JJs in perpendicular magnetic field are shown in Fig.5.1 for both inner and outer junctions. The main feature of the dependence is that the both junctions are nearly insensitive to the magnetic field over a broad range of it.

Also in Fig.5.1 the localization of the AV is illustrated. The junctions

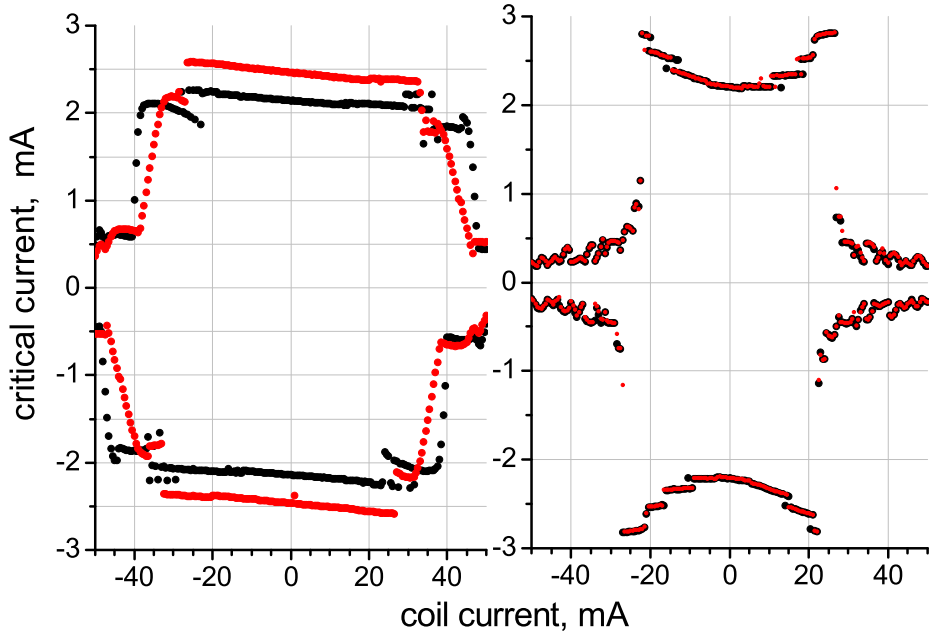

Figure 5.1: The magnetic diffraction pattern for the delta-biased junctions (sample 1). Left: inner junction. Right: outer junction. Black - without trapped AVs. Red - with trapped AVs. $T = 4.2K$

were heated and cooled several times in order to obtain the distribution of the critical current. During some of the cycles one or several AVs were trapped in the inner junction. The critical current then increased by $\approx 15\%$. The magnetic diffraction pattern taken in this state, is shown by red dots in the figure. Then without heating the sample the magnetic diffraction pattern was recorded also for the outer junction. For the outer junction no difference with the previous case was found. To check that the trapped magnetic field did not escape during measurements the diffraction pattern of the inner junction was taken one more time and it overlapped with the red curve. Thus the magnetic field from AVs is localized and leads to drastic change in the critical current if it is close to the inner junction area. If it is not close to the junction area its influence is negligible.

In Fig. 5.2 the field cooling measurements are presented for the inner junction of sample 1. As was mentioned in Chap.4 each junction has a distinct set of levels. The main difference from the short junctions is that in the long junctions trapped AVs increase the critical current. It was demonstrated already in Fig.5.1. But still as in the case of the short junctions the critical current changes in a step-like manner. The field cooling experiments were made with large τ_Q, i.e. a pulse width 10 ms.

A slight asymmetry of the investigated junction in regard of positive and

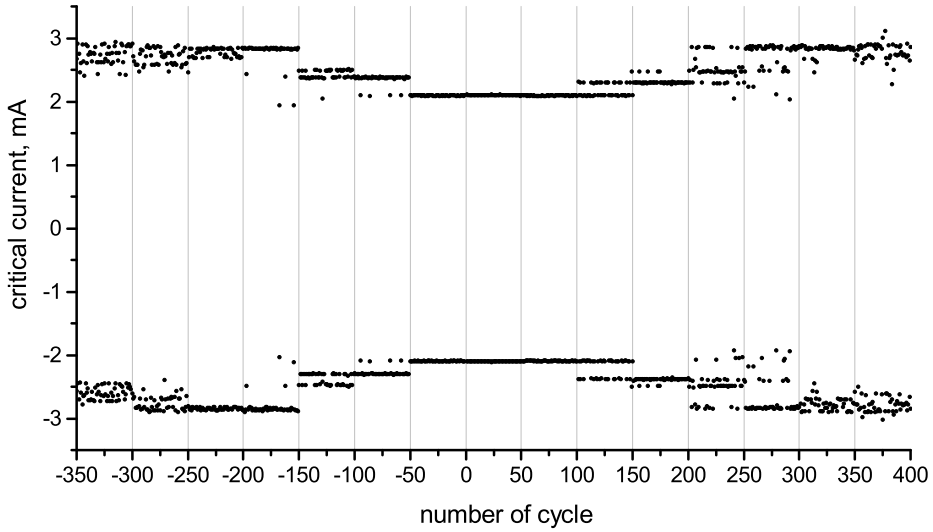

Figure 5.2: Calibration for inner junction of sample 1. Current I_{coil} (the magnetic field) changes from -1400μA to $+1400\mu$A with step 200μA for every 50 cycles. Pulse width = 10 ms

negative magnetic field helps to separate vortices with different polarity. This was also possible for samples 1, 3 and 5, but not for samples 2 and 4, since their magnetic patterns were completely symmetrical. Due to inevitable spread in parameters during fabrication each junction appears to have slightly different parameters, such as the critical current, the gap current, the magnetic diffraction pattern and others.

For slow transitions with zero I_{coil} the inner junction of sample 1 does not trap AVs and its critical current is always the same. This picture changes for faster cooling rates. The coil is disconnected during these measurements. The results are presented in Fig. 5.3 for two transition rates. The top plot is taken for rather large τ_Q (pulse width is 500μm) but, however, faster than during the calibration. The junction was heated and cooled 3300 times, and after every cycle the critical current was measured. Only 8 times the critical current was found to be different from the value 2.1 mA. The bottom plot is for a shorter τ_Q (pulse width is 20μm). Except for a few points all values lay on the well defined levels. Under the term "level" we understand the systematically repeated value of the critical current. This may be interpreted as that every time AVs are trapped in the same place. In both plots most of points are above the zero-field critical current.

Each level may be associated with a certain pinning center (PC). The fact that the plot which we get in the field cooling experiment (for example in Fig. 5.2) is perfectly symmetric with respect to rotation by 180° corrobates

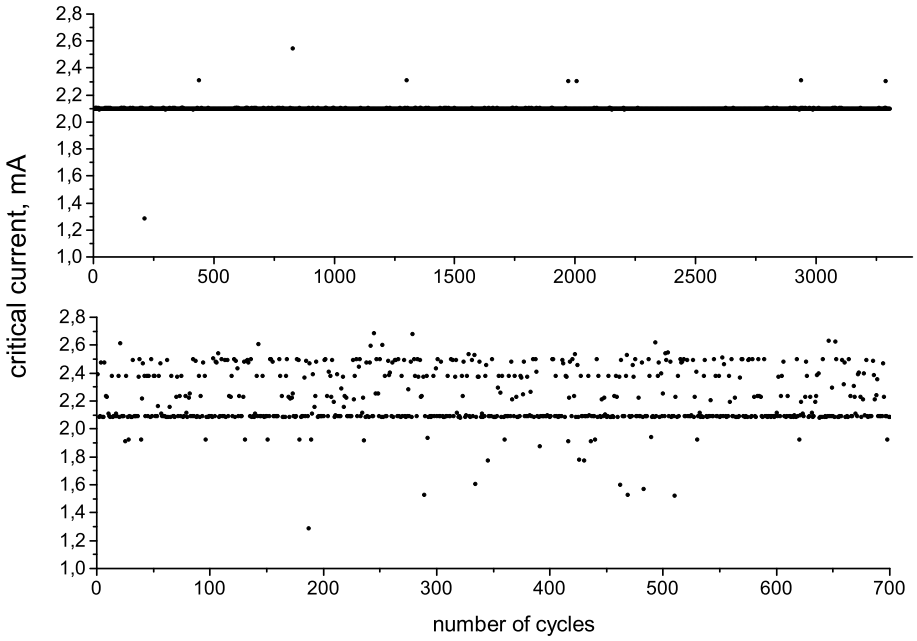

Figure 5.3: I_c of junction 1 in Kibble-Zurek experiment, zero feild. Measurement temperature 4.2 K. Top: Pulse width 500μs. 3300 cycles. Bottom: Pulse width 20μs. 700 cycles.

the assumption that the same pinning centers participate in trapping both in positive and negative magnetic field.

It is also worth to mention that the places where vortices are trapped are the same in the following situations: when trapping is imposed by an external field or when the transition is too fast to allow the vortices to annihilate or escape before they freeze in.

As one can see from Fig. 5.3 there is a clear dependence of the trapping rate on the transition time. In the next sections of this chapter this dependence will be investigated in details.

5.1.1 Probability of trapping versus quality of a junction

Here we discuss trapping probability of AVs. In this section we compare results for two junctions, which have the same critical current density, geometry and size but different quality of the tunnel barrier. Their IV-curves are in Fig. 5.4, on the top plot.

Let us define the probability of trapping in the case of AVs. For a given number of cycles N we count the cycles (N_{trap}) for which the critical current is different from the zero-field value found without trapped vortices. The ratio $P = N_{trap}/N$ is called the probability of trapping and it is this quantity

which is plotted in all figures in this chapter.

The measurement procedure is the following. Since we apparently have a small residual dc magnetic field we need to find its magnitude and compensate for it. Otherwise the probability of trapping P will be determined by the residual field and can happen to have any value from 0 to 0.5 at a fixed τ_Q depending on the magnitude of the field. For samples with asymmetrical levels one can conclude that the residual field is compensated correctly when numbers of positive and negative trapped vortices are equal. In this situation the main level (nothing trapped) is populated with the highest rate. The levels for plus and minus single vortex are equally populated with probabilities P_{+1} and P_{-1}. Above all the sum of probabilities $P_{+1} + P_{-1}$ is the smallest when magnetic field is compensated. The last fact gives a possibility to find residual magnetic field even for symmetrical samples for which it is impossible to discriminate between vortices and antivortices. While the residual magnetic field is found it is compensated by the external coil, which then remains connected during measurements at all times.

The probability of trapping measured by the inner junction of sample 1 is presented in Fig. 5.4. With decreasing pulse width the picture which we observed on the upper plot of Fig. 5.3 changes gradually to the bottom plot. There is more behind the term "gradually". Two regimes are to be specified when we go from large τ_Q towards smaller values. When trapping just starts (long transitions) we see only one level in addition to the main one for the symmetrical junctions and two additional levels for the asymmetrical junctions. For faster transitions these two levels become more and more populated. Let us define this behavior as the "first regime". Now τ_Q gets even smaller and we observe that along with populating the already existed levels new levels come into play. At this point the "second regime" begins. For junction 1 this happens after $\tau_Q = 10ms$ or pulse width 400μs.

Defined as described above the quantity P has different meaning for different τ_Q. For slow transitions, when no more than one vortex can be trapped at once, we indeed count the events of trapping of a single vortex or antivortex. And in this case P means exactly the probability of trapping of one Abrikosov vortex/antivirtex. For smaller τ_Q we have more levels and not for all of them the exact number of trapped vortices can be determined. Usually we can only establish the event of trapping. Therefore P now includes probabilities of trapping one, two, three or probably more vortices.

By comparing the IV-curves of the junctions and their trapping rates in Fig. 5.4 the obvious conclusion can be drawn. The lower the quality of the junction the more Abrikosov vortices it traps.

5.1.2 Probability of trapping versus size of the system

It is important to check the effect of the sample size on the trapping rate. Such measurements will give a clue about places where vortices are trapped.

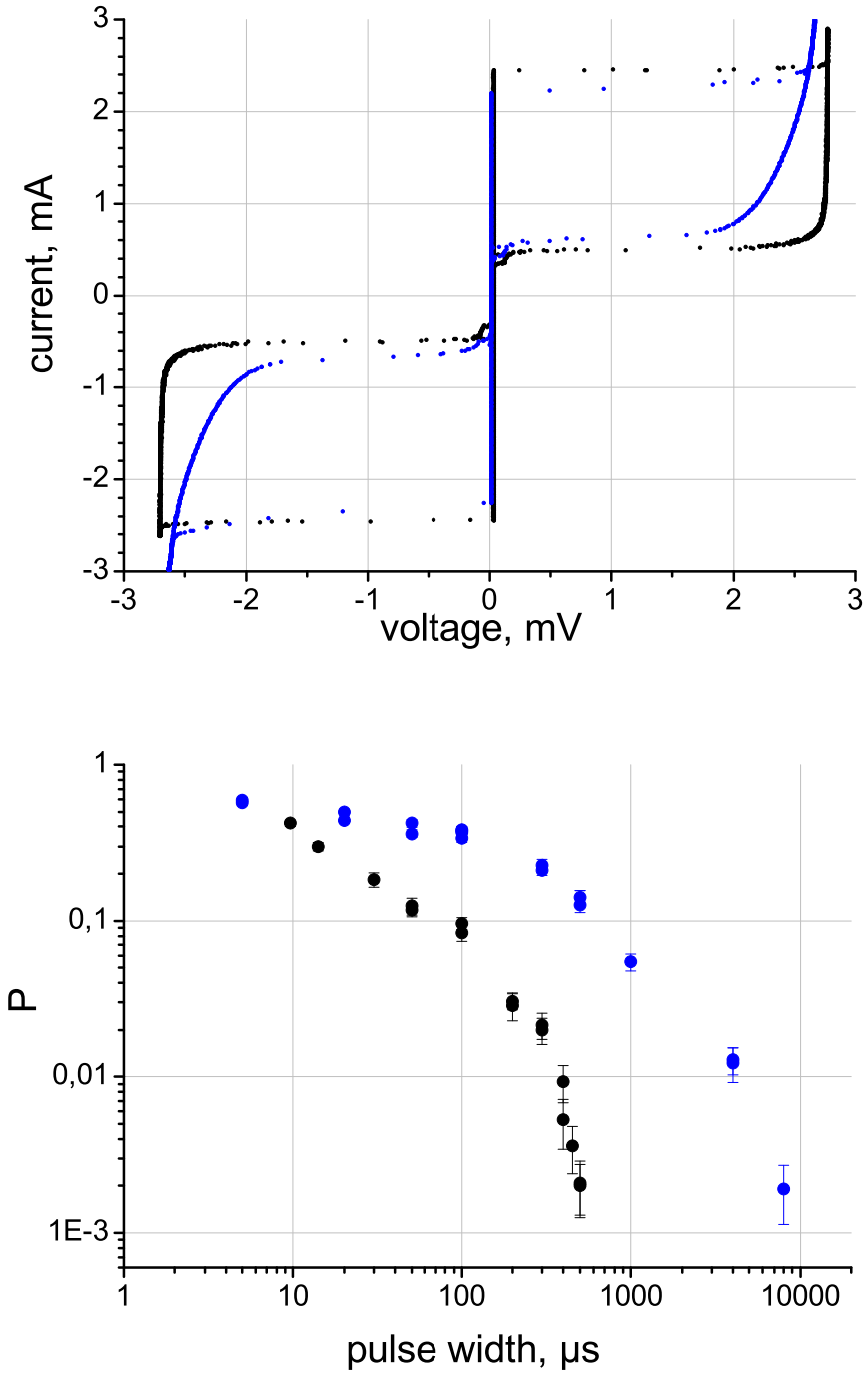

Figure 5.4: Comparison of two samples of different quality from Tab. 5.1. For both plots: black - sample 1, blue - sample 3. Top: IV-curves. T = 4.2K. Bottom: Probability of trapping of Abrikosov vortices by inner junction versus transition time τ_Q. Residual magnetic field is compensated.

Below we examine the hypothesis that the pinning centers are randomly distributed over the junction electrodes with an average distance which depends on film properties. Thus the smaller the area of the electrodes the fewer pinning centers are expected.

In this section we compare the trapping probability for the inner junctions of samples 1 and 5 from table 5.1. The areas of the junctions are $400\mu\text{m}^2$ and $164\mu\text{m}^2$, respectively. Therefore if our assumption about randomly distributed pinning centers is valid the ratio of trapping probabilities for these samples will be of the order of 3. Significant deviation from this expectation indicates that the pinning centers are determined by the other factors, for example, are due to the geometry of the samples.

The results of measurements are presented in Fig. 5.5. Again the IV-curves of the studied samples are compared on top plot and probabilities of trapping on bottom plot. There is a large difference in trapping rates for two samples. The smaller sample traps significantly less. Precisely the ration of trapping probabilities for those two junctions is about 30. Hence the number of pinning centers does not scale with the area of a junction. This value can not be explained in the framework of the above assumption.

5.1.3 Other samples

Three junctions considered so far have a unified characteristic: for large τ_Q the probability of trapping decays faster than a power-law. Among measured samples we have two more samples those behavior is different. They will be considered in this section.

One of them (number 4 from Table 5.1) has size and geometry as two already described samples 1 and 3. Another junction (number 2) is placed on a broader ring and therefore shorter than number 4.

Trapping probabilities of all samples are plotted in Fig. 5.6 versus the pulse width.

Sample number 2 fits very well sample 1 in a certain range of the pulses despite of different geometrical parameters. Disagreement starts from 400μs: sample 1 decays very fast but sample 2 gets saturated.

Sample 4 is a difficult one. It was published in [74] with different interpretation, before it was realized that what we saw was AVs trapping rather than fluxoid trapping. The aim of measurements here is to repeat the published result and to get more precise values of probability. in Fig. 5.6 this sample is presented by green color. The published result was repeated. However one can notice two deviant green points fallen out of the common trend. This is an illustration of importance of residual magnetic field. All points except two lowest were obtained with disconnected coil. Then the residual magnetic field was found according to the recipe given above. And with compensated field we got two points significantly lower. It means that the previous result is misleading since it is dictated by external parameters

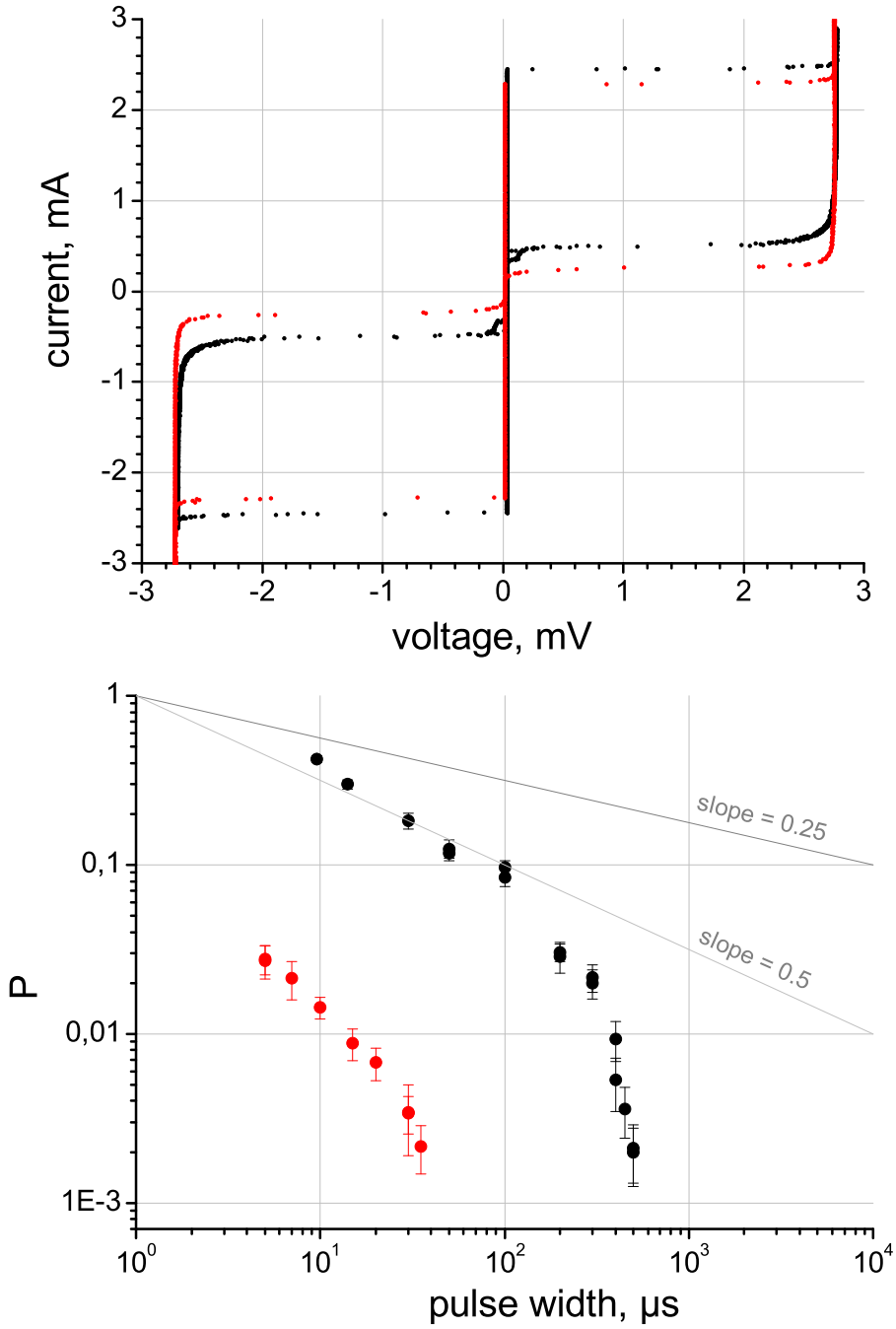

Figure 5.5: Comparison of two samples of different size from Tab. 5.1. For both plots: black - sample 1, red - sample 5. Top: IV-curves. T=4.2K. Bottom: Probability of trapping of Abrikosov vortices by inner junctions versus pulse width. Residual magnetic field is compensated.

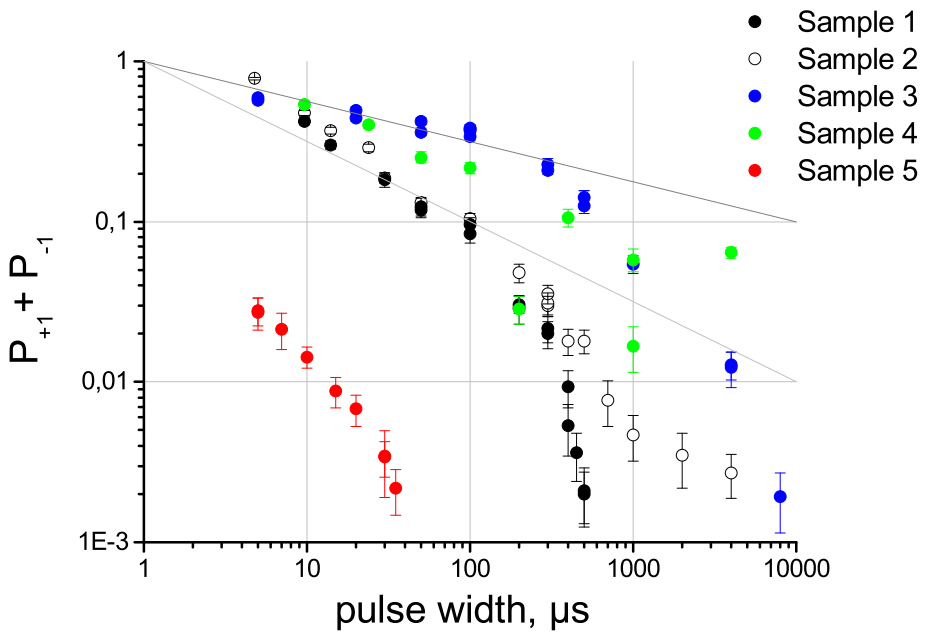

Figure 5.6: Probability of trapping of Abrikosov vortices versus pulse width. Electrical heating. T=4.2K. $H = H_{comp}$.

and does not characterize the sample itself. After this finding the sample 4 was not measured anymore.

5.2 Discussion

The probabilities of trapping are different for different samples. On the one hand this result is not surprising. The lower quality of the junction the more pinning centers are there, inside or near JJ, and the probability to trap the AV increases. But is this assumption enough to explain all results? Or can one get a more detailed picture?

Let us try to compose a general picture which can explain the variety of presented measurements. The analysis of the measurements can be done on basis of two postulates. First, the number of pinning centers is different for each sample. Second, the pinning centers are not equivalent. They can be classified, for example, by their strength and temperature dependence.

Some of the PCs begin to trap at higher temperatures, some of them at lower. The higher the temperature of trapping the weaker the pinning center.

The PC traps when two conditions are fulfilled. First, its strength is more than energy of thermal activation at a freeze-in temperature. Second, at this

temperature there are AVs available around, which have not annihilated or escaped yet.

It is impossible to trace what happens when many pinning centers are active (regime 2), but for rather slow transitions when only two or one center remains (regime 1) we can take a closer look at each sample.

Sample 1 has one dominant pinning center which is "stronger" than the others. This center is activated first. It is responsible for the very fast decay of the trapping probability.

Sample 2 also has one dominant PC which is more active than the others. But the type of this center is not similar to the one in sample 1. It is a long-lived pinning center which continues trapping also for so slow transitions when other centers do not trap anymore. And probability to trap by this center does not depend on the cooling rate.

Sample 3 has two dominant pinning centers with nearly equal parameters. This conclusion follows from the observation that instead of two additional levels there are four for this junction: two for positive vortices and two for negative. The same four levels appear during field cooling and again simultaneously, at one magnetic field. They trap both with equal probability even at the largest pulse width 8000μs.

Sample 4 has two competitive pinning centers. But since this junction was not measured properly it is not known how these centers behave at larger transition times.

Sample 5 is a unique. It traps in a much narrower range of pulses. But the interesting thing about this sample is that in the whole range from 5μs till 35μs only one pinning center is active. Therefore this sample allows us to monitor the probability of trapping of an AV by a certain pinning center. If we compare this sample with sample 1, we see that for sample 1 the pinning center "turns on" faster. This difference might originate from a different temperature dependence. However this question needs further theoretical and empirical investigation.

A more adequate way of measuring would be to measure the number of trapped vortices and then to plot the average number of them per cycle. This is however not possible with our present technique. If we had the possibility to measure the exact number of trapped Abrikosov vortices we would find larger values for probabilities. For correct comparison with theoretical results we need the second quantity.

The fact that we don't count all vortices was mentioned several times in this chapter. But let us summarize three reasons for this.

First. Only vortices inside or close to the junction area can be detected. Those which are far away are not visible for the junction.

Second. We can not say from our data how many vortices are trapped. With our setup we can only detect that something was trapped. But positions and number remain unclear.

Third. Some of vortices can be inside the junction but still do not

manifest their presence. This situation is described in [75]. According to the theoretical analysis it happens when the vortex, more precisely a monopole, does not interact with the Josephson phase if it is in the middle of the junction. The closer to the boundaries the stronger the interaction energy is.

Let us discuss the effect of the junction shape, since it is nontrivial for our samples. What is the role of the junction shape in the presented results? From comparison with the square and circular junctions in Chap.4 we conclude that the shape is important. A complicated geometry of the junctions, for example, sharp corners, favors the formation of pinning centers.

But we can guess that for study of the trapping probability versus the quench time the shape is not important. In the next chapter we will use similar junctions, also following the ring shape. In comparison with the design in this chapter the next design differs mainly by the position of the current leads and the smaller sector of the ring covered by the junction. It is easy when only one parameter of the system is changed, in this way we know what already appeared and what is new. Therefore it is reasonable to study similar junctions in this chapter to understand better the next samples.

5.3 Conclusion

It was demonstrated that the probability of AV trapping depends on the quench rate of the phase transition. The slower the transition the less vortices are trapped. However from the presented results it is difficult to specify an exact law according to which the probability scales with τ_Q. Undoubtedly there is a strong correlation between the quality of a sample and its trapping rate. None of five tested samples showed overlapping results. The only overlap is between sample 1 and sample 2 but not in the entire range of τ_Q. Also sample 5 was not expected to overlap with other samples because of its different size. However samples 1, 3 and 4 have identical physical parameters, such as geometry, size and the critical current density. Moreover samples 1 and 4 were produced on the same substrate in one technological run. Each of those three has a unique result not overlapping with others.

For most of the samples it is possible to avoid trapping of AVs if time of transition is larger a certain value, as a value common for all samples, we recommend $\tau_Q = 0.1s$. However one sample has a particular pinning center which traps with probability independent on τ_Q.

Chapter 6

Long inline Josephson junctions

In this chapter we consider Josephson junctions sensitive to one flux quantum trapped in the ring. The sensitivity was improved in comparison with the samples from Chap.5 due to the inline geometry of the junctions (Sec.1.4).

This design is a modification of the design described in the previous chapter. But in this chapter we have to account for two effects: Abrikosov vortices trapping and fluxoid trapping.

The aims of this chapter are

1. to separate trapping of fluxoids in the ring from trapping of AVs in the body of the ring or in the JJs,
2. to find the dependence of the probability of fluxoid trapping on the transition rate,
3. to check whether the junctions on the ring influence the probability of the trapping of flux quanta in the ring.

In contrast to Chap.5 the green laser is used as a heater for all measurements presented below.

6.1 Samples

The samples are shown in Fig. 6.1. There are two rings on each chip. The rings differ by the width: 10 and 6 μm for upper and lower rings respectively. The inner and the outer radii for the upper ring are 50 and 60 μm and for the lower ring 50 and 56 μm. Both rings carry two inline Josephson junctions. The length of all junctions is 100μm and the width is 2μm. λ_J is about 7μm, i.e. junctions are long $L = 14\lambda_J$ and narrow $w \ll \lambda_J$. Junctions are called A, B, C and D.

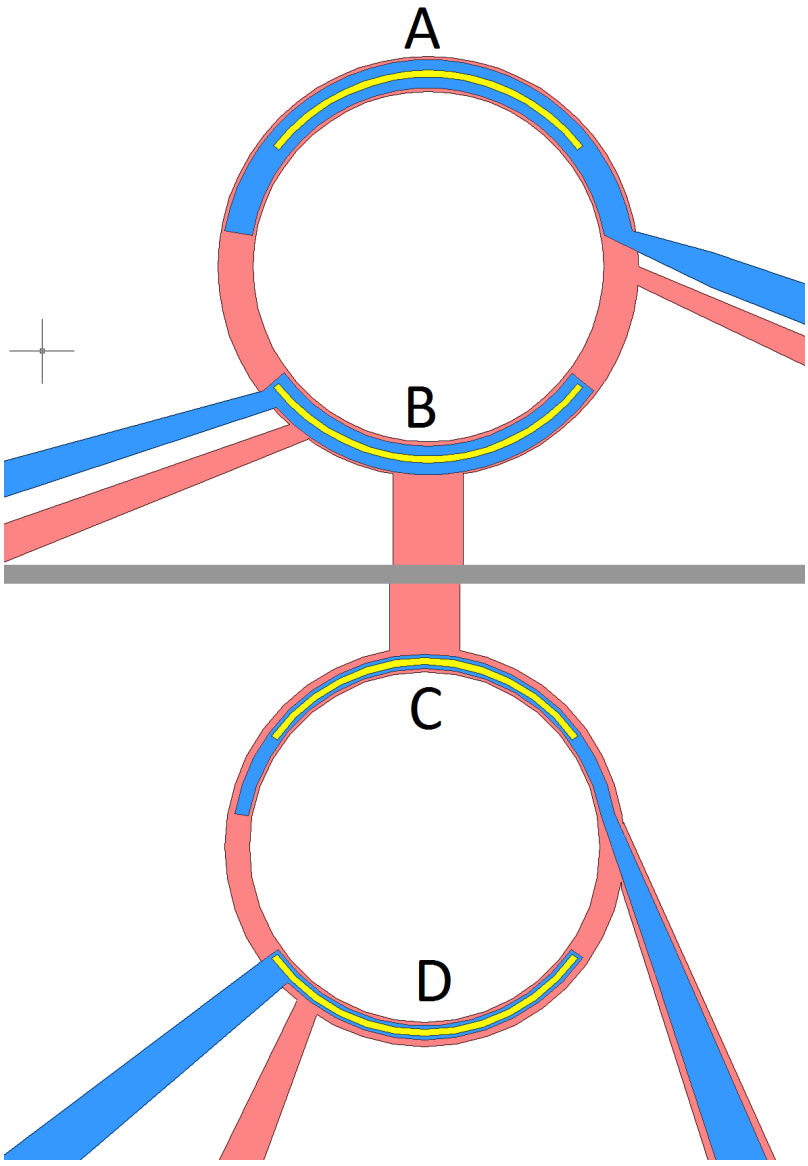

Figure 6.1: Layout of the sample with inline Josephson junctions. Red - first superconducting layer, forms the ring and is used also as bottom electrode for all four inline Josephson junctions, called A, B, C and D. Blue - second superconducting layer, used as top electrode for the junctions. Yellow - region between two superconducting layers where Josephson relation is valid.

Four samples were tested in this chapter. On each sample only one junction was measured: three times junctions A (called in this chapter junctions $1i$, $2i$, $3i$) and once junction D (called $4i$). The IV-curves of the junctions and their magnetic diffraction patters are shown in Fig 6.2. The magnetic diffraction patterns are taken in perpendicular magnetic field. The coil factor is 5μT/mA.

All junctions have reasonably good quality ($R_j/R_n \approx 20$), $3i$ is the worst of them ($R_j/R_n = 10$) but is still suitable for our purpose. Two junctions $1i$ and $2i$ demonstrate a magnetic diffraction pattern similar to theoretical in Fig. 1.7. However junctions $3i$ and $4i$ have a peculiarity: the main lobe is split into two near the maximum. The origin of this split is analyzed in the next section by means of numerical simulations.

6.1.1 Barrier inhomogeneity. Numerical simulations.

The hypothesis which we are going to check in the current section is the following: the change of the shape of the I_c versus B curve, observed for junctions $3i$ and $4i$, is a consequence of barrier inhomogeneities. The effect may be caused by other reasons. We will show that the same effect can be obtained in the framework of the conventional sin-Gordon equation with included inhomogeneities.

An inhomogeneity in the tunnel barrier can change locally the Josephson current density j_c. Therefore in order to model it we will use the coordinate dependent current density $j_c = j_c(x)$, where $j_c(x) = 1$ outside the inhomogeneity and $j_c(x) = 1 - k$ inside the inhomogeneity. In our case $k > 0$, i.e. the Josephson current is suppressed. This method has been used in several works, see for example [75] and [76].

In the resistive model the evolution of the Josephson phase ϕ is described by the sine-Gordon equation:

$$\frac{\partial^2\phi}{\partial x^2} - \frac{\partial^2\phi}{\partial t^2} - \alpha\phi_t = j_c(x)\sin(\phi). \tag{6.1}$$

where $\alpha = \omega_p/\omega_c$ is the Ohmic loss parameter, ω_c is the characteristic frequency, ω_p is the plasma frequency. Time and space are normalized by ω_p and λ_J, respectively. All currents are normalized by the critical current I_c More details about the numerical simulations can be found elsewhere [77].

In the asymmetric inline junctions a bias current I_b enters the equation through the boundary conditions along with magnetic field I_H:

$$\frac{\partial\phi}{\partial x}\,|_{x=0} = I_H + I_b, \quad \frac{\partial\phi}{\partial x}|_{x=L} = I_H, \tag{6.2}$$

Notation in Eq.6.2 repeats the notation in the book [36]. I_H is a current proportional a magnetic field parallel to the junction plane.

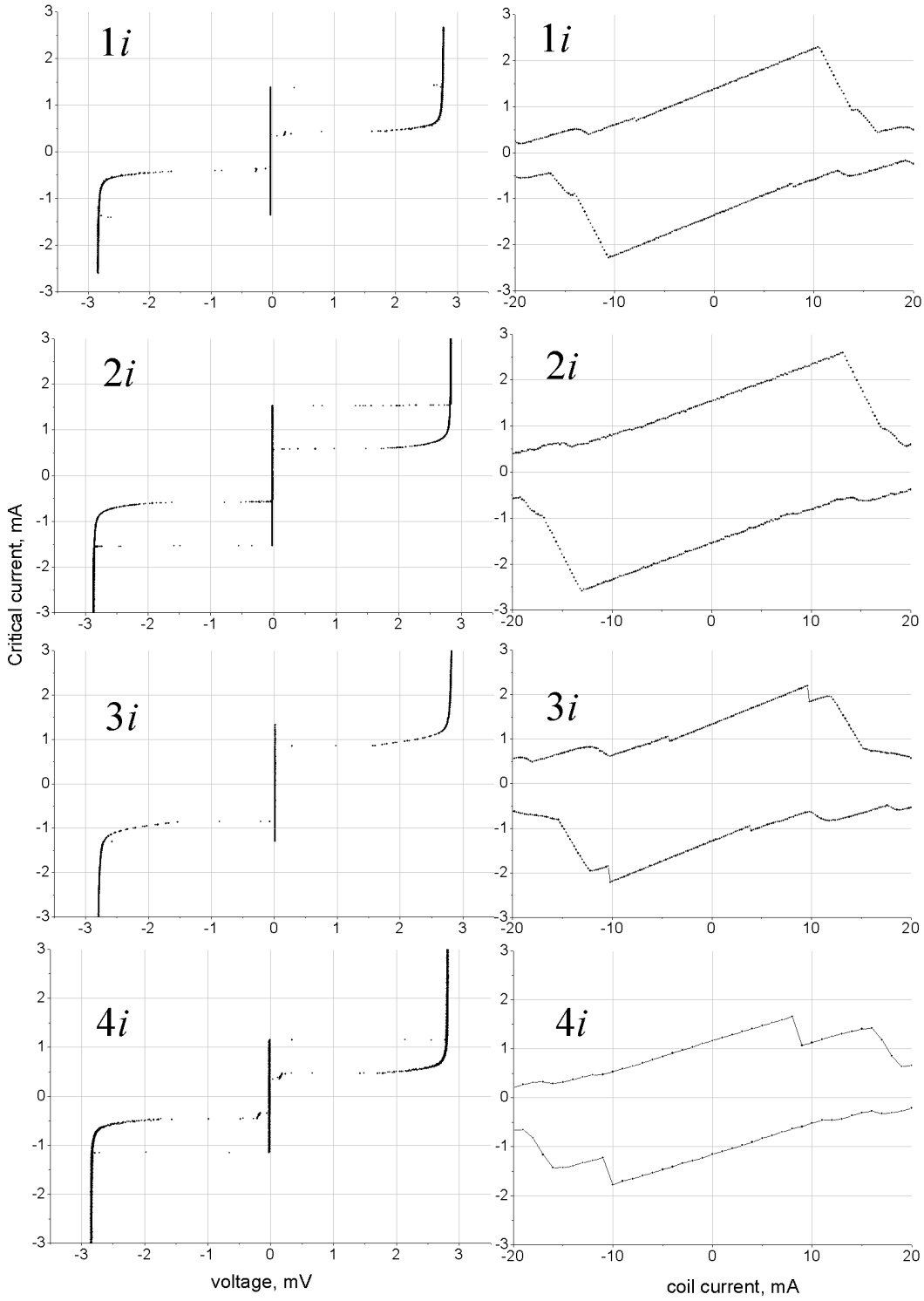

Figure 6.2: Characteristics of measured inline JJs. Left: IV-curves. Right: magnetic diffraction patterns in perpendicular magnetic field. Details can be found in the text. T=4.2K.

The simulations are dynamical. At the initial moment $\phi(x) = 0$. The bias current I_b is increased by a small step (0.02) until the phase starts moving. The current when it happens is defined as the critical current. After every increasing of I_b there is a waiting time to let the phase reach the stable distribution under the new conditions. In such a way simulations repeats the experimental situation, when the bias current applied to the junction is ramped.

We started the simulation from a test of the model, the theoretical plot 1.7 was repeated in case of homogenous barrier $j_c(x) = 1$. Now let us insert one test inhomogeneity $j_c(x) = 0.2$ close to the end of the JJ where the bias current is injected. The coordinates of the inhimigeneity are $1 < x < 2$, i.e. it is of the size of λ_J. The total length of the junction is set to 15 in dimensionless units.

The results of the simulations are shown in Fig.6.3. The top plot is the magnetic diffraction pattern of the inline junction with the inhomogeneity described above. One sees that the main lobe has double solution. The color arrows point out two possible solutions: red arrow is for the first solution and blue arrow is for the second one. Close to the maximum the second solution (with lower critical current) is realized more frequently than the first solution, in experiment this can be seen as a split top. Visa verse in the direction of positive magnetic field the second solution almost completely disappears.

The bottom plot in Fig.6.3 represents the profiles of the Josephson phase for both solutions. Again red color corresponds to the first solution and blue to the second one. The region with suppressed critical current is marked by gray. One can see that the inhomogeneity gives an ambiguity for ϕ: it goes above or below the homogeneous solution, shown by the gray dashed line. Thus the inhomogeneity pushes the phase out of the region with suppressed Josephson current. The magnetic field for all three curves on the bottom plot was 14 in dimensionless units. If we chose other values from say -25 to 10 we find phase distributions qualitatively similar to the one shown in Fig.6.3.

The size and position of the inhomogeneity can be fitted more precisely to the experimental plots. But this procedure is time consuming and was not the main goal of the investigation. The main goal was to demonstrate that an inhomogeneity in the barrier can introduce the "double"-solutions of the Josephson phase.

6.1.2 Fluxoids versus Abrikosov vortices

The calibration procedure is identical to the one described in the previous chapters. The sample is cooled in magnetic field and after the critical current is measured. Both a fluxoid trapped by the ring and an Abrikosov vortices trapped somewhere in the body of the ring or penetrating through the

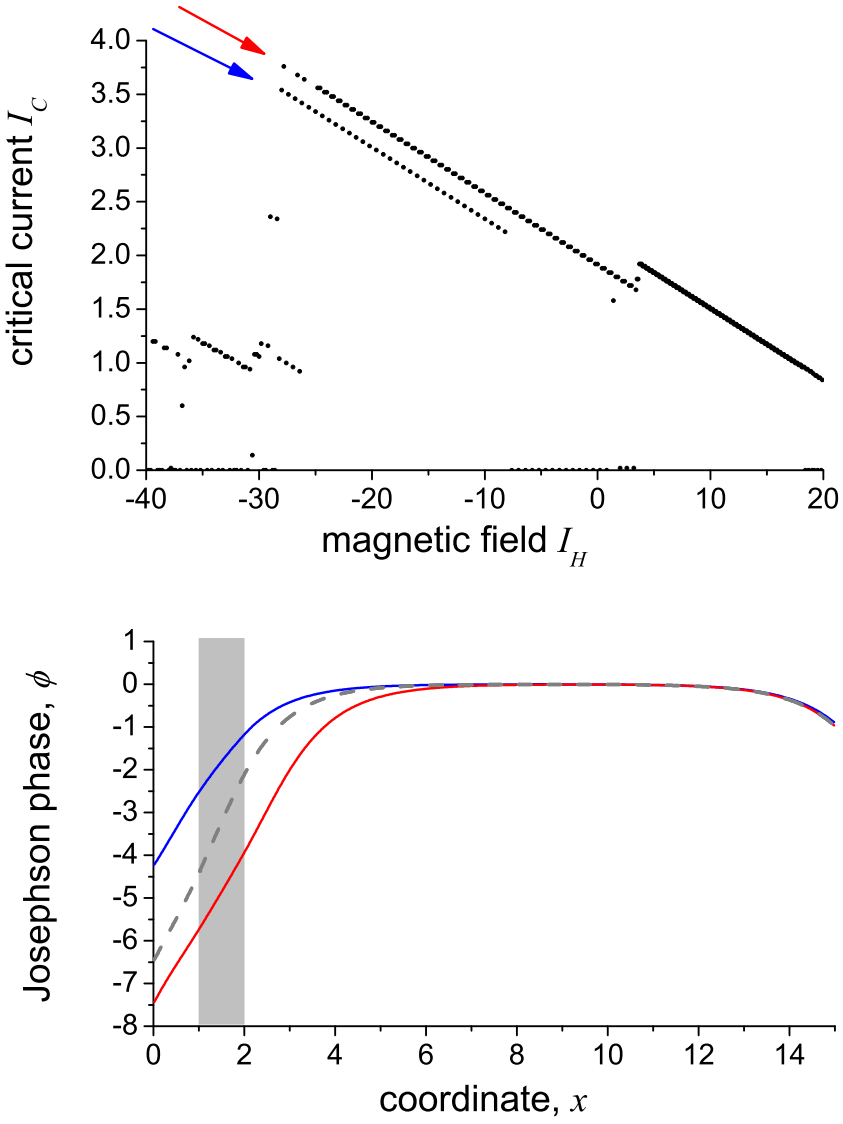

Figure 6.3: Results of numerical simulations of a long asymmetric inline JJ with an inhomogeneity of width $\Delta x = 1$ placed at $x = 1$ to 2. Top: magnetic diffraction pattern. Arrows indicate two solution for the critical current caused by two possible phase distributions. Bottom: Two phase distributions at $I_H = -14$. Gray color indicates the region with suppressed Josephson current. In both plots red - first solution, blue - second solution. The dashed line shows how the phase profile would be in the homogeneous case for the same magnetic field.

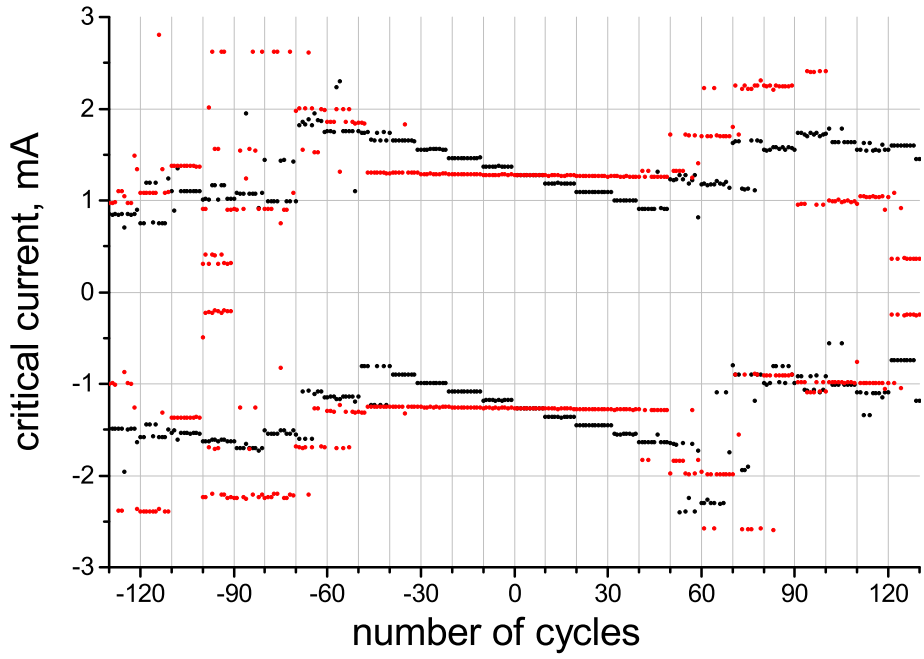

Figure 6.4: Field-cooling measurements of a long inline JJ places on a ring. Black: when the sample is cold the magnetic field is removed. Red: magnetic field remains unchanged during the transition and measurements. For both plots: after 10 cycles the coil current is changed by 1 mA (corresponding to about $22\Phi_0$ in the ring. T = 4.2K)

electrodes of the JJs change the critical current of the JJ. How to distinguish between them?

First criterion is the magnitude of the external field during the cooling. To trap one Abrikosov vortex significantly larger magnetic field is required than to trap one fluxoid.

Second criterion is to measure every time the I_c versus B dependence. In case of AVs we will see qualitative change, while in case of fluxoid the dependence will be simply shifted without disturbances of its shape. However this method is very time consuming. Moreover there is a technical difficulty related to the very different scales of both effects, which imposes two mutually exclusive regimes of operation. If we need to measure the effect from one trapped fluxoid we use a larger gain of the amplifies, so that only a small part part of the IV-curve can be seen, the rest saturates the amplifier. If we need to observe the $I_c(B)$ pattern, which implies much larger current range, the amplifier gain is to be reduced and noise in this regime becomes comparable to the change in I_c corresponding to trapping of one fluxoid.

Third criterion. Suppose that the ring has been cooled down in a field and after this the external magnetic field is switched off. At the first moment

after switch off the field, the magnetic flux through the ring decreases and, according to Faraday's law of electromagnetic induction, induces a current in the ring which will be persistent from this moment [22]. In other words to detect whether the flux quanta were trapped the field has to be switched off.

In contrast to it the trapping of AV can be seen both with the external field and without it. We can use this fact to distinguish AVs and fluxoids in the calibration procedure.

The results of the field-cooling experiments (rough calibration) are presented in Fig. 6.4. Two sets of data (black and red) are obtained under absolutely identical conditions except one: for black points external field is removed before measurements and for red points magnetic field remains the same as during the cooling. Thus in the black points the information about the trapped fluxoids and also the AVs is hidden, whereas the red points are free from influence of currents screening the flux quanta trapped in the ring.

In zero field the current is the same for both calibrations. Therefore the black markers are not visible behind the red ones(cycles form 1 to 10).

From the red data the magnitude of the magnetic field sufficient for AV trapping can be found. The first time new values of the critical current, signalizing AV trapping, appears at the coil current +4mA in positive field and at −5mA in negative field. These currents are 100 times higher than needed to trap one flux quantum in the ring.

Now the set of black points can be analyzed. In analogy with red data one can expect that the AV trapping starts at the currents $>$ 4mA. At higher fields both AVs and fluxoids are trapped. At lower fields the change of the critical current is caused by fluxoids only. Change of the coil current by 1mA results in the equidistant change of the critical current by 0.1mA. In this plot the distance between neighboring levels is about $22\Phi_0$.

In Fig. 6.5 the fine calibration is presented: the effect from every single flux quantum trapped in the ring is visible. After 10 cycles the coil current changes by 45μA in positive direction and -45μA in negative direction. Such coil current adds approximately one flux quantum (or minus one flux quantum) in the ring area. Sometimes when the field gives fractional magnetic flux we can observe two levels, that means the ring traps $n\Phi_0$ or $(n+1)\Phi_0$.

The system is calibrated now and it is shown that the detector is ample sensitive to detect one flux quantum in the ring. Therefore it can be used for Kibble-Zurek measurements - trapping probability as a function of the quench rate.

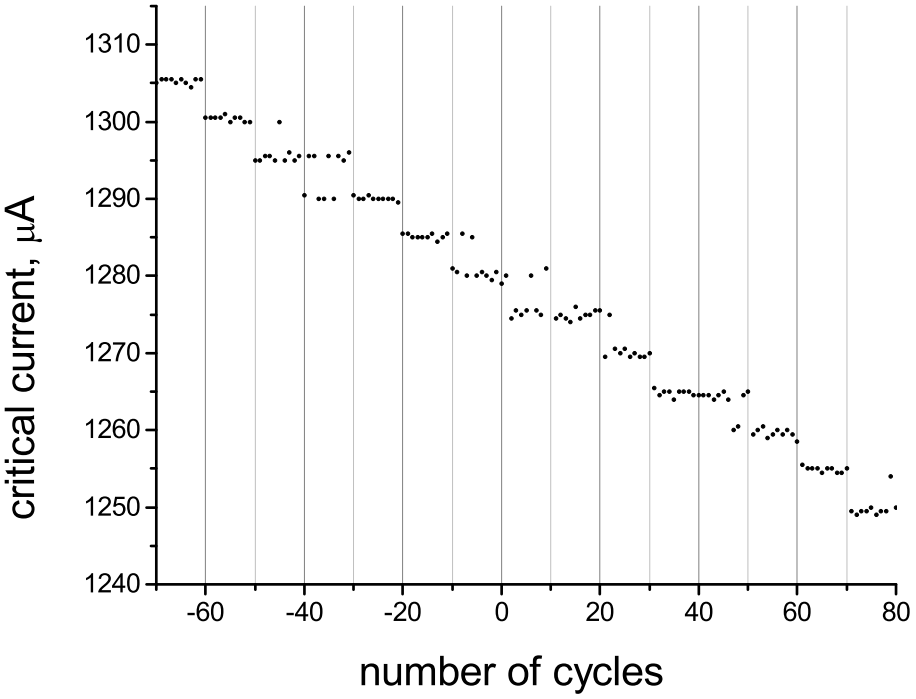

Figure 6.5: Field-cooling measurements of a long asymmetric inline JJ placed on a ring.

6.2 Results

To perform measurements of spontaneously trapped magnetic flux quanta it is necessary to find the magnitude of the residual magnetic field first. While the field is found, it is compensated by the coil, which is connected constantly during the measurements for a given τ_Q.

An alternative is to cool the sample in the compensated field, and then turn off the field and measure the sample in the residual field. In this way, however, current, applied to the coil, may not correspond to the current seen by the superconductor at the moment of going through the critical temperature due to the transient process in the coil. The current in the coil rises with time as $I = I_0(1 - e^{-t/\tau})$, where I_0 is applied current. A characteristic time scale needed to charge the coil is given by $\tau = L/R$, where L and R are inductance and resistance of the coil, respectively. A rough estimation gives $\tau \approx 60\mu$s for our coil. But the experimental value is longer. For such method of measurements the coil should be connected every time in advance to be sure that all transient processes decayed when ring goes through the transition temperature. That is more time consuming. All measurements presented here are obtained by the first method, i.e. with

permanently connected coil.

In the next Fig.6.6 the main result of the thesis is shown: probability of trapping of flux quanta P as a function of the quench time τ_Q for four samples. The quantity P includes both probability of trapping one flux quantum P_{+1} and probability of trapping minus one flux quantum P_{-1}.

The first property of the plot is that the robability of trapping decreases with τ_Q for all four samples. The second property, perhaps the most striking, is that the results are sample-dependent. Below each sample is discussed separately.

Sample $1i$. This sample shows the lowest trapping rate of all four samples. The experimental data are fitted quite well by a power-law with exponential coefficient $B = 2.8 \pm 0.1$.

Sample $2i$. This sample demonstrates a behavior similar to the sample $1i$. However $2i$ was more difficult to analyze, because there were several points which did not correspond to any integer number of flux quanta in the ring. Such points were ignored in the analysis. $B = 2.0 \pm 0.3$

Sample $3i$. Shows a non-monotonous probability of trapping. Also the probability decays rather fast but does not go to zero in the measured range of τ_Q as it does for samples $1i$ and $2i$. $B = 1.3 \pm 0.1$

Sample $4i$. Shows the largest trapping rate with the weakest dependence on τ_Q. $B = 0.4 \pm 0.1$

This kind of junctions rarely suffers from AV trapping. However sometimes the critical current was very large - a signature of trapped AV (see Fig.6.4). Is there a correlation between the rates of AV trapping and flux quanta trapping?

Junction $1i$ trapped AVs 30 times from the total number of cycles 13500, i.e. in 0.002 per cent of all cases. Junctions $2i$, $3i$ and $4i$ trapped in 0.009, 0.0006 and 0.007 per cent of cases, respectively. Hence there is no direct correlation between AV trapping and the quanta trapping.

Despite the AV trapping is a rare event it may complicate the analysis of results (only sample $2i$ has this problem). Trapped Abrikosov vortex can result in any change of the critical current, both large or small. Vortices trapped a bit far from JJ can still change the critical current. But this change can be as small as the current noise (2μA in our setup) and in this case, of course, not detectable. Or it can be slightly larger, for example 5μA, of the order of the effect from one flux quantum. In this case it is hard if possible at all to say whether we deal with one flux quantum or AV.

However the probability, that a pinning center happens to be exactly in such a place that the effect from it is equal to the effect from one flux quantum, is small.

Moreover this problem has a solution, proposed and implemented by Roberto Monaco in April 2011. As one can notice in Fig.6.1 each ring has two junctions on top. If the ring traps one flux quanta both junctions must detect it. On the contrary if an Abrikosov vortex is trapped sufficiently

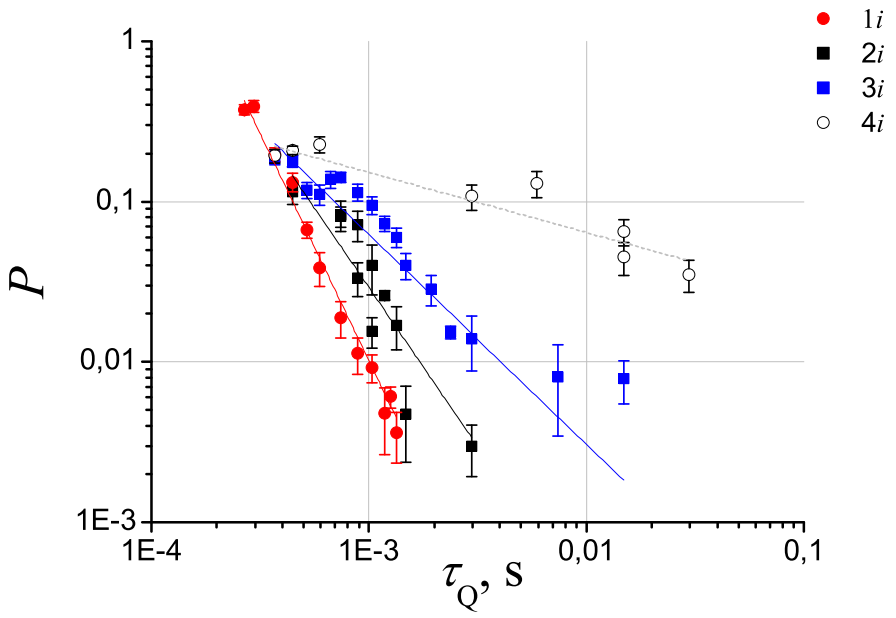

Figure 6.6: Probability of trapping of flux quanta in the ring versus the quench time τ_Q for four samples. Experimental points are fitted by a power dependence $P = A(\tau_Q)^{-B}$. Exponential coefficient B equals 2.8, 2.0, 1.3 and 0.4 for samples $1i$, $2i$, $3i$ and $4i$, respectively.

close to one of the junctions, it is too far away from the other, so that the indications of the junctions are not correlated. Therefore by reading two junctions simultaneously and looking for the correlation between them one can exclude the cases of AV trapping completely. However, this method was not implemented for results presented here, all data relay on measurements of a single junction.

6.3 Discussion and Conclusion

The samples, investigated in this chapter, consists of a superconducting ring and two inline Josephson junctions on top. Junctions serve as detectors of flux quanta trapped by the ring during phase transition. It is shown that this kind of junctions indeed can detect one trapped flux quantum in the ring. The measurements of trapping probability versus the quench time are performed for four samples. Below we discuss several factors, which could influence the trapping rate, such as residual magnetic field and Josephson junctions.

In spite of magnetic shielding some residual magnetic field is still present

in the setup. Its value corresponds to approximately $0.3 - 0.5\Phi_0$ in the ring area. Besides it is slightly different for each sample. With this kind of junctions it is impossible to determine where zero magnetic field is. Therefore in reality we may have, for example, $0.3\Phi_0$ plus some integer number of Φ_0. Large default number is not expected due to good quality shielding can made of high-T_c superconductor, but 1 or -1 is reasonable to assume. Does it affect the trapping rate?

From Chap.3 it is known that the dependence of the trapping rate on the external field is periodic, see Fig.3.4. For example, to measure spontaneous trapping in the first period, we find, first, the field for which probability not to trap is maximal. At this field we measure probability P to trap $+1\Phi_0$ and $-1\Phi_0$. If we move to the next period and find the field for which probability to trap $+1\Phi_0$ is maximal, we will see that at this field probability to trap $+2\Phi_0$ and $0\Phi_0$ is the same P. Therefore it is not important in which period we are.

Let us discuss now why the probability is so different for different samples. One possible reason is a film property. For example, rings made from films with more pinning centers trap more frequently. However in the previous two chapters we collected the evidence that difference between results for Abrikosov vortex trapping can not be explained by the quality of the films. This conclusion may be extended to this chapter as well. It is unlikely that quality of the film varies from chip to chip on one substrate significantly for the present technology of fabrication.

Another possible reason is the Josephson junctions on top of the ring. The ring plus the JJs compose a complex system, each component of which influences the others. A ground for this assumption can be a correlation between junction quality and trapping rate of the ring. The quality of the junctions is judged from the parameter R_j/R_n and from the shape of magnetic pattern. From their patterns, shown in Fig.6.2, one can conclude that something is wrong with junctions $3i$ and $4i$. If we look at the trapping probability we will see that it is the largest for samples $3i$ and $4i$. Thus, there could be a correlation. However four samples are not enough to make a solid conclusion. More samples have to be measured to prove this guess.

Conclusion

The observation of the dependence of the trapping rate on the transition speed is the main results of the thesis. For convenience the most important measurements are reproduced here again on one page in Fig.6.7. The left and the right plots show the probability of trapping versus the quench time for Abrikosov vortices and for flux quanta in the rings, respectively. The left plot was shown in Chap.5 with the pulse width instead of the quench time on the X-axis. The plot preserves its qualitative view in new units. At least three features are common for both plots:

- Production of both Abrikosov vortices and fluxoids depends on the cooling rate. The faster the sample is cooled the more frequently it traps magnetic fluxes.

- Trapping probability strongly depends on a sample. Particular sample properties is one of the factors influencing the trapping.

- For most of the samples the probability drops to zero much faster than a power low with exponent -0.5. Such fast decay is observed for the first time in this thesis.

Thus the mechanism of trapping of magnetic field for our samples is such, that unique characteristics of each sample contribute to the result.

Another factor, increasing the trapping probability, is the electrical heater. All measurements in Chap.5 are done with the electrical heater. In Chap.3 we observed that the trapping decreases if laser heating is used in place of electrical, what means that the electrical heater is a source of noise.

Since we observed the difference in trapping rates for different samples and when using electrical or laser heating, we can not assert that the trapping is caused by the KZ-mechanism only. Definitely, in our experiments additional factors play a significant role and interrupt the trapping.

But these findings do not cancel the hypothesis that one common mechanism (by this we mean the KZ-mechanism) is active for all samples. We believe that the KZ-mechanism plus sample effects plus external factors (such as electrical heater) all together compose the observed probability of

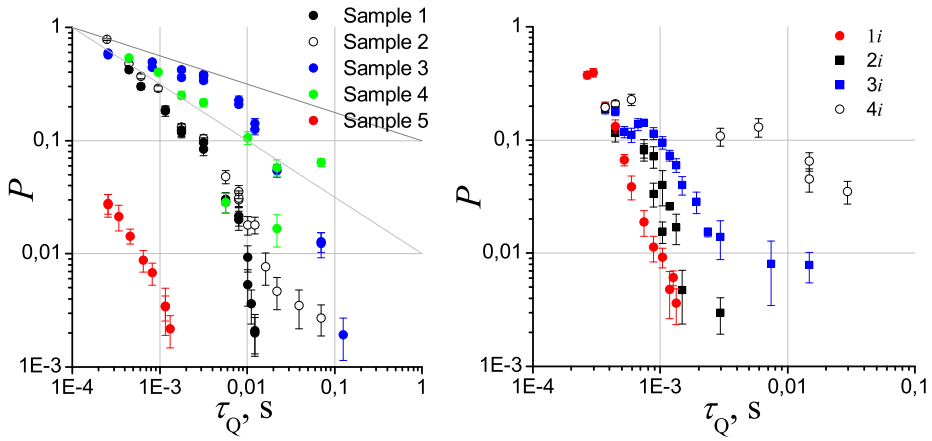

Figure 6.7: The main results of Chap.5 and Chap.6. Left: Probability of trapping of Abrikosov vortices versus the quench time. Right: Probability of trapping of flux quanta in the ring versus the quench time.

trapping. The question is how to distinguish the contribution from KZ-mechanism and form other effects. How are our results related to the KZ-theory?

There is a lower limit in the trapping rate which curves approaches for both plots in Fig.6.7. It is not obvious where this limit came from. Let us make an assumption, which looks rather reasonable, that the KZ-mechanism gives the lower boundary of the effect. I.e. other factors can only increase probability of trapping but do not decrease it. It gives a right to assert that all samples demonstrating larger trapping rate are influenced by some other factors whereas the samples with the lowest trapping rate can not be used for comparison with the KZ-theory. But before doing this, let us make one very important remark, discussed already earlier.

The KZ-theory was created for systems of infinite size, i.e. many and many defects appear during the transition. And the quantity to estimate their density is the average distance between them. In real systems the defects, being initially created, annihilate afterwards. That is why annular geometry, preventing the defects from annihilation, is so attractive for experiments. But in that case only one defect is created and measured. And instead of distance between the defects the probability of appearance of one defect is measured. The recognition of difference between these two situations (many defects versus only one defect) did not come easily because neither theory nor experiment could cover both cases. Fortunately theory and experiment has been linked by means of numerical simulations, for which no constrains exist.

By the argument above we should compare measurements with simulations rather than with the theory. Simulations say that below 0.3 the trapping probability decreases exponentially with the quench time.

For comparison we choose samples 1, 3, 5 and 1i and 2i for the following reason. For samples 2, 4, 3i and 4i there are undoubtedly some factors not related to Kibble-Zurek picture, which increased the trapping rate.

For chosen samples the results are consistent with numerical simulations. In case of Abrikosov vortices the decay is indeed exponential. Whereas in case of flux quanta the decay is fitted by a power law rather than exponent, however with very large exponential coefficient - 2.8 and 2.0 in comparison to the KZ-scalings 0.25 or 0.5.

However comparison with simulations can be only qualitative.

Simulations [29] are made in the framework of second-order Langevin equation with Ginzburg-Landau potential. Such description is a very idealized and simplified model of a superconductor, so no quantitative agreement with experiment is expected. More realistic simulations require the incorporation of a dynamical electro-magnetic field. Nevertheless with all limitations this model reproduces the Kibble-Zurek scaling $\sigma = 0.25$ for one-dimensional systems.

Another model, widely used for description of superconductors, is a time-dependent Ginzburg-Landau model. Time-dependent Ginzburg-Landau theory generalizes the usual GL theory to include relaxation processes for nonequilibrium superconductivity. The validity of it is much more limited. The TDGL equations, being exact in the gapless superconductors, are known to describe the dynamics only qualitatively in other cases [78]. However they are still used to get qualitative picture, because there is no anything better.

Also let us not forget that neither Kibble or Zurek included external fields in the analysis. In this sense the simulations are closer to the theory whereas the experiment stays apart.

Finally, could the presented result be useful for understanding of the Universe evolution? Such experiments provide a system in which the microscopic dynamics underlying the important mechanisms in a non-equilibrium phase transition can be probed, understood and controlled. Whether they can be used to model the early evolution of the Universe remains to be seen, but they look promising for providing new insights into these, traditionally difficult to study, phase transitions.

Outlook

As it is seen at the moment two main directions for the further experiments can be denoted.

The first direction is the improvements of conditions of experiments. By conditions we mean the environment of the samples. The most important improvement is to isolate the sample from the influence of a magnetic sensor.

In this sense the optical detection is still looks very attractive and may be realized in future. Next improvement may concern the base temperature of the experiment, for example from 4.2K down to 2K or lower. It would be very informative check whether the trapping rate is determined by the transition speed at the critical temperature of niobium (9.2K) or by surrounding noise.

The second direction is a modification of magnetic sensor on top of the ring. New design of samples is in production at the moment. In this design size of the detector should be decreased significantly in comparison with inline junctions, the most successful design by now.

The important question remained unanswered at the moment of writing the thesis is why the offset field changes with the quench time. No explanation has been figured out so far.

Bibliography

[1] T. Kibble. Phase-transition dynamics in the lab and the universe. *Physics today*, pages 47–52, 2007.

[2] L. Pitaevskii and E. Lifshitz. *Physical Kinetics*. London: Pergamon Press, 1981.

[3] A. Larkin and A. Varlamov. *Theory of Fluctuations in Superconductors*. Oxford University Press, 2005.

[4] H. E. Stanley. *Introduction to phase transitions and critical phenomena*. Clarendon Press, Oxford, 1971.

[5] M. Hindmarsh and A. Rajantie. Defect formation and local gauge invariance. *Physical Review Letters*, 85(22):4660(4), 2000.

[6] N. D. Antunes, P. Gandra, R. J. Rivers, and A. Swarup. The creation of defects with core condensation. *arXiv:hep-ph/0601130v2*, 31 Mar 2006.

[7] W. Zurek. Cosmological experiments in condensed matter systems. *Physics Reports*, 276:177–221, 1996.

[8] R. Monaco, R. Rivers, and E. Kavoussanaki. Testing the Zurek-Kibble causality bounds with annular Josephson tunnel junctions. *Journal of Low Temperature Physics*, 124(1/2):85–99, 2001.

[9] R. Monaco, J. Mygind, and R. J. Rivers3. Zurek-Kibble domain structures: The dynamics of spontaneous vortex formation in annular Josephson tunnel junctions. *Physical Review Letters*, 89(8):080603(4), 2002.

[10] T. W. B. Kibble. Topology of cosmic domains and strings. *J. Phys. A: Math. Gen.*, 9, 1976.

[11] A. Kogut, J. Dunkley, C. L. Bennett, O. Dore, B. Gold, M. Halpern, G. Hinshaw, N. Jarosik, E. Komatsu, M. R. Nolta, N. Odegard, L. Page, D. N. Spergel, G. S. Tucker, J. L. Weiland, E. Wollack, and E. L. Wright. Three-year Wilkinson microwave anisotropy probe (wmap)

observations: foreground polarization. *The Astrophysical Journal*, 665:355–362, 2007.

[12] T. Kibble. Some implications of a cosmological phase transition. *Physics Reports*, 67(1):183–199, 1980.

[13] M. E. Dodd, P. C. Hendry, N. S. Lawson, P. V. E. McClintock, and C. D. H. Williams. Nonappearance of vortices in fast mechanical expansions of liquid 4He through the lambda transition. *Physical Review Letters*, 81(17):3703(4), 1998.

[14] C. Bäuerlea, Y. M. Bunkov, S. N. Fisher, H. Godfrin, and G. R. Pickett. Laboratory simulation of cosmic string formation in the early Universe using superfluid 3He. *Nature*, 382:332–334, 1996.

[15] E. A. S. Mark J. Bowick, L. Chandar and A. M. Srivastava. The cosmological Kibble mechanism in the laboratory: String formation in liquid crystals. *Science*, 263(5149):943–945, 1994.

[16] A. Rajantie. Local gauge invariance and formation of topological defects. *Journal of Low Temperature Physics*, 124(1/2):5–16, 2001.

[17] M. Hindmarsh and A. Rajantie. Phase transition dynamics in the hot Abelian Higgs model. *Physical Review D*, 64:065016(13), 2001.

[18] P. Laguna and W. H. Zurek. Critical dynamics of symmetry breaking: Quenches, dissipation, and cosmology. *Physical Review D*, 58:085021(4), 1998.

[19] M. Tinkham. *Introduction to superconductivity, 2nd Edition.* McGraw-Hill, 1996. ISBN: 0070648786.

[20] A. Abrikosov, L. Gorkov, and I. Dzyaloshinskii. *Quantum Field Theoretical Methods in Statistical Physics*, volume XII. Pergamon Press, Oxford, 2nd edition, 1965.

[21] N. Kopnin. *Vortices In Type-II Superconductors: Structure And Dynamics.* L.D. Landau Institute for Theoretical Physics Moscow, Russia and Laboratoire de Physique des Solides, Universite Paris-Sud, Bat 510, 91405 Orsay, 1995 - 1996.

[22] V. V. Schmidt. *The Physics of Superconductors.* Springer-Verlag Berlin Heidelberg, 1997.

[23] L. H. Allen and J. H. Claassen. Technique for measuring the elementary pinning force in thin films. *Physical Review B*, 39:20542059, 1989.

[24] W. Goodman and B. Deaver. Detailed measuments of the quantized flux states of hollow superconducting cylinders. *Physical Review Letters*, 24, 1970.

[25] J. R. Kirtley, C. C. Tsueia, and F. Tafuri. Thermally activated spontaneous fluxoid formation in superconducting thin film rings. *Physical Review Letters*, 90(25):257001(4), 2003.

[26] R. Monaco, J. Mygind, M. Aaroe, R. J. Rivers, and V. P. Koshelets. Zurek-Kibble mechanism for the spontaneous vortex formation in Nb-Al/Al_{ox}/Nb Josephson tunnel junctions: New theory and experiment. *Physical Review Letters*, 96:180604(4), 2006.

[27] R. Carmi, E. Polturak, and G. Koren. Observation of spontaneous flux generation in a multi-Josephson-junction loop. *Physical Review Letters*, 84(21):4966(4), 2000.

[28] P. Laguna and W. H. Zurek. Density of kinks after a quench: When symmetry breaks, how big are the pieces? *Physical Review Letters*, 78(13):2519(4), 1997.

[29] D. J. Weir and R. J. Rivers. Fluxoid formation: size effects and non-equilibrium universality. *Journal of Physics: Conference Series 286*, page 012056(7), 2011.

[30] A. Yates and W. H. Zurek. Vortex formation in two dimensions: When symmetry breaks, how big are the pieces? *Physical Review Letters*, 80(25):5477(4), 1998.

[31] I. Montvay and G. Münster. *Quantum fields on a lattice*. University Press, Cambridge, 1994.

[32] M. Ghinovker, B. Y. Shapiro, and I. Shapiro. Spontaneous magnetic-flux generation in superconducting ring. *Europhysics Letters*, 53(2):240–245, 2001.

[33] D. Golubchik, E. Polturak, and G. Koren. Evidence for long-range correlations within arrays of spontaneously created magnetic vortices in a Nb thin-film superconductor. *Physical Review Letters*, 104:247002(4), 2010.

[34] H.-J. Barthelmess, S. Krey, S. Ostertun, and M. Schilling. Sensitive Josephson magnetometry of flux quantization in a normal conducting hole in a narrow $YBa_2Cu_3O_7$ line. *Applied Physics Letters*, 77(12):1882–1884, 2000.

[35] A. Golubov, E.P.Houwman, J. Gijsbertsen, V. Krasnov, J. Flokstra, H. Rogalla, and M. Kupriyanov. Proximity effect in superconductor-insulator-superconductor Josephson tunnel junctions: Theory and experiment. *Physical Review B*, 51(2):1073(17), 1995.

[36] K. K. Likharev. *Dynamics of Josephson junctions and circuits*. Gordon and Breach science publishers, 1984.

[37] A. Barone and G. Paternò. *Physics and Applications of the Josephson Effect*. John Wiley and sons Inc., 1982. ISBN: 0471014699.

[38] A. Franz, A. Wallraff, and A. V. Ustinov. Magnetic field penetration in a long Josephson junction imbedded in a wide stripline. *Journal Of Applied Physics*, 89(1):471–476, 2001.

[39] V. N.Gubankov, M. P. Lisitskii, I. L.Serpuchenko, and M.V.Fistul. Influence of trapped Abrikosov vortices on the critical current of the Josephson tunnel junction. *Sup. Sci. Tech.*, 5:168–173, 1992.

[40] R. Monaco, J. Mygind, V. P. Koshelets, and P. Dmitriev. δ-biased josephson tunnel junctions. *Physical Review B*, 81, 2010.

[41] R. Monaco, M. Aaroe, J. Mygind, and V. P. Koshelets. Static properties of small Josephson tunnel junctions in an oblique magnetic field. *Physical Review B*, 79:144521, 2009.

[42] A. Hebard and T. Fulton. Josephson junctions in transverse magnetic fields. *Physical Review Letters*, 35(19):1310–1311, 1975.

[43] S. Miller, K. Biagi, J.R.Clem, and D. Finnemore. Critical currents of cross-type superconducting-normal-superconducting junctions in perpendicular magnetic fields. *Physical Review B*, 31:2684–2693, 1985.

[44] S. Basavaiah and R. Broom. Characteristics of in-line Josephson tunneling gates. *IEEE Trans. on Magn.*, MAG-ll, 1975.

[45] A. M. van den Brink and H. Dekker. Josephson-junction thermodynamics and the superconducting phase transition in a squid device. *Physical Review B*, 55(14):8697(4), 1997.

[46] T. Kibble and G. Volovik. On phase ordering behind the propagating front of a second-order transition. *JETP Letters*, 65(1):102–107, 1997.

[47] J. Dziarmaga, P. Laguna, and W. H. Zurek. Symmetry breaking with a slant: Topological defects after an inhomogeneous quench. *Physical Review Letters*, 82(24):4749(4), 1999.

[48] V. L. Ginzburg. Nobel lecture: On superconductivity and superfluidity what i have and have not managed to do! as well as on the physical minimum at the beginning of the xxi century. *Reviews Of Modern Physics*, 76:981(18), 2004.

[49] P. Selzer and W. Fairbank. Thermally generated magnetic fields in an anisotropic metallic crystal at low temperatures. *Physics Letters*, 48A(4):279–280, 1974.

[50] D. V. Harlingen, D. Heidel, and J. Garland. Experimental study of thermoelectricity in superconducting indium. *Physical Review B*, 21(5):1842–1857, 1980.

[51] D. V. Harlingen. Thermoelectric effects in the superconducting state. *Physica*, 109 and 110B:1710–1721, 1982.

[52] M. Kartsovnik, V. Ryazanov, and V. Schmidt. Observation of the thermoelectric effect in SNS-junctions. *Pis'ma Zh. Eksp. Teor. Fiz.*, 33(7):373–376, 1981.

[53] P. N. Dmitriev, A. B. Ermakov, A. G. Kovalenko, V. P. Koshelets, N. N. Iosad, A. A. Golubov, and M. Y. Kupriyanov. Niobium tunnel junctions with multi-layered electrodes. *IEEE Trans. on Appl. Supercond.*, 9(2):39703973, 1999.

[54] V. Koshelets, S. Kovtonyuk, I. Serpuchenko, L. Filippenko, and A. Shchukin. High quality Nb-AlOx-Nb junctions for microwave receivers and SFQ logic devices. *IEEE Transactions on Magnetics*, 27(2):3141–3144, 1991.

[55] P. N. Dmitriev, I. L. Lapitskaya, L. V. Filippenko, A. B. Ermakov, S. V. Shitov, G. V. Prokopenko, S. A. Kovtonyuk, and V. P. Koshelets. High quality Nb-based tunnel junctions for high frequency and digital applications. *IEEE Transactions On Applied Superconductivity*, 13(2):107–110, 2003.

[56] U. L. Olsen. *DTU, Physics.* Master's thesis, 2006.

[57] Thermal conductivity: Silicon. *http://www.efunda.com/materials/elements/.*

[58] J. V. Goicochea, M. Madrid, and C. Amon. Hierarchical modeling of heat transfer in silicon-based electronic devices. *Journal Of Heat Transfer*, 132(10):1–11, 2010.

[59] R. F. Broom. Some temperature-dependent properties of niobium tunnel junctions. *Journal of Applied Physics*, 47(12):5432–5439, 1976.

[60] R. Monaco, M. Aaroe, J. Mygind, R. J. Rivers, and V. P. Koshelets. Experiments on spontaneous vortex formation in Josephson tunnel junctions. *Physical Review B*, 74(14):144513(9), 2006.

[61] M. Aarøe. *Symmetrybreaking in superconducting phase transitions*. Ph.D. thesis, Denmark Technical University, DTU Physics, 2009.

[62] J. Ramos, V. Zakosarenko, R. IJsselsteijn, V. Schultze, and H.-G. Meyer. Mutual inductance and noise of high-Tc, SQUIDs with flip-chip and integrated input coils. *IEEE Transactions on Applied Superconductivity*, 11(1):1118–1121, 2001.

[63] T. V. Duzer. *Principles of Superconductive Circuits and Devices*. Prentice Hall, 1998. ISBN: 0521624355.

[64] J. Clarke and A. I. Braginski. *Vol.I: Fundamentals and Technology of SQUIDs and SQUID Systems, Vol.II: Applications of SQUIDsand SQUID Systems*. WILEY-VCH Verlag GmbH and Co. KGaA, Weinheim, 2004.

[65] T. Ryhänen and H. Seppä. SQUID magnetometers for low-frequency applications. *Journal of Low Temperature Physics*, 76, 1989.

[66] V.P.Koshelets, A.N.Matlashov, I.L.Serpuchenko, L.V.Filippenko, and Yu.E.Zhuravlev. Dc-SQUID preamplifier for dc-SQUID magnetometer. *IEEE Transactions On Magnetics*, 25:1182 – 1185, 1989.

[67] S. K. H. Lama and D. L. Tilbrook. Development of a niobium nanosuperconducting quantum interference device for the detection of small spin populations. *Applied Physics Letters*, 82(7):1078(3), 2003.

[68] Q. Li, J. R. Clem, and D. K. Finnemore. Nucleation and motion of an isolated Abrikosov vortex. *Physical Review B*, 43(16):12843–12847, 1991.

[69] O. Hyun, J. Clem, and D. Finnemore. Motion of a single superconducting vortex. *Physical Review B*, 40:175–181, 1989.

[70] M. P. Lisitskiy and M. V. Fistul. Fiske steps and Abrikosov vortices in Josephson tunnel junctions. *Physical Review B*, 81:184505, 2010.

[71] M. Y. Kupriyanov, K. Likharev, and V. Semenov. Boundary between static and dynamic state in long Josephson junctions. *Fizika Nizkih Temperatur*, 2:1252–1256, 1976.

[72] K. Likharev, V. Sernenov, O. V. Snigirev, and B. I. Todorov. Josephson junction with lateral injection as a vortex transistor. *IEEE Transactions On Magnetics*, 15(1):420–423, 1979.

[73] N. Uchida, K. Enpuku, Y. Matsugaki, S. Tomita, and F. Irie. Flux trapping in Josephson tunnel junctions. *Journal of Applied Physics*, 54(9):5287–5292, 1983.

[74] R. Monaco, J. Mygind, R. J. Rivers, and V. P. Koshelets. Spontaneous fluxoid formation in superconducting loops. *Physical Review B*, 80:180501(4), 2009.

[75] A. Golubov and A. Ustinov. Interaction energy of Abrikosov and Josephson vortices in a long Josephson junction. *Physics Letters A*, 162(5):409–414, 1992.

[76] O.Yu.Andreeva, T.L.Boyadjiev, and Yu.M.Shukrinov. Influence of position and parameters of inhomogeneities on vortex structure in long Josephson junctions. *Journal of Physics: Conference Series 129*, page 012036(5), 2008.

[77] A. V. Gordeeva and A. L. Pankratov. Defect formation in long Josephson junctions. *Physical Review B*, 81:212504(4), 2010.

[78] N. B. Kopnin. Introduction to Ginzburg-Landau and Gross-Pitaevskii theories for superconductors and superfluids. *Journal of Low Temperature Physics*, 129:219–262, 2002.

List of Figures

Appendix A

Appendixes

A.1 Samples

Below the original notation of the samples adopted by the producer is given with corresponding notation used in the thesis.

Chapter 4

$HD22\sharp2-07$**, JJs 2,3 and 4:** short overlap junctions

$HD22\sharp7-05$**, inner JJ:** short delta-biased Josephson junctions

Chapter 5

$HD22\sharp1-18$**, inner JJ:** sample 1

$HD22\sharp1-8$**, inner JJ:** sample 2

$HD22\sharp2-18$**, inner JJ:** sample 3

$HD22\sharp1-5$**, inner JJ:** sample 4

$HD22\sharp1-6$**, inner JJ:** sample 5

Chapter 6

$HD24\sharp2-5$**, JJA:** sample 1i

$HD24\sharp3-5$**, JJA:** sample 2i

$HD24\sharp1-5$**, JJA:** sample 3i

$HD24\sharp2-18$**, JJD:** sample 4i

Fig.A.1 shows the layouts of the samples investigated in chapters 3 - 6.

A.2 Equipment

List of the hardware used in the setup:

```
Function generator: HAMEG HM 8030
HP Triple output DC power supply:
E3631A HP DAQ/Switch Unit, 34970A
Tektronix analogue Oscilloscope
rack 7613 (storage)
  70A22 Differential amplifier
  70A22 Differential amplifier
Tektronix analogue Oscilloscope rack 7603
  70A22 Differential amplifier
  70A22 Differential amplifier
  7B53A  Time base
Tektronix TDS 410A Digitizing oscilloscope
  ADA400A   Differential Preamplifier
  ADA400A   Differential Preamplifier
Tektronix 1103 Tekprobe power supply
  ADA400A   Differential Preamplifier
  ADA400A   Differential Preamplifier
HP 34401A Multimeter HAMEG rack
  HM8040-2  Triple power supply
  HM8040-2  Triple power supply
Hewlett Packard
  E-3611A DC Power Supply
  E-3611A DC Power Supply
  8110A Pulse generator
Keithley
  230 Programmable voltage source
  2400 Source meter
  2400 Source meter
Pentium 4, 3.00GHz
  1.49 GB of RAM
  Microsoft Windows XP Pro SP2
  National Instruments LabVIEW Express 7.0
  NI PCI-GPIB
  NI PCI-6023E DAQ card
```

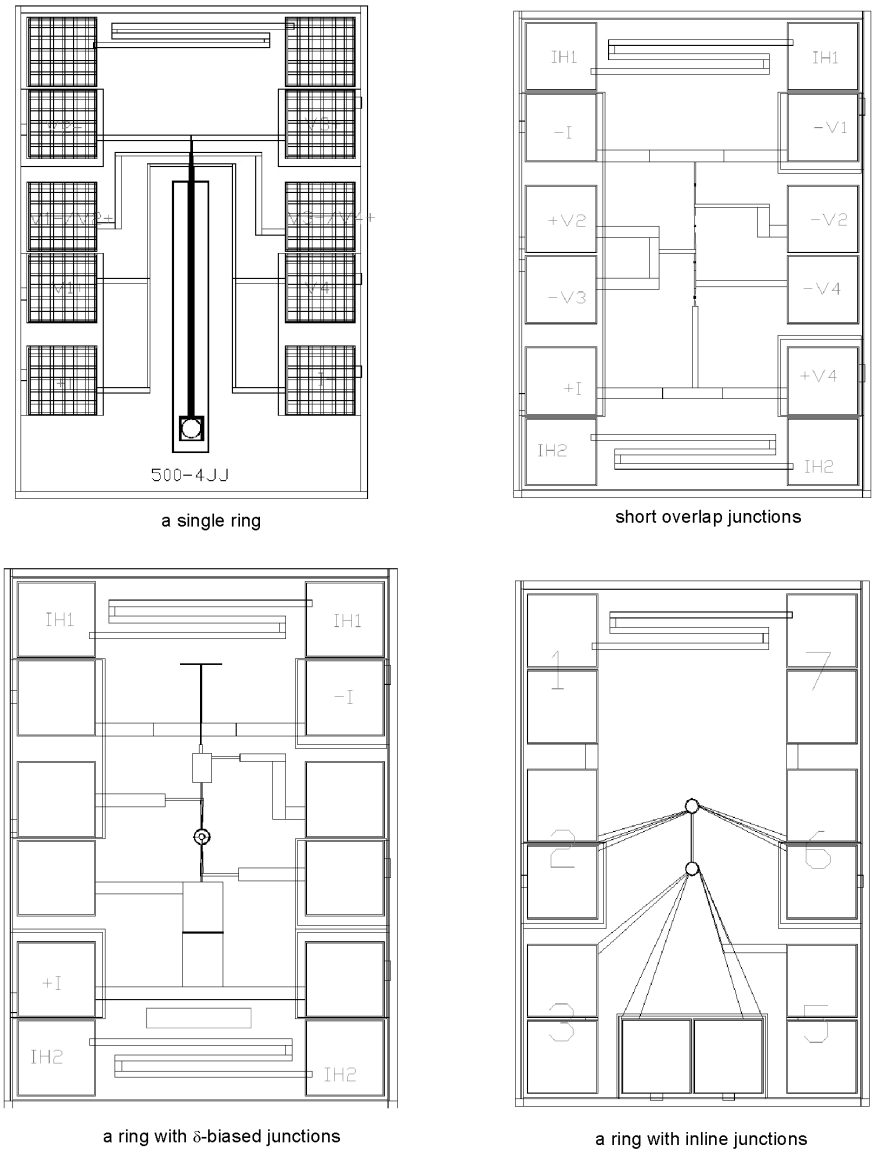

Figure A.1: Layouts of the samples.

A.3 Amplifierbox layout

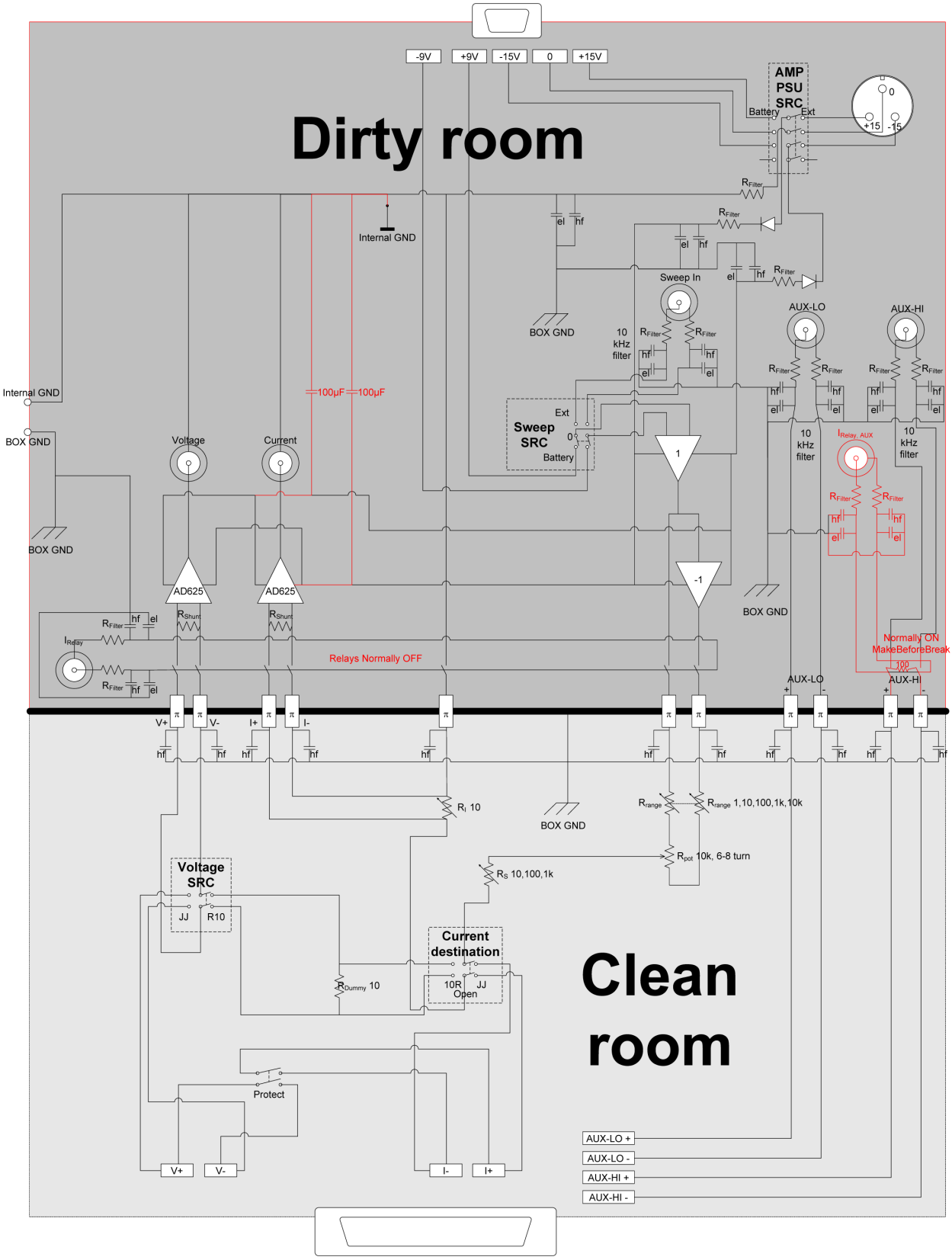
Dirty room
Clean room
-9V
+9V
-15V
0
+15V
AMP PSU SRC
Battery
Ext
Internal GND
BOX GND
Sweep In
Sweep SRC
10 kHz filter
AUX-LO
AUX-HI
100µF
100µF
Voltage
Current
AD625
Relays Normally OFF
Normally ON MakeBeforeBreak
V+
V-
I+
I-
Voltage SRC
JJ
R10
Current destination
10R
Open
Protect
AUX-LO +
AUX-LO -
AUX-HI +
AUX-HI -